UPGRADING NATURAL GAS TO VALUE-ADDED LIQUID PRODUCTS IN AQUEOUS SYSTEMS UNDER AMBIENT CONDITIONS

A Thesis by

Farshad Houtaham

Bachelor of Science, South Tehran Azad University, 2008

Submitted to the Department of Mechanical Engineering
and the faculty of the Graduate School of
Wichita State University
in partial fulfillment of
the requirements for the degree of
Master of Science

July 2017

UPGRADING NATURAL GAS TO VALUE-ADDED LIQUID PRODUCTS IN AQUEOUS SYSTEMS UNDER AMBIENT CONDITIONS

The following faculty members have examined the final copy of this thesis for form and content, and recommend that it be accepted in partial fulfillment of the requirement for the degree of Master of Science with a major in Mechanical Engineering.

_____
Shuang Gu, Committee Chair

_____
Ramazan Asmatulu, Committee Member

_____
Kim Cluff, Committee Member

DEDICATION

To my beloved parents

“The only source of knowledge is experience.”

Albert Einstein

ACKNOWLEDGMENTS

I would first like to thank my thesis advisor Prof. Shuang Gu form the Mechanical Engineering Department at Wichita State University (WSU). The door to Prof. Gu office was always open whenever I ran into a trouble spot or had a question about my research. His guidance helped me in all the time of research and writing of this thesis. I could not have imagined having a better advisor and mentor for my Master's study.

My sincere thanks also goes to Prof. Ramazan Asmatulu from Mechanical Engineering Department and Prof. David M. Eichhorn chair of the Chemistry Department at WSU who provided me an opportunity to conduct my experiments by giving access to the laboratory and research facilities. Without they precious support it would not be possible to conduct this research.

Besides my advisor, I would also like to acknowledge Dr. Kevin Langenwalter NMR/Instrumentation manager of the Chemistry Department at WSU. I am gratefully indebted to him for his continuous support, patience, motivation, and immense knowledge. I could not have done it without his valuable comments and guidance.

Finally, I must express my very profound gratitude to my parents and to my friends Giw, Pejman, Behdad and Ali for providing me with unfailing support and continuous encouragement throughout the process of researching and writing this thesis and my life in general. This accomplishment would not have been possible without them. Thank you.

The financial support provided by Start-Up Grant from the Collage of Engineering at WSU is gratefully acknowledged.

ABSTRACT

A novel method of upgrading natural gas into value-added liquid products is presented, in which the methane is activated by a decoupled oxidation approach with metal-surface facilitation in aqueous system under ambient conditions.

A facilitation effect of metal surfaces was discovered to be the critical step for methane activation, and three different liquid products can be produced: methanol, methyl formate, and formic acid. Our results showed that the activation rate of methane on metal surface is strongly correlated with the CH_3−M binding energy: The higher binding energy leads to greater activation rate. At the same time, product evolution as well as its final decomposition was also observed along with activation time.

In order to understand the evolution of activation products, we studied the decomposition reaction of formic acid in the same aqueous system with tuned conditions. A pseudo-first-order kinetics was observed to well fit the decomposition behavior of formic acid. The results revealed a volcano-shape correlation between the decomposition rates of formic acid with the O−M binding energy.

The fundamental understanding of the methane activation and the product decomposition will enable us to further develop this novel methane-upgrading method for industrial scale.

TABLE OF CONTENTS

TABLE OF CONTENTS (continued)

TABLE OF CONTENTS (continued)

Chapter Page

LIST OF TABLES

LIST OF TABLES (continued)

LIST OF FIGURES

Figure Page

LIST OF FIGURES (continued)

Figure Page

LIST OF FIGURES (continued)

Figure Page

LIST OF FIGURES (continued)

Figure Page

LIST OF ABBREVIATIONS/NOMENCLATURE

CoPc	Cobalt phthalocyanine
CW	Continuous Wave
DHHC	Dehydrohalogenative Coupling
DME	Dimethyl Ether
DSS	3-(Trimethylsilyl)propionic acid-D4 sodium salt
FFT	Fast Fourier Transform
FID	Free Induction Decay
FT	Fourier Transform
F-T	Fisher-Tropsch
GHG	Greenhouse Gas
GWP	Global Warming Potential
LNG	Liquefied Natural Gas
MMO	Monooxygenase
MO	Molecular Orbitals
NMR	Nuclear Magnetic Resonance
OCM	Oxidative Coupling of Methane
TMS	Trimethylsilyl Cyanide
UV	Ultra Violate

CHAPTER 1

INTRODUCTION

1.1 Background

Methane is the major component of natural gas, and it is the simplest alkane with the chemical formula CH_4 which has one atom of carbon and four atoms of hydrogen. Methane is a colorless and odorless gas at room temperature under ambient pressure. The normal boiling point of methane is −161 °C (−257.8 °F), and it is flammable in gaseous state over concentrations of 5.4%−17% in air [1].

As shown in Figure 1.1, structurally methane molecule is a tetrahedral compound with four identical C–H bonds.

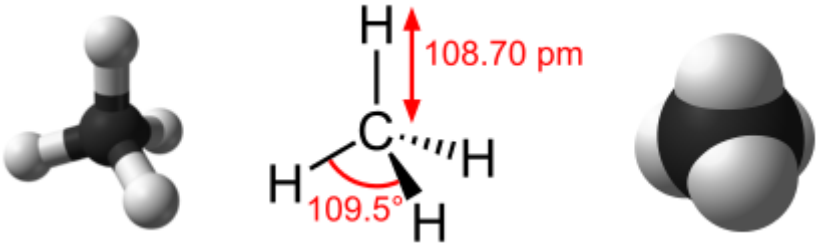

Figure 1-1. Methane structure and bonding (molecular model from left to right: ball-and-stick, geometry, and spall-filling) [2]

The electronic structure of methane is characterized by four bonding Molecular Orbitals (MOs) resulted from the overlap of valance orbitals on the central carbon atom and four hydrogen atoms.

Methane occurs naturally, and it can also be generated by industrial routes. The formation of natural methane is through either geological pathway or biological one. The geological pathway could further be divided to two subcategories as organic geological pathway and inorganic one. In the organic geological pathway, methane is generated by the thermal break-up of organic matters

at intensive temperatures and pressures in deeper stratus of earth, and the generated methane in such way is generally referred to as thermogenic methane. Natural gas resources primarily consist of thermogenic methane. In the inorganic geological pathway, methane is formed as a result of water-rock reaction, without involving organic matters. This type of methane generation occurs at low temperatures and pressures [3, 4].

Another major source of natural methane is the biological pathway in which an anaerobic respiration process, consisting of multistep reactions, is used by some microorganisms and enzymes as catalysts. This kind of methane is generated in landfills, cattle and termite's colonies where these microorganisms are found.

Although there are many methods to produce methane, the practice of synthetic methane production is limited to very special cases due to the great abundance of natural methane resources. In those special cases, methane can be generated from biomass in industrial plants, through previously explained, biological route. Another synthetic method is the hydrogenation of carbon dioxide (methane as the major product) or carbon monoxide (methane as a byproduct).

Naturally generated methane is most under the sea floor or below the ground. Once methane reaches the Earth surface, it is referred to as atmospheric methane. The very high heat of combustion (891 kJ/mol) of methane makes it a remarkable fuel. However, capturing, storing, and transporting gaseous methane is rather inconvenient, compared with liquid products. [5].

Generally, chemical reactions involving methane are difficult to control. The typical chemical reactions of methane include combustion, steam reforming to syngas, and halogenation. The partial oxidation of methane to methanol or other liquid products is very attractive, but it is challenging because the reaction prefers to continue all the way to full oxidation of methane forming carbon dioxide and water. The most used reaction is the steam reforming to produce

syngas which can also be used for many industrial chemical processes including the production of ammonia and methanol.

Under appropriate conditions, methane can react with different halogens such as fluorine, chlorine, bromine and iodine. And this reaction is used to produce chemical compounds such as dichloromethane (CH_2Cl_2), chloroform ($CHCl_3$), and, ultimately, and carbon tetrachloride (CCl_4) [6].

Methane can be liquefied by cooling (below its boiling point), and the liquefied natural gas (LNG) can be used as a fuel for automobiles. Highly refined liquefied methane can also be used as rocket fuel [7, 8].

1.2 Motivations of Methane Upgrading

Great abundance and increasing production of methane make methane upgrading an appealing topic for commercial and research investment. Methane has significantly lower cost than many oxygenated carbonaceous compounds (oxycarbons). The huge difference in product value provides a beneficial market to efficiently upgrade methane into other value-added liquids.

Liquid products produced from methane upgrading are highly preferred over the liquefied methane (LNG). The liquefaction of methane demands the use of energy-intense and thus costly cryogenic methods of storage and transport. Moreover, methane is often released from the handling of LNG, not only endangering infrastructure safety but also raising concerns over its strong greenhouse effect.

1.2.1 Great Methane Abundance

Methane (natural gas) frequently is produced along with liquid petroleum and in most of the cases producer is required to take the gas along with the oil. According to U.S Energy Information Administration, the annual production of natural gas reached its highest record in

2015, and the growth in production rate continues to rise. The production increase of natural gas is largely the result of new technical breakthroughs of hydraulic fracturing and horizontal drilling such as shale gas-rich shales and tight sand gas. The Figure 1.2 shows a schematic of different natural gas resources.

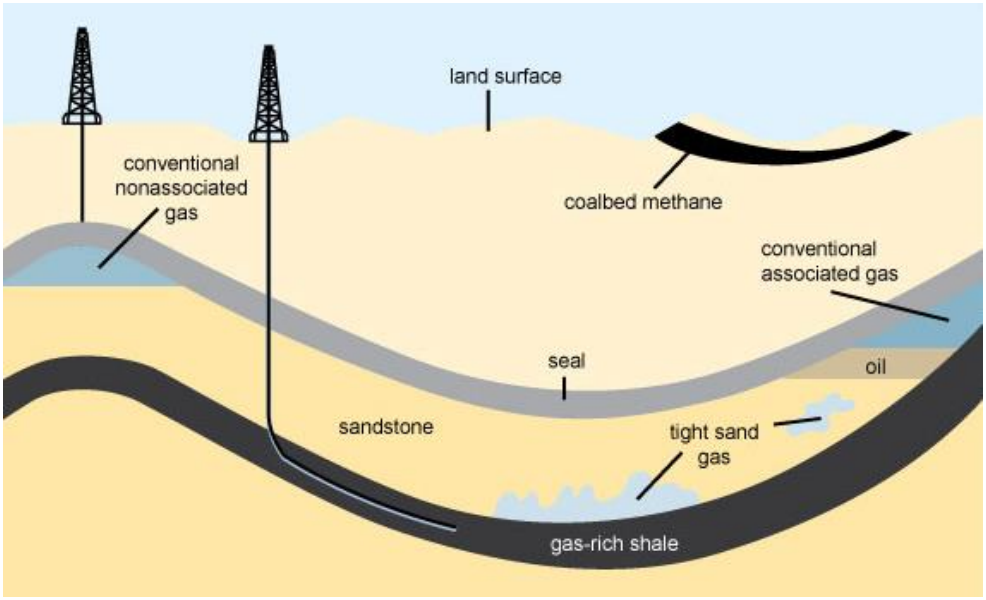

Figure 1-2. Schematic geology of natural gas resources
(Geological Survey factsheet 0113-01)

The Figure 1.3 shows that the production of natural gas in US is projected to increase by 30% and 55% in 2025 and 2040, respectively.

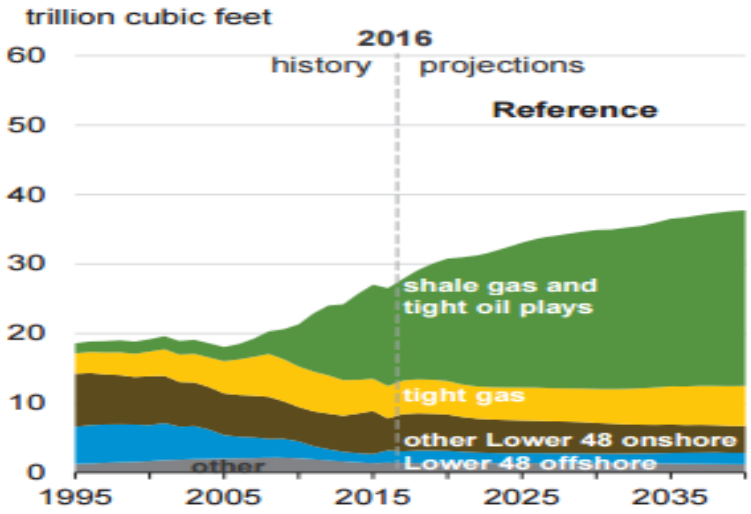

Figure 1-3. U.S. natural gas production: history and projections. Reference case, 1995−2040. (Annual Energy Outlook 2017, US/EIA)

This projection shows that the oil-to-gas price ratio will increasefrom 3.0 in 2016 to 3.1 and 4.9 in 2025 and 2040, respectively (Fig 1.4, Reference case).

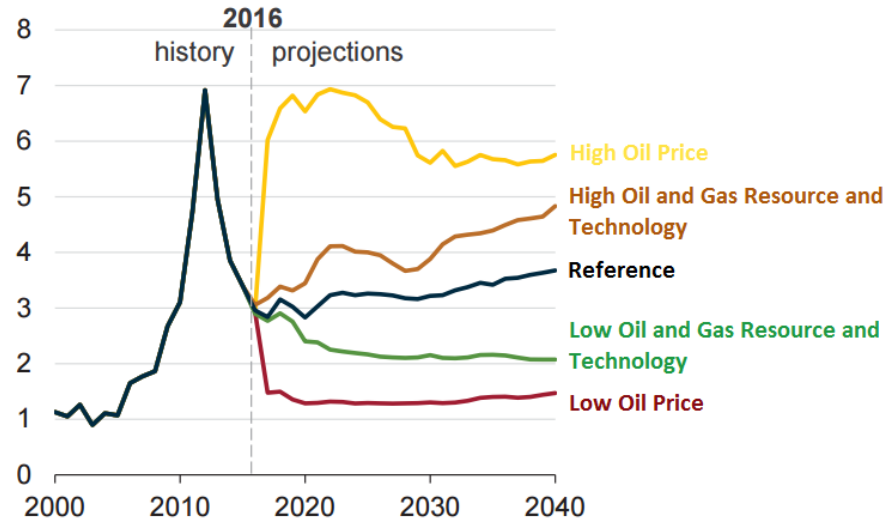

Figure 1-4. Oil-to-gas price ratio: history and projections. Reference case and other scenarios, 2000−2040. (Annual Energy Outlook 2017, US/EIA)

1.2.2 Low Energy Cost

Due to the great abundance of natural gas and its increasing production, the price of methane is much lower than that of crude oil in terms of same amount of energy. Obviously, oxycarbon liquids have even higher value than the crude oil. Currently, the prices of oxycarbon liquids are generally around 10−20 times as much as that of natural gas based on the same carbon molarity. For example, as shown in Table 1, the price of methanol (CH_3OH), formic acid (HCOOH), and methyl formate ($HCOOCH_3$) is 6.9, 11.1, and 17.5 times as much as that of natural gas based on market values in the first half year of 2017.

Great abundance and low cost of natural gas provide a clear motivation and unique opportunity for upgrading methane, the dominant component of natural gas, to value-added and handling-convenient oxycarbon liquids. There is also the opportunity of using methane as a platform to produce more valuable chemicals used in other industries.

TABLE 1

THE COMPARISON OF CURRENT MARKET PRICES BETWEEN METHANE AND SOME OXYCARBON LIQUID PRODUCTS OF INTEREST

Reactant/Products		**Price in Weight ($/ton)**	**Price in Molarity ($/kmol-C)**	**Value Addition[f]**
Reactant	CH_4	115.2[a]	1.8	0
Products	**CH_3OH**	386[b]	12.4	6.89 times
	HCHO	878[c]	26.4	14.7 times
	HCOOH	865[d]	19.9	11.1 times
	$HCOOCH_3$	1,050[e]	31.5	17.5 times

[a] Average price ($2.25/mmBTU natural gas) on Quarter 1, 2016: http://oilprice.com/Energy/Energy-General/Natural-Gas-Prices-Are-Unsustainably-Low.html.
1 kg natural gas is equivalent to 54 MJ/kg (1 mmBTU = 1.055 MJ).
[b] Average price in June, 2017: https://www.methanex.com/our-business/pricing
[c] Average price ($300−$350/ton @ 37% concentration) in June, 2017: http://www.made-in-china.com/
[d] Average price ($700−$770/ton @ 85% concentration) in June, 2017: http://www.icis.com/
[e] Average price ($1,000−$1,100/ton) in June, 2017: http://www.made-in-china.com/
[f] Value addition is based on 100% carbon efficiency.

In order for the liquid products to be considered as fuel applications, it is necessary to compare their heats of combustion. The Figure 1.5 shows HCOOH has much lowered combustion heat, compared with CH_3OH and $HCOOCH_3$. From the perspective of fuel application, it would be useful to produce more CH_3OH and $HCOOCH_3$ products than HCOOH one. Regardless of the heat of combustion, the all of them can be used as valuable additives to liquid fuels.

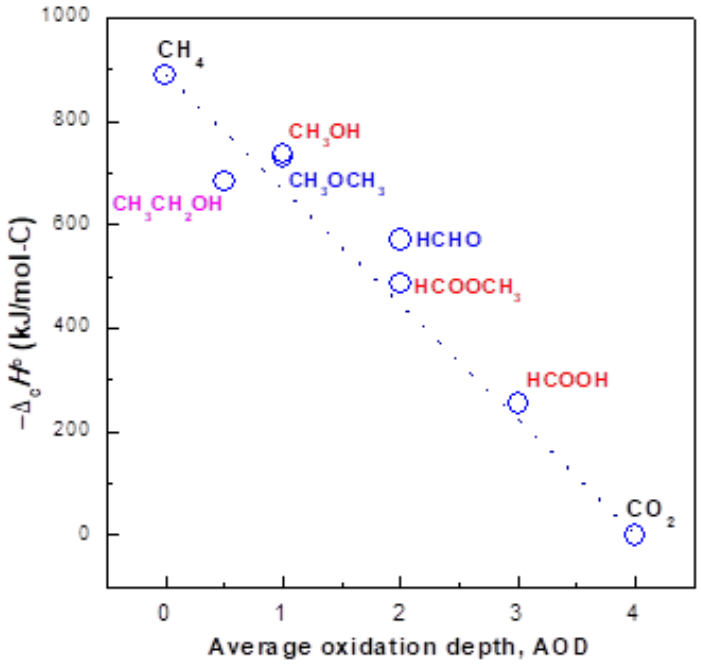

Figure 1-5. Standard combustion enthalpies ($\Delta_c H°$) of oxycarbon products of interest

1.2.3 Storage and Delivery Challenges

Natural gas resources are mostly located in inconvenient and remote locations. Most of the time, pipelines are built for transporting natural gas to potential markets.

Alternatively, natural gas can be physically liquefied, called liquefied natural gas (LNG), via a cooling process involving very low temperatures of −160 °C. The transportation of LNG, especially from off-shore resources by ocean-going vessels, is expensive. There are also some safety and quality debates on LNG conversion and transportation. First of all, it is almost

impossible to add any odorant to LNG because of the very low temperature. This absence of odorant raises the leak detection concern as methane is odorless and colorless. Secondly, the cryogenic temperatures required by LNG arises several safety concerns over bulk storage and delivery. For instance, intensive temperature control is required at the cost of constantly consuming fuel, because of the extreme temperature difference between ambient and LNG storage tank. Finally, we may note that cryogenic temperatures used for LNG changes the fuel properties of methane to some extend and care should be taken once using this liquefied gas in different applications.

Due to the hurdles mentioned above, approximately 11% of methane gas is reinjected, and unfortunately, another 4% is flared or vented, which is a waste of a hydrocarbon resource. Therefore, the conversion of methane to more energy-dense liquid derivatives, or a value-added product, as the source would significantly increase its utilization on a world-wide scale [9].

1.2.4 High Greenhouse Effect

Greenhouse gases (GHGs) are referred to any compound in the atmosphere of the earth that is capable of absorbing and emitting the infrared radiation. As a result, these gases warm the Earth by absorbing energy and decreasing the rate at which the energy escapes to space. In other words, they act as a blanket and insulate the Earth. Some of the primary greenhouse gases of earth's atmosphere could be named as water vapor, carbon dioxide, methane, nitrous oxides, and ozone. The impact of different GHGs on increasing the Earth's temperature is different, compared to one another. The main two key parameters for determining the impact of different GHGs are:

a) Radiative efficiency, which is defined as how able to absorb energy

b) Lifetime, which is defined as how long to stay in the atmosphere

In order to allow comparisons of the global warming impacts of different gases, The Global Warming Potential (GWP) was developed. GWP is defined as the measure of how much energy the emissions of 1 ton of a gas will absorb over a given period of time, relative to the emissions of 1 ton of carbon dioxide (CO_2). The GWP for any particular gas is calculated as:

$$GWP_i = \frac{\int_0^{TH} a_i(t)c_i(t)dt}{\int_0^{TH} a_c(t)c_c(t)dt}$$

where "*TH*" is the time horizon over which the GWP is calculated. In this equation a_i is relative efficiency of the gas in W m^{-2} kg, and c_i is the time dependent decay of the compound. The subscript "*i*" in the equation indicates the compound for which is being investigated and subscript "*c*" indicates the same parameter for the reference compound. Generally for GWP calculation, the reference gas is CO_2. The larger the GWP means the more powerful that a given gas warms the Earth, compared to CO_2 over a specific period of time. This time period usually used is 100 years. Methane decay time is about a decade on average, but the more dominating factor for methane's GWP is radiative efficiency which is much larger compared to that of the carbon dioxide. As a result, methane (CH_4) is calculated to have a GWP of 21–36 over 100 years [10, 11].

The concentration of methane in Earth's atmosphere has increased by about 150% since 1750. This increase accounts for 20% of the total radiative forcing from all of the long-lived and globally mixed greenhouse gases [12, 13]. As is clear the releasing methane into atmosphere should not be encouraged.

CHAPTER 2

LITERATURE REVIEW

Methane has been a major source for producing some important chemicals such as methanol and ammonia. Methane is much cleaner than petroleum and coal due to the higher ratio of hydrogen to carbon.

Currently, thermal processes are the most dominating ones for methane upgrading, and high rate of methane activation and high concentration of products have been achieved for industrial scale application. However, these thermal processes are highly energy-intense and require capital-intensive infrastructures. New methods are needed to overcome the problems of the thermal processes. For example, advanced catalysts have been designed to lower the energy consumption for directly or indirectly upgrading methane.

More interestingly, electrochemical approaches have been proposed to activate methane without the needs for high temperature and high pressure. Figure 2.1 shows a schematic chart for different available methods of methane upgrading. A brief description for each method is presented in following subsections.

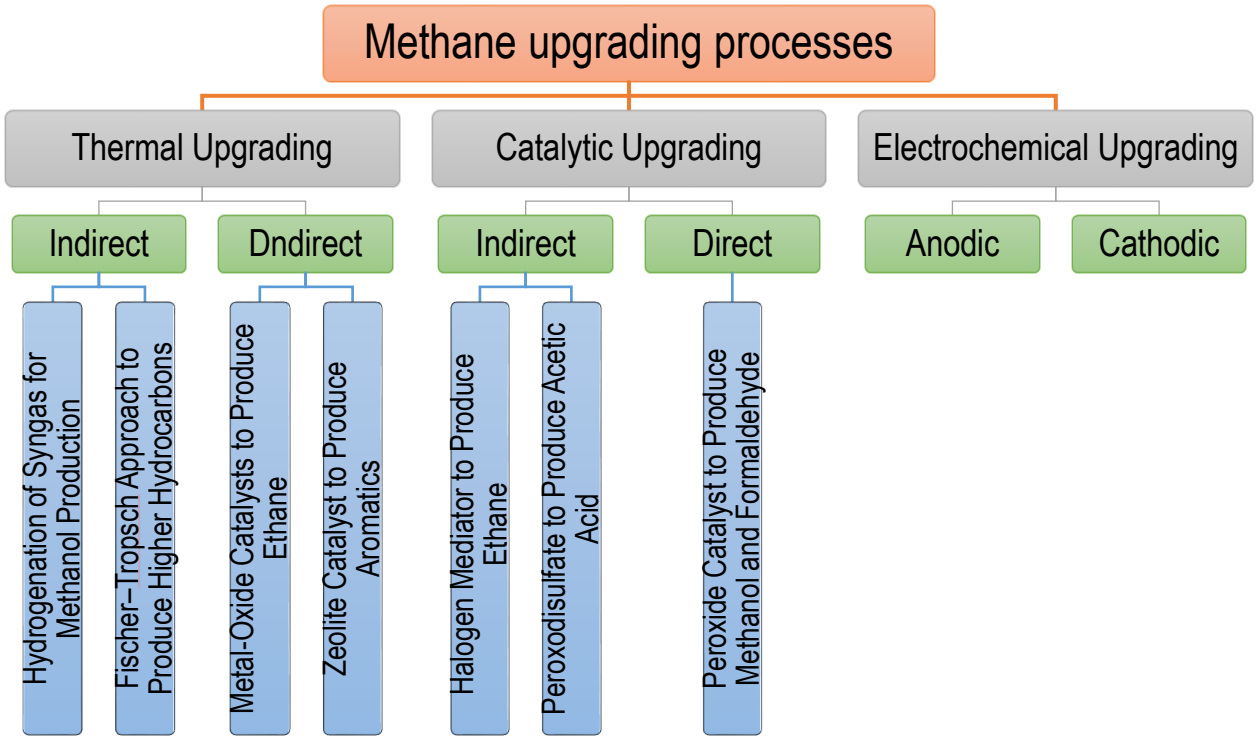

Figure 2-1. Flowchart for different methods of methane upgrading

2.1 Thermal Upgrading of Methane

The thermal upgrading approach includes the indirect thermal upgrading (via syngas) and the direct one.

2.1.1 Indirect Thermal Upgrading

Currently, the indirect thermal upgrading is the most mature method: an intermediate fuel gas (called syngas) is generated, followed by the synthesis of final products such as methanol and ammonia.

Syngas or synthesis gas is a fuel mixture that primarily consists of hydrogen, carbon monoxide, and carbon dioxide in some cases. Generally, syngas is generated by the following reactions with methane:

a) Steam reforming

$$CH_4 + H_2O \rightleftharpoons CO + 3H_2 \qquad (\Delta H° = 206 \text{ kJ/mol})$$

b) Carbon dioxide reforming

$$CH_4 + CO_2 \rightleftharpoons 2CO + 2H_2 \qquad (\Delta H° = 247 \text{ kJ/mol})$$

c) Partial oxidation

$$CH_4 + 0.5O_2 \rightleftharpoons CO + 2H_2 \qquad (\Delta H° = -35 \text{ kJ/mol})$$

The ratio of H_2/CO could be adjusted in the reformers utilizing the following reaction:

$$CO + H_2O \rightleftharpoons CO_2 + H_2 \qquad (\Delta H° = -41 \text{ kJ/mol})$$

Both steam reforming and carbon-dioxide reforming reactions are extremely energy-intensive. Such high energy demand is not only because of the strongly-endothermic reaction heat due to the high dissociation enthalpy of the C−H bonds (105 kcal/mol, highest among all alkanes) [14], but also because of the great reaction barrier due to the high kinetic activation energy (17.9 kcal/mol, highest among all alkanes as well) [15].

Given that steam reforming is the most mature process among the aforementioned syngas-generating processes, there are still severe safety concerns over implementing this method in industrial plants. The major concern is such that this process involves very high temperatures and pressure for pure oxygen and mixture of CH_4/O_2. Moreover, the large-scale production inevitably involves the handling and storing of larger amounts of highly pure oxygen and syngas, raising concerns over safety management. Some rare dramatic report such as explosion in Shell F-T plant in their oxygen purification site was reported as the consequences of not precisely following the safety regulations.

2.1.1.1 Hydrogenation of Syngas for Methanol Production

Once the syngas is generated, it can be used to product different products using their corresponding reactions. The thermal activation of C−H bonds in methane requires high temperature (typically, 700−1,000 °C) and the presence of metal-based heterogeneous catalyst. Generally, the chemical reaction for methanol formation from syngas could be expressed as hydrogenation of either CO or CO_2 [16].The following two reactions can be used to produce methanol from syngas:

$$CO + 2H_2 \rightleftharpoons CH_3OH \qquad \Delta H° = -90.55 \text{ kJ/mol}$$
$$CO_2 + 3H_2 \rightleftharpoons CH_3OH + H_2O \qquad \Delta H° = -49.34 \text{ kJ/mol}$$

A catalyst is required for the methanol formation. For instance, it has been shown that palladium supported on La_2O_3 [17] or promoted by SiO_2 [18, 19] can selectively and actively catalyze methanol formation in slurry reactors.

Furthermore, the produced methanol in such plants might be used for producing dimethyl ether (DME), which is an attractive alternative for diesel fuel application[20]. It might be worth mentioning that, other products such as ethylene and propylene could also be produced in large scale form methane, via methanol.

The energy efficiency of the steam reforming in industry is approximately 70%. Note that the recent breakthrough in catalyst can realize the one-step synthesis and also lower the temperature down to 180 °C [21-23]. Also, some metal or non-metal centered free radicals are able to activate methane at ambient temperature, but significant amount of energy is required to generate these ultra-high-energy radicals [24, 25].

2.1.1.2 Fischer–Tropsch Approach to Produce Higher Hydrocarbons

In addition to the hydrogenation of syngas to produce methanol, the syngas can be used to produce hydrocarbons and higher alcohols in industrial scales. Since 1926 Fischer and Tropsch

introduced a method of using syngas to produce gasoline over cobalt and iron as catalyst, many modifications have been made in different aspects over the original process. The syngas enters the reactor and in the presence of catalyst, liquid hydrocarbons of ordered composition can be produced [26]. Its main reactions could be summarized as:

$$(2n+1)H_2 + nCO \rightarrow C_nH_{(2n+2)} + nH_2O$$
$$2nH_2 + nCO \rightarrow C_nH_{2n} + nH_2O$$

Initially, the catalysts used in Fischer–Tropsch process were based on cobalt (Co) or iron (Fe). Adding copper (Cu) to cobalt or iron catalysts can help increase the reduction of deactivating alkali species on catalyst surface, while the addition of SiO_2 and Al_2O_3 helps increase structural support of the catalyst. It has also been shown that adding some manganese (Mn) can improve the selectivity control while adding ruthenium (Ru) improves the yield of waxes. By far, Ru is the most active catalyst and it can work at lowest temperature among other catalysts. Ru catalyst is able to produce the hydrocarbons with higher molecular weight in the cleaner mode [27].

As mentioned earlier, Fisher-Tropsch is dominating process in industrial scale as it can easily be modified for various products with high yields. The main downside is very high temperatures and pressures of operations which imposes huge energy consumption to this method.

2.1.2 Direct Thermal Upgrading

2.1.2.1 Metal-Oxide Catalysts to Produce Ethane

Instead of going through syngas as intermediate, methane can be thermally upgraded directly. In the direct thermal upgrading, methane is directly oxidized to from ethane at high temperatures but in moderate pressures. Ethane is often turned into ethylene as final product via dehydrogenation. Such direct thermal upgrading is also known as oxidative methane coupling (OCM). At temperatures of 500 to 800 °C with the help of a catalyst, one C−H bond of methane goes through hemolytic cleavage, forming one methyl radical. Subsequently, two methyl radicals

are coupled to produce one ethane molecule in gaseous phase[28]. The mainly used catalyst for this type of reaction is magnesium oxide (MnO_2). By controlling the low partial pressure of methane, the selectivity of the products is typically around 60%. The reactions involved in this direct thermal upgrading are as follows [29, 30].

$$2CH_4 \xrightarrow{2O^{2-}} 2CH_3\bullet$$
$$CH_3\bullet + CH_3\bullet \rightarrow C_2H_6$$

Since such direct thermal upgrading is a single integrated process for methane upgrading, we may expect a large decrease in operational cost, compared with the indirect thermal upgrading. In addition, the products (ethane or ethylene) of the direct thermal upgrading is often more valuable than those of the indirect thermal upgrading. By implementing more advanced catalysts such as SrO/La_2O_3 [31] and $Mn/Na_2WO_4/SiO_2$ [32, 33], researchers were able to increase the product selectivity to about 80% for C_2, but the conversion rate of methane is generally limited to 20%. One explanation for such a low conversion rate is that the exothermic reactions over the catalyst surface may cause temperature differences of about 150 °C to 300 °C on the catalyst surface compared to external temperature. These hot spots can reduce the yield of C_2 significantly. It seems the heat management for higher yields of C_2 is more important engineering problem than the catalyst design [34, 35].

To avoid using pure oxygen as an expensive feed in this reaction, a $NaMnO_4/MgO$ catalyst was used while separate pulses of methane and air was blown over the catalyst. The only limitation observed with this method was that the oxygen capacity was limited and as a result very large amounts of catalyst were required to be able to produce commercially reasonable amount of C_2 products [36].

The main drawback for the direct thermal upgrading is very high temperature and challenging control over the coupling reaction of methyl radicals, which leads to deeper oxidized

products. Compared with the indirect thermal upgrading, the products of the direct thermal upgrading are limited to C_2 species, and methanol or other important oxycarbon products cannot be obtained. [37, 38].

2.1.2.2 Zeolite Catalyst to Produce Aromatics

Another example of direct thermal upgrading is using zeolite as catalyst, and such method was developed to eliminate the need for oxygen. Utilizing Mo/H-ZSM-5 zeolite catalyst, benzene, toluene, or naphthalene can be produced [36, 39-41]. The proposed reaction for this mechanism is as follows:

$$3MoO_3 + CH_4 \rightleftharpoons CO + 2H_2O + 3MoO_2$$
$$4MoO_3 + CH_4 \rightleftharpoons CO_2 + 2H_2O + 4MoO_2$$

Followed by dehydrogenation of methane and formation of CH_3 and as a result recombination of it, in various form of hydrocarbons as shown below.

$$CH_4 + O_{(s)} \rightleftharpoons CH_3\bullet + OH_{(s)}$$
$$2OH_{(s)} \rightleftharpoons H_2O + O_{(s)}$$

$$2CH_3\bullet \rightleftharpoons C_2H_6$$
$$2CH_2\bullet\bullet \rightleftharpoons C_2H_4$$
$$C_2H_4 + CH_3\bullet \rightleftharpoons C_3H_7$$

This method still needs development in terms of low conversion rate of methane and high temperatures required for reaction. For instance, conversion rate at 700 and 750 °C is only 11% and 18%, respectively [42].

2.2 Catalytic Upgrading of Methane

To lower the high cost and hazards imposed by elevated temperatures and high pressures, non-thermal methods are introduced using some powerful catalysts to upgrade methane under

much milder conditions. Similarly to the thermal upgrading, there are two major categories for catalytic upgrading: direct catalytic upgrading and indirect one.

2.2.1 Indirect Catalytic Upgrading

2.2.1.1 Halogen Mediator to Produce Ethane

Using halogen (X_2, X = Cl or Br) as mediator, methane can be turned into some light olefins (typically, ethylene). In this method, methane first reacts with a suitable halogen such as chlorine (Cl_2), bromine (Br_2), or a mixture of them. Olefins are then generated through either condensation process or dehydrohalogenative coupling (DHHC) process. The reactions involved with halogen-mediated catalytic upgrading are shown as below, where X_2 is a suitable halogen.

$$2CH_4 + 2X_2 \rightarrow 2CH_3X + 2HX$$
$$2CH_3X \rightarrow C_2H_4 + 2HX$$
$$4HX + O_2 \rightarrow 2H_2O + 2X_2$$

The overall reaction of the whole processes: $2CH_4 + 2O_2 \rightarrow C_2H_4 + 2H_2O$

Compared with thermal upgrading, the catalytic upgrading require much lower temperatures: 80−220 °C. Another advantage of halogen-mediating approach is that methanol can be produced shown in Figure 2.2

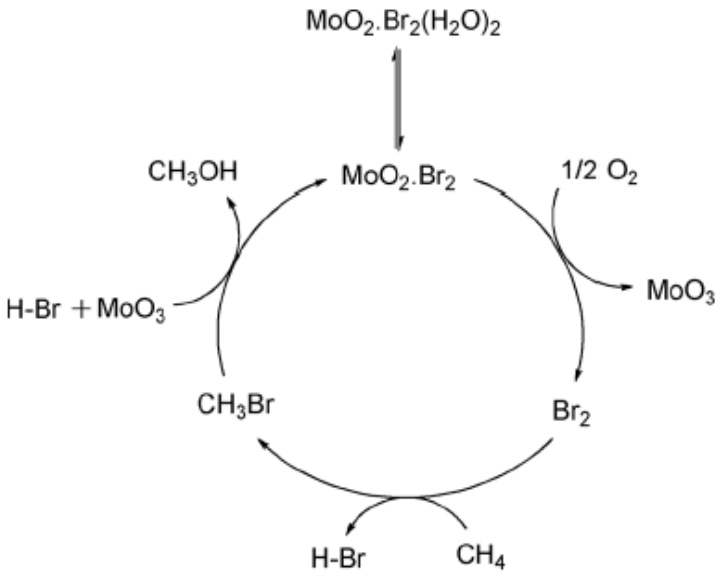

Figure 2-2. Methanol synthesis via the bromine-mediated indirect catalytic upgrading of methane catalyzed by Zn-MCM-48 supported dibromo-(dioxo)molybdenum(VI) [43]

The 14% conversion rate for halogenation step shall be improved to enable significant light olefins production. The limited conversion rate is the result of forming polyhalogenated alkanes that eventually lead to the formation of heavier and long-chained alkanes and aromatics [44-46]. Compared with Cl_2, using Br_2 have advantages of good control over halogenation path or easy handling of liquid products, , but the selectivity for methanol production is lowered In addition, reactivity of Br_2 is also lower than that of Cl_2 [47].

2.2.1.2 Peroxodisulfate Initiator to Produce Acetic Acid

Another example of indirect catalytic upgrading is using peroxodisulfate as radical initiator to catalytically upgrade methane to acetic acid. This is a less explored method, and $RhCl_3$ is used as the critical catalyst. Along with methane, carbon monoxide and oxygen are also introduced to participate into the process[48]. In current industry, acetic acid is generated through oxidative carbonylation of methanol in the presence of Rh catalyst. Well, the peroxodisulfate initiator provides a different radical-based mechanism. The yield of acetic acid is up to 20% at low

temperatures of about 80°C. Figure 2.3 shows a schematic cyclic production of acetic acid using oxidative carbonylation method [49].

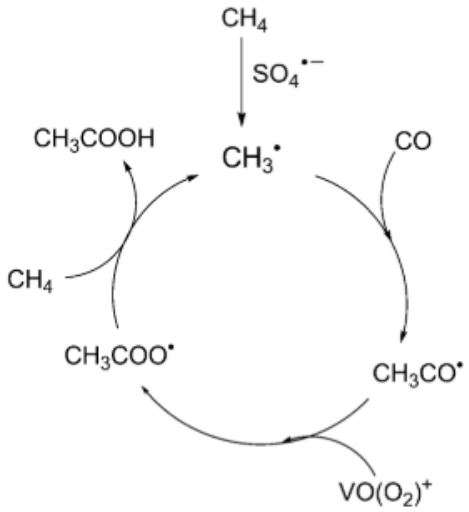

Figure 2-3. Radical-based carbonylation mechanism proposed by Kirillova et al. for the carbonylation of methane to acetic acid [50]

2.2.2 Direct Catalytic Upgrading

Compared with indirect catalytic upgrading where an intermediate species is involved, direct catalytic upgrading can directly catalyze methane to form products. Below are two examples of such direct catalytic upgrading of methane.

2.2.2.1 Peroxide Catalyst to Produce Methanol and Formaldehyde

The first example of direct catalytic upgrading of methane is using peroxide catalysts. One of the most interesting catalysts introduced for this process is $FePO_4$, and both H_2 and O_2 are needed as reagents, along with methane [50].

As seen in Figure 2.4 in more details, alternatively introducing hydrogen gas (H_2) and oxygen gas (O_2), peroxide groups are formed on the surface of $FePO_4$ catalyst, and the methane is introduced and reacted with peroxide groups forming methane as final product.

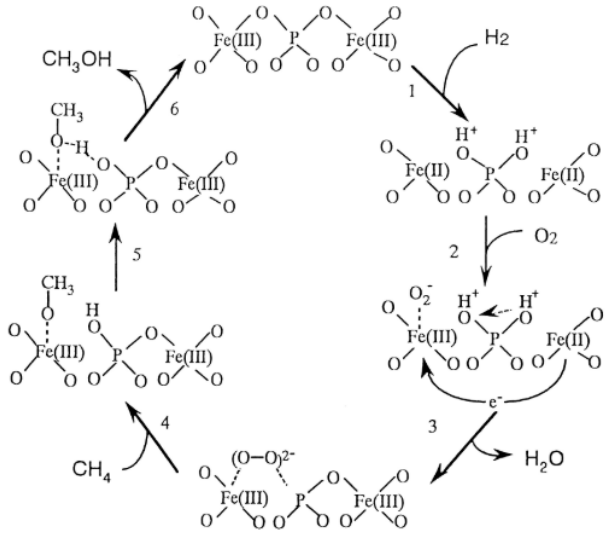

Figure 2-4. Proposed catalytic cycle for the conversion of CH_4 to CH_3OH

As shown in the Figure 2.4, both hydrogen and oxygen are needed, and hydrogen is a costly chemical. Such peroxide catalyst based direct catalytic upgrading suffers a very low conversion rate of methane (currently no more than 0.6%) [9]. By using bipyrimidyl platinum (II) complex in concentrated sulfuric acid at high temperatures of 220 °C, 90% of methane will react to sulfuric acid in catalytic manner. However, this will arise another issue of regeneration of concentrated acid in order to complete a cycle [22].

2.3 Electrochemical Upgrading of Methane

Electrochemical upgrading of methane is fundamentally more energy-efficient than thermal upgrading or catalytic upgrading. From electrochemical perspective, upgrading methane to methanol only requires a quite small amount of electrical energy input: 121 kJ/mol of Gibbs free energy, or 0.628 V of standard electrolytic voltage is theoretically needed to convert methane and water to methanol and hydrogen. General formulation for that could be expressed as:

$$CH_4 + H_2O \rightarrow CH_3OH + H_2 \qquad (\Delta rG° = +121 \text{ kJ/mol, or } E° = -0.628 \text{ V})$$

Depending on the design of electrochemical cell, the required electrical energy varies. Among many electrolytes of choices for electrochemical activation of methane, aqueous systems

are particularly interesting due to reliability and simplicity. Based on the role of working electrode, there are two major approaches to electrochemically activate methane: direct oxidation (or anodic oxidation) and indirect one (or cathodic oxidation).

2.3.1 Anodic Electrochemical Upgrading

The direct-oxidation approach is to directly oxidize methane on working electrode (anode) to form oxycarbon products such as methanol, formaldehyde, and formic acid in either aqueous or nonaqueous system. A schematic draft of such a device is shown in Figure 2.6.

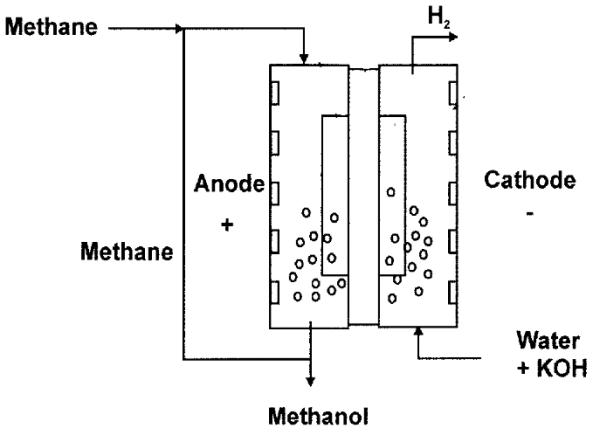

Figure 2-5. Electrochemical method to convert methane to methanol [52]

Different metals and their alloys have been tested as electrodes for this method including platinum, gold, palladium, ruthenium, and rhenium etc. Also surface treatments have been applied for some cases to investigate the molecular scale details of this reaction series. Almost in all cases, unfavorable deeply-oxidized product species were detected [53-60]. Electrochemical upgrading of methane has been carried out in low-temperature fuel cell with a polymer membrane as electrolyte, and high-surface area Pt and/or Pt–Ru as electrocatalysts. The products of this fuel cell were reported to vary with respect to materials used for electrode[55].

However, under the anodic conditions, the products or intermediates are kinetically more prone to further oxidation than the starting methane molecules. This phenomenon is called “over-

oxidation challenge" [14]. As a result, CO and CO_2 (both with deeper oxidation depth) are often the major products, instead of the desired oxycarbon products such as methanol, formaldehyde, or formic acid. For example, one of the best results showed that the carbon (atomic) efficiency towards methanol from methane reached 60% at 50 °C, using a PdAu/C as anode catalyst. At the same time, the conversion rate of methane was only 0.012% [61].

2.3.2 Cathodic Electrochemical Upgrading

The indirect electrochemical upgrading utilizes a powerful radical as the activating agent, and both hydroxyl radical (HO•) and superoxide (anion) radical (O_2•$^-$) have been introduced to react with methane. These radicals are typically generated form H_2O_2 which could be generated electrochemically from working electrode (cathode). This is the reason why this method is sometimes called as "cathodic activation". As early as 1990, Cook and Sammells reported the ground-breaking study on such indirect electrochemical upgrading for methane in aqueous system [62]. First, the working electrode reduces oxygen to selectively form hydrogen peroxide (H_2O_2). Methane molecules are then activated by HO• that are catalytically generated from hydrogen peroxide. As a result, CH_3• are formed to produce different hydrocarbons and oxycarbons such as methanol, formaldehyde, and formic acid.

One of the main advantages of indirect electrochemical upgrading over the direct one is the decoupling ability of the oxidizing agent production and methane activation reaction. The following reactions are involved in the generation of HO•:

$$O_2 + 2H^+ + 2e^- \rightarrow H_2O_2$$
$$H_2O_2 + Fe^{2+} + H^+ \rightarrow HO\bullet + Fe^{3+} + H_2O$$

Once the hydroxyl radicals are generated, the methyl radical can be created:

$$CH_4 + HO\bullet \rightarrow CH_3\bullet + H_2O$$

In that study, 0.1 M H_2SO_4 containing 0.005 M $FeSO_4$ was used as aqueous electrolyte, and cobalt phthalocyanine (CoPc) was used as cathodic catalyst. Among the activated methane, the 10% carbon atoms went to alcohols (CH_3OH, C_2H_5OH, and n-C_3H_7OH), 67% to HCHO, and ~25% to HCOOH, without the sign of CO or CO_2 in the product.

In another study by Frese in 1991, the alkaline aqueous systems were introduced and superoxide (anion) radical (O_2•$^-$) was the activating agent, and similar products were detected and almost 100% carbon efficiency was confirmed again [63]. Note that for both indirect electrochemical upgradings, the H_2O_2-generating working electrode is cathode, and thus an anode is required as counter electrode to complete the electrical circuit typically by either hydrogen oxidation reaction (requiring H_2) or oxygen evolution reaction.

In both cases, the H_2O_2 electrochemical production, HO• or O_2•$^-$ radical generation, methane activation, and product formation are heavily coupled at the same place, making the individual step unclear. The "over-activation dilemma" still holds here, as shown in Table 2, the C−H bonds of any oxycarbon products are more prone to further activation than those of methane molecules, because of the lowered dissociation enthalpy.

TABLE 2

THE C−H BOND DISSOCIATION ENTHALPIES (DH_{298}(C−H)) AND THE FORMATION ENTHALPIES ($\Delta_F H_{298}$) OF SPECIES/COMPOUNDS OF INTEREST (ALL DATA FROM [64] UNLESS OTHERWISE NOTED)

Group	**Compound of Interest**	***DH*$_{298}$(C−H)[a]** (kcal/mol)	**Δ_f*H*$_{298}$[b]** (kcal/mol)
Methane	CH_4	105.0	−17.9
C_1 radicals	CH_3•	110.4	35.1
	CH_2••	101.3	93.3
	CH•••	80.9	142.5
C_1 oxycarbons	**CH_3OH**	96.1	−49.0
	HCHO	88.1	−27.7
	HCOOH	96.0	−90.6
C_2 oxycarbons	CH_3OCH_3	93.3 [65]	−44.0
	H−$COOCH_3$	92.7 [66]	−80.6

[a] ***DH*$_{298}$(C−H)**: dissociation enthalpy at 298 K for C−H bond, 1 kcal/mol = 4.18 kJ/mol
[b] **Δ_f*H*$_{298}$**: formation enthalpy at 298 K in gas phase for the compound.

For example, the C−H's bond strength in CH_3OH, HCHO, and HCOOH is 96.1, 88.1, and 96.0 kcal/mol, respectively, of which are 8.5%−16% lower than that of methane (105.0 kcal/mol) [64]. One of the challenges in radical-enabled activation of methane is the explanation of why this reaction favors the oxycarbons as the majority of products, instead of carbon oxides such as CO or CO_2. Understanding this matter, would enable us to develop more advanced catalytic systems for methane conversion and tackle obstacles such as low concentration and selectivity.

2.4 Research Objective

The current study extends the indirect electrochemical upgrading of methane in search of the understanding of the unreconciled explanation of methane activation, and a decoupled electrochemical upgrading is designed in acidic aqueous system to specifically focus on the process of the methane activation. ,Specifically, we are proposing a unique process for methane upgrading at ambient temperature and pressure, based on the discovery of metal surface facilitation phenomenon which in fact is the key step for methane activation by HO• radicals. Base on this

discovery, we are enabled to decouple the oxidative agent production process and methane activation process and consequently engineer each of them separately. The decoupling ability will help us eliminate over-activation dilemma. With the established electrochemical system, two major parts of research have been conducted. In the first part, using metal surfaces as catalyst to facilitate the methane upgrading is proposed. As a result, the correlation between metal surface and methane activation will help us to understand the fundamentals of methane activation (both in terms of rate and product species). In the second part, the focus is laid on the decomposition of the generated compounds, as one of the most critical limiting problems for commercialization of this method.

CHAPTER 3

STUDY OF SOLUTION CONDITION

3.1 Objective

As explained earlier, hydroxyl radicals (HO•) are generated form reduction of hydrogen peroxide (H_2O_2) by utilizing a reductive agent in aqueous system. Choice of pH, selection of the reductive ligand and concentrations of hydrogen peroxide and reductive agent in solution are important. This chapter is to investigate and establish the optimal solution conditions for methane activation.

3.2 Methods and Devices

The proton Nuclear Magnetic Resonance (^{1}H NMR) spectroscopy is the major instrumental technique used to study solution conditions by monitoring products produced in reaction solution. The Varian Mercury VX Oxford NMR 300MHz is the spectrometer used in this study (available in the Chemistry Department at Wichita State University), shown in Figure 3.1.

By properly locking and shimming samples, the spectroscopy can be achieved, and by comparing the known concentration of solute in the solution, we are able to calculate the concentrations of all other proton-containing compounds presented in reaction solution. For more details and information on NMR spectroscopy and its operation procedure, please refer to the Appendix A.

Figure 3-1 NMR Varian Mercury VX 300 MHz in the Chemistry Department at Wichita State University

3.3 The pH Selection

In literature, the effect of pH on the generation and yield of hydroxyl radical from hydrogen peroxide has been widely investigated. The acidic environment is generally required generate hydroxyl radicals, and the typical pH range is from 1.2 to 7.4. Depending on the external supply of H_2O_2, the pH has different impacts on the generation of hydroxyl radicals. Without supplying H_2O_2 , increasing pH can enhance hydroxyl-radical production; while with supplying H_2O_2, increasing pH has no significant impact on the production of hydroxyl radicals [67].

The effect of pH was also studied for removal of organic substances from water. It was shown that the best production of OH• radicals was achieved at pH values between 2.5 and 4 [68-70]. In this study, the pH of 3 was chosen for generating hydroxyl radicals for methane activation.

3.4 Selection of Fenton's Reagent

In general, hydroxyl radicals are effectively formed via Fenton process, in Fe^{2+} is used to catalyze H_2O_2 to generate HO• radicals [71, 72]. Since the Fe^{2+} ions are eventually consumed in oxidative environment, utilizing UV irradiation to regenerate Fe^{2+} from Fe^{3+} has been suggested [73, 74]. It has been shown ligands with greater ratio of oxygen to carbon ratio usually possess higher photoreduction ability [75].

In this study, in order to eliminate the doubt over external sources of carbons in our system, both $FeCl_2$ and $FeSO_4$ could be the chosen as the Fenton's reagent, since they are free of any carbon atoms in their ligands. This will make the balance of carbon atoms accurate and straightforward.

On the other hand, chlorine can be strongly adsorbed on the surface of some transition metals (e.g., Pt and Ag), which causes "surface contamination" that could interfere with the methane upgrading [76, 77]. As such, $FeSO_4$ was chosen over $FeCl_2$ to serve as the Fenton's reagent in this study.

3.5 Concentrations of Hydrogen Peroxide and Ferrous Sulfate

The effect of the concentration of hydrogen peroxide on the generation of methyl radicals has been studied [78, 79]. In order to simply the reaction system, we only control the initial, yet sufficient, concentration of H_2O_2, since H_2O_2 is the only source of HO• radicals.

. The generation of HO• radicals from H_2O_2 is catalyzed by an agent. As explained in Section 3.2 earlier, $FeSO_4$ is used to serve for this need. The generally-accepted generation mechanism goes through the following step: $H_2O_2 + Fe^{2+} \rightarrow Fe^{3+} + HO\bullet + OH^-$. $FeSO_4$ agent offers one of the highest reaction kinetics among the chain reactions [80, 81].

In our preliminary studies, the concentration ratio of H_2O_2 to Fe^{2+} ion has been investigated, and the optimal concentration ratio was obtained. Higher D_2O_2 concentration (e.g., 50 mM) than the optimal one (5 mM) will lead to no product of methane activation, as shown in Figure 3.1 (a) and (b); and this is also true for the Fe^{2+} concentration, seen in Figure 3.2 (a) and (b). .

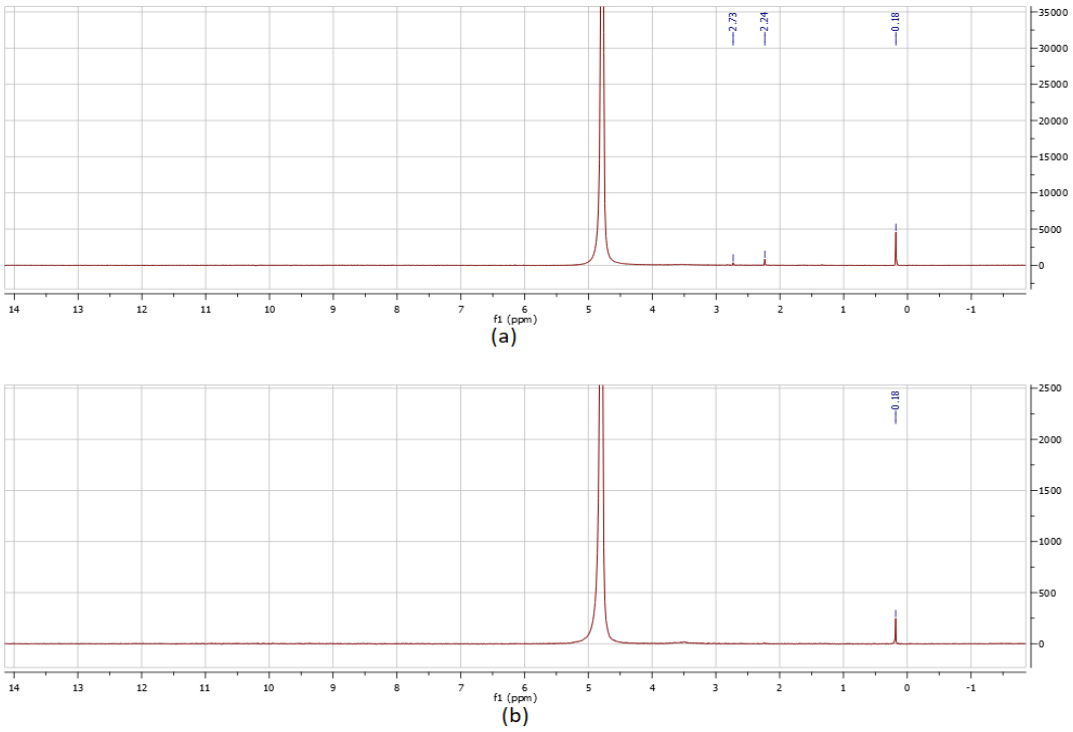

Figure 3-2. ^1H NMR spectra of reaction solution for methane activation with $[Fe^{2+}]$ = 0.025 mM and different D_2O_2 concentrations: (a) $[D_2O_2]$ = 5 mM and (b) $[D_2O_2]$ = 50 mM

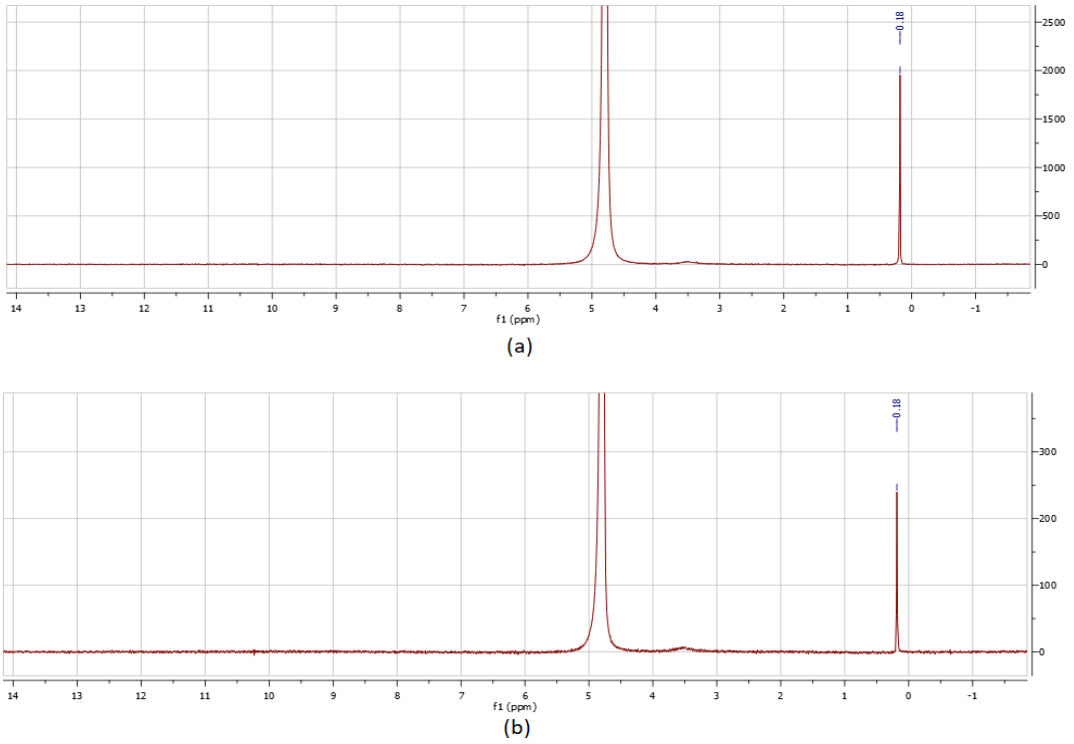

Figure 3-3. ^{1}H NMR spectra of reaction solution for methane activation with $[D_2O_2]$ = 5 mM and different Fe^{2+} concentrations: (a) $[Fe^{2+}]$ = 0.25 mM and (b) $[Fe^{2+}]$ = 0.025 mM

The ratio of $[H_2O_2]$ to $[Fe^{2+}]$ is rather important, and thus a range of $[H_2O_2]/[Fe^{2+}]$ ratios were examined: 1, 10, 50 and 200, with different combinations of concentrations. The $[H_2O_2]/[Fe^{2+}]$ ratio of 50 was chosen for the following studies due to the highest product concentration in the same time (2 hours). .

3.6 Chapter Summary

The optimal conditions for methane activation in our system are summarized as:

- pH is adjusted as 3 using H_2SO_4
- The initial concentration of Fe^{2+} is 0.25 mM, using $FeSO_4$
- The initial concentration of D_2O_2 is 12.5 mM.
- The initial molar ratio of D_2O_2 to Fe^{2+} is 50:1.

CHAPTER 4

METHANE UPGRADING

4.1 Discovery of Facilitating Effect of Metal Surfaces

It was reported that the methane upgrading occurred where the H_2O_2 generation was present [82]. In order to simply the reaction system and to better understand the methane activation, we separated the methane upgrading from HO• generation (from H_2O_2). Surprisingly, as will be discussed in detail in Section 4.3, methane activation was not observed using the optimal solution condition determined, and this is apparently contradicting with the general understanding. When we introduced a piece of metal foil in the reaction solution, different products of methane activation were obtained, and such a phenomenon has never been reported or recorded. It turns out that the metal surface plays a key role of "facilitation" that enables the methane activation.

4.2 Methodology

The facilitating effect of metal surfaces on the methane activation was studied by testing different metals. The selection of metals is based on the stability against the acidic environment: Platinum, palladium, copper, gold, rhenium, and silver. The relationship between the binding energy of metals with methane and the production rates of activation products was investigated to gain a deeper understanding.

4.2.1 Materials and Reaction Conditions

High-purity D_2O (99.9%) and $FeSO_4$ (99.0%) were form Sigma-Aldrich. The solution of D_2O_2 in D_2O with 35 wt. % was from Icon Isotopes; and sulfuric acid (98%) was supplied by Fisher-Scientific Company. Very pure methane gas (99.999%) was supplied by Cal Gas Direct Inc. Platinum, copper, gold, rhenium, and silver metal foils were obtained from Alfa, and they have the same foil size of 1 inch square and the same thickness of 25 μm.

4.2.2 Testing Method of Methane Upgrading

For each test, both D_2O_2 and $FeSO_4$, are introduced in 12 mL of D_2O solvent. The pH is then accurately set as 3 by adding H_2SO_4. The initial concentration of Fe^{2+} is 0.25 mM, and the initial molar ratio of D_2O_2 to Fe^{2+} is 50:1 (the D_2O_2 concentration: 12.5 mM). The Figure 4.1 shows

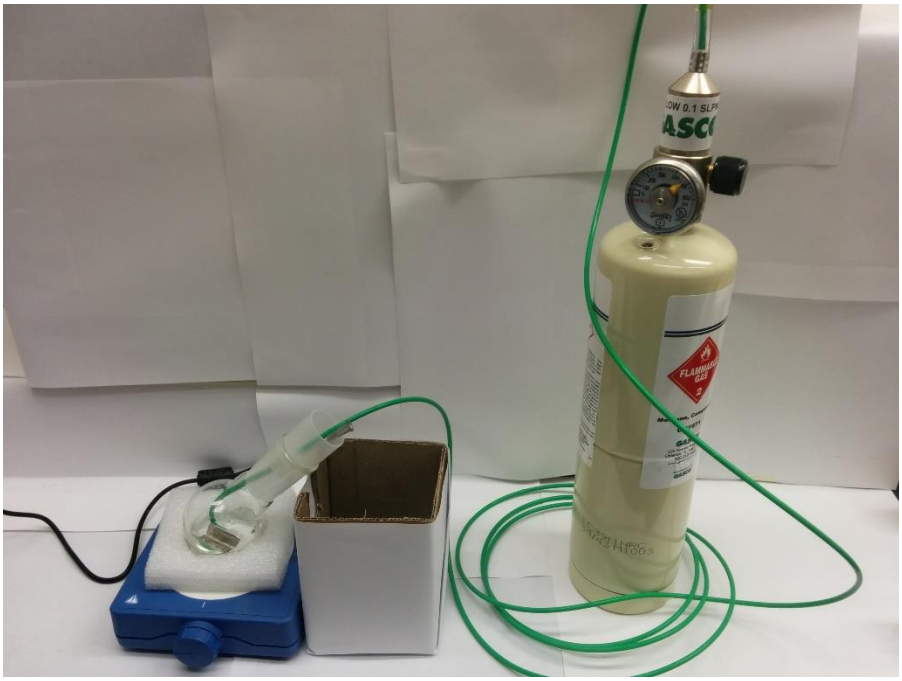

Figure 4-1 Photograph of experimental setup for methane activation reaction

the methane gas was introduced to the solution using Teflon tubing at a constant flow rate of 100 mL/min. A thin syringe needle was used to serve as the vent to discharge unused methane and gas products if any. Chances of external contaminations from atmosphere are minimized by tight sealing using a silicon rubber stopper.

The whole solution was held in a 50−mL round glass flask with constant magnetic stirring. Before introducing methane gas, the reaction system was stirred for ~10 min to generate HO•.

After a certain reaction time, a small amount of reaction solution was sampled for NMR testing. For each ^1H NMR sample, 0.7 mL of the reaction solution was inserted into NMR tube. The ^1H NMR spectroscopy was obtained with a number of 256 scans for every sample.

4.3 Facilitating Effect of Metal Surfaces on Methane Upgrading

4.3.1 The Absence of Metal Surface

The experiment was conducted in a 12-hour duration, and ^{1}H NMR results are shown in Figure 4.2.

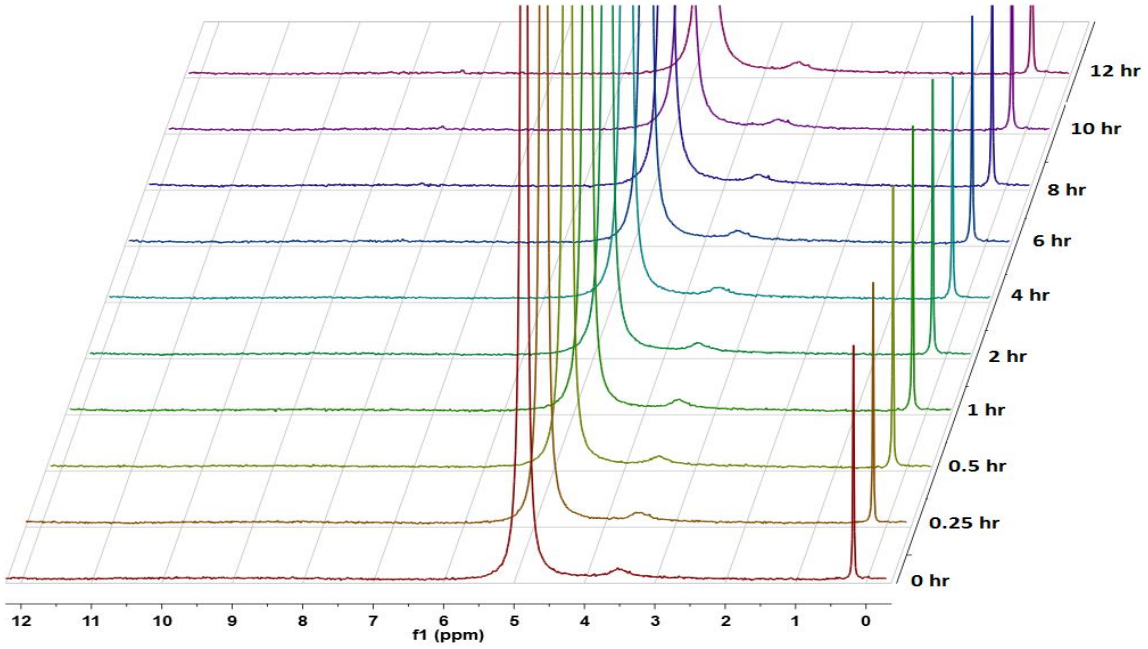

Figure 4-2. ^{1}H NMR spectra of reaction solution for methane activation without any metal surfaces

On each NMR spectrum, there are two sharp peaks: 4.76 ppm as water solvent and 0.18 ppm as the dissolved methane. Note that, a wide peak around 3.6 ppm was confirmed to be a signal noise caused by the long-used NMR spectrometer. Clearly, over 12 hours of reaction duration, no product was observed of methane activation.

4.3.2 Platinum

One of the most common metals used as a catalyst in different reactions is Platinum. In this time, a platinum foil (1 inch square in size and 25 μm in thickness) was place in the reaction solution and all other conditions are kept the same. The Figure 4.3 shows the NMR results when

Pt foil was used in the solution. New products emerged in solution and growing along with time: 3.36 ppm which is from C<u>H</u>$_3$OH, 3.87 ppm from HCOOC<u>H</u>$_3$, and 8.25 ppm from <u>H</u>COOC<u>H</u>$_3$ and/or <u>H</u>COOH. Note that, we have already verified their identifications by matching those pure substances in ^{1}H NMR. The methane activation is so fast in the present of Pt foil that we are able to detect the activation products in even 5 mins (i.e., 0 hour in Figure 4.3).

Compared with the case in the absence of metal, the presence of a simple platinum foil makes a huge difference for the methane activation under exactly the same test conditions. The most reasonable explanation is that the metal surface serves as a catalyst or a mediator to effectively and critically facilitate the methane activation.

The increasing trend of new peaks for reaction products becomes complicated after a couple of hours, which indicates the product evolution and/or decomposition.

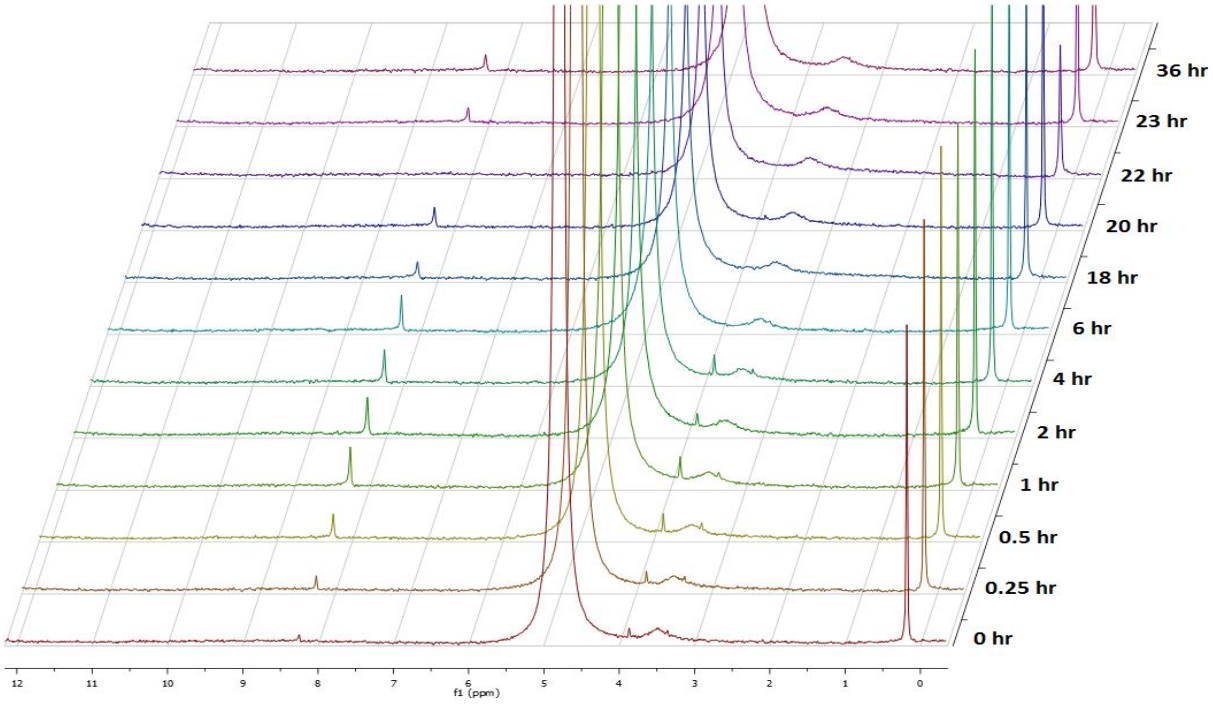

Figure 4-3. ^{1}H NMR spectra of reaction solution for methane activation in the presence of a Pt metal foil

To quantitatively analyze the data form ^{1}H NMR spectroscopy, the peaks were integrated for each sample. Methane peak at 0.18 ppm is normalized at the value of 4.00 as it represents CH_4 with four H atoms. The integration results are as presented in Figure 4.4 (a) to (l).

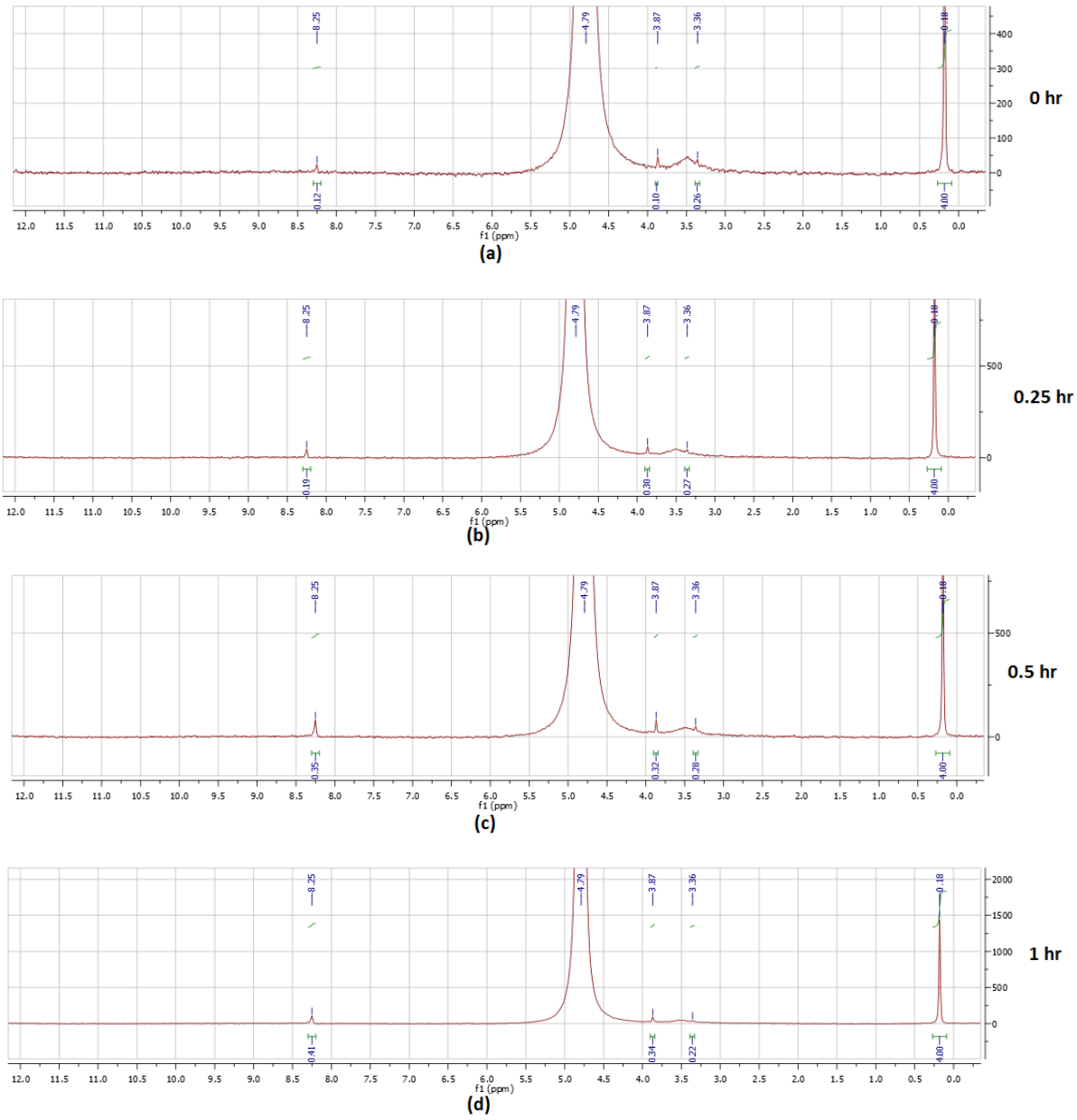

Figure 4-4. Integrated area for observed peaks of methane activation in the presence of platinum sheet

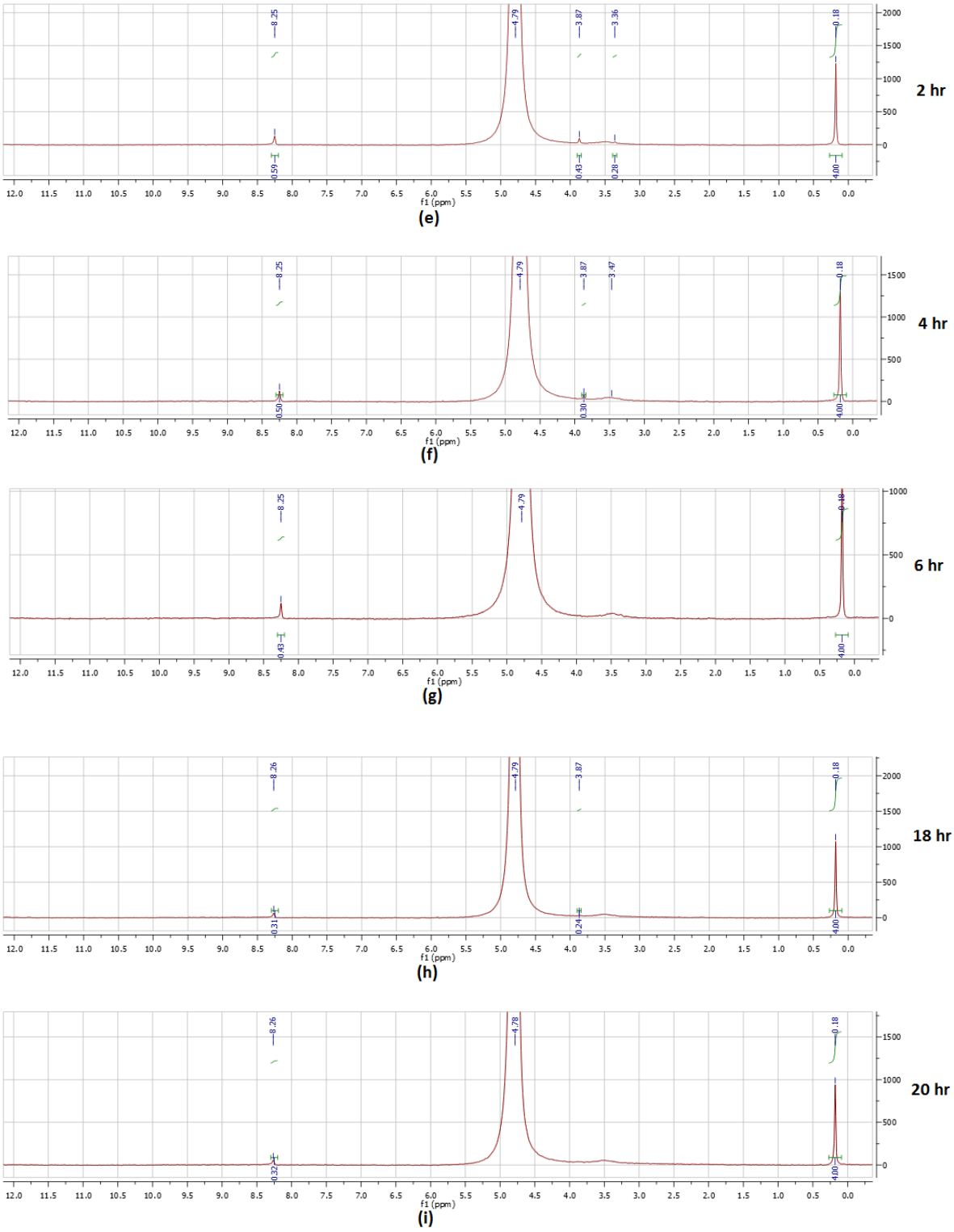

Figure 4 4. (continued)

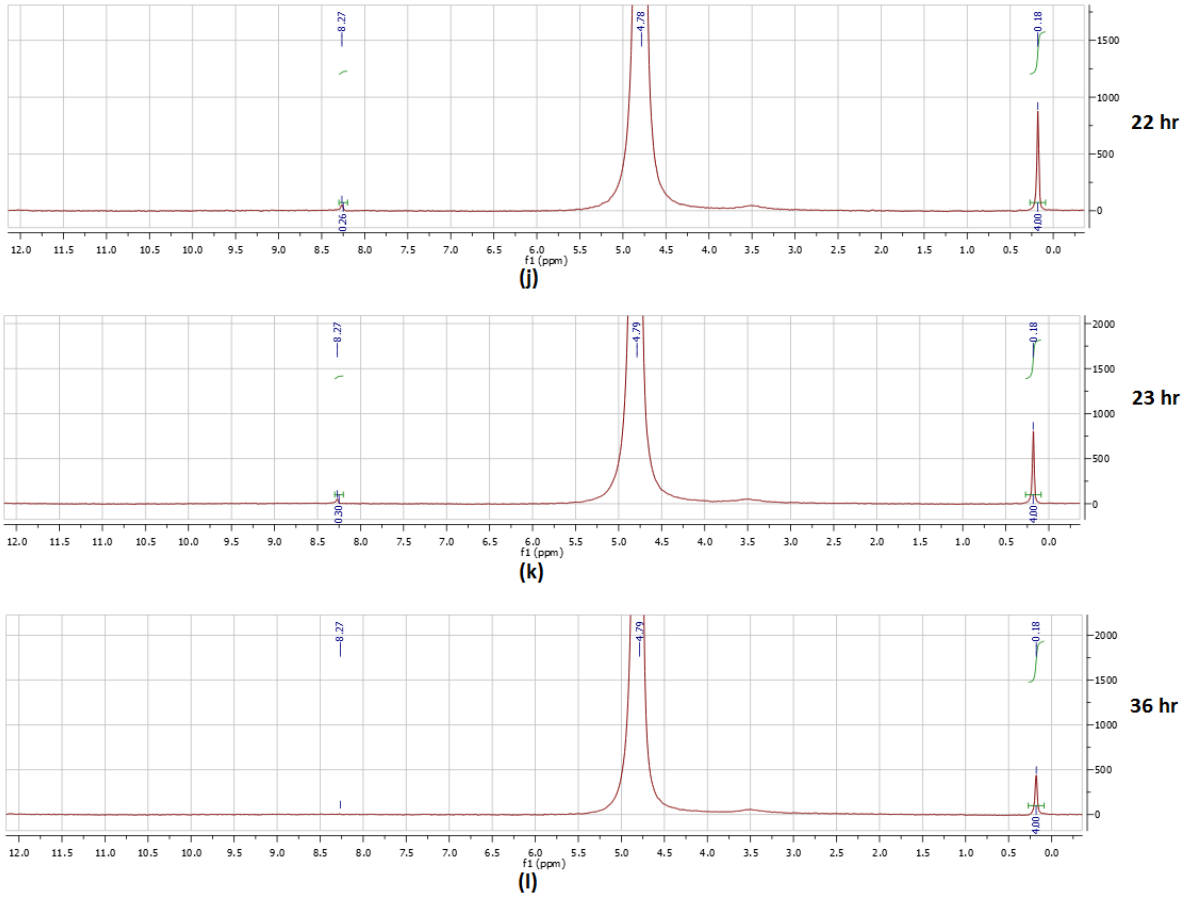

Figure 4 4. (continued)

The solubility of methane in water is 1.44 mM at 25 °C under 1 atm. and thus by assigning the integrated area for methane peak as 1.44 mM, we can calculate the concentrations of other emerging products. The peaks in ^{1}H NMR spectra represent the concentrations of protons in a particular molecule. For instance, the peak at 0.18 ppm represents four hydrogen atoms available in methane. The peak at 3.36 ppm represents three protons of methyl formate, while 8.25 represents the single proton from both methyl formate and formic acid. The concentration of formic acid can be obtained by deducting the contribution on the peak 8.25 ppm from methyl formate. The data for different peaks integrated area along with reaction time are summarized in Table 3.

TABLE 3

PEAK INTEGRALS IN THE 1H NMR SPECTRA FOR THE CASE OF PLATINUM (Pt)

Time (hr.)	Methanol (3.36 ppm)	Methyl formate (3.87 ppm)	Methyl formate (8.25 ppm)	Formic acid (8.25 ppm)
0	0.00	0.00	0.00	0.00
0.25	0.26	0.10	0.03	0.09
0.5	0.27	0.30	0.10	0.09
1	0.28	0.32	0.11	0.24
2	0.22	0.34	0.11	0.30
4	0.28	0.43	0.14	0.45
6	0.00	0.30	0.10	0.40
18	0.00	0.24	0.08	0.23
20	0.00	0.00	0.00	0.32
22	0.00	0.00	0.00	0.26
23	0.00	0.00	0.00	0.30
36	0.00	0.00	0.00	0.00
Methane peak at 0.18 ppm is considered the standard peak with a normalized value of 4.00				

The area integral of those NMR peaks are used to calculate the concentration of each compound As the methane is constantly supplied to the system, its concentration is assumed to be constant and equal to 1.44 mM. Since we assigned normalized value of 4.00 for methane's integrated peak, each unit of integrated area will represent 1.44 mM of concentration. As such, the following equation can be used for calculating the concentration for other products:

$$[PR] = (A_{PR}/N) \times [CH_4]$$

In the equation above, [PR] is the concentration of a product, and A_{PR} is the integrated area for its peak, and N is the number of protons represented in its chemical formula, and $[CH_4]$ is the concentration of methane which is equal to 1.44 mM. Specifically, for each of the products we have:

$[CH_3OH] = (A_{3.36\ ppm}/3) \times 1.44\ mM$

$[HCOOCH_3] = (A_{3.87\ ppm}/3) \times 1.44\ mM$

$[HCOOH] = (A_{8.25\ ppm}/1) \times 1.44\ mM$

$A_{3.36\ ppm}$, $A_{3.87\ ppm}$, and $A_{8.25\ ppm}$ stand for the area integrals of the peaks at 3.36 ppm, 3.87 ppm, and 8.25 ppm, respectively. Table 4 shows the calculated concentrations based on the above method.

TABLE 4

CALCULATED CONCENTRATIONS OF ACTIVATION PRODUCTS IN THE CASE OF PLATINUM (Pt)

Time (hr.)	$[CH_3OH]$ (mM)	$[HCOOCH_3]$ (mM)	[HCOOH] (mM)
0	0	0	0
0.25	0.125	0.048	0.125
0.5	0.130	0.144	0.130
1	0.135	0.154	0.350
2	0.106	0.163	0.427
4	0.134	0.206	0.643
6	0	0.144	0.576
18	0	0.115	0.331
20	0	0	0.461
22	0	0	0.374
23	0	0	0.432
36	0	0	0

CH_4 concentration in solution is considered a constant of 1.44 mM for calculating other concentrations.

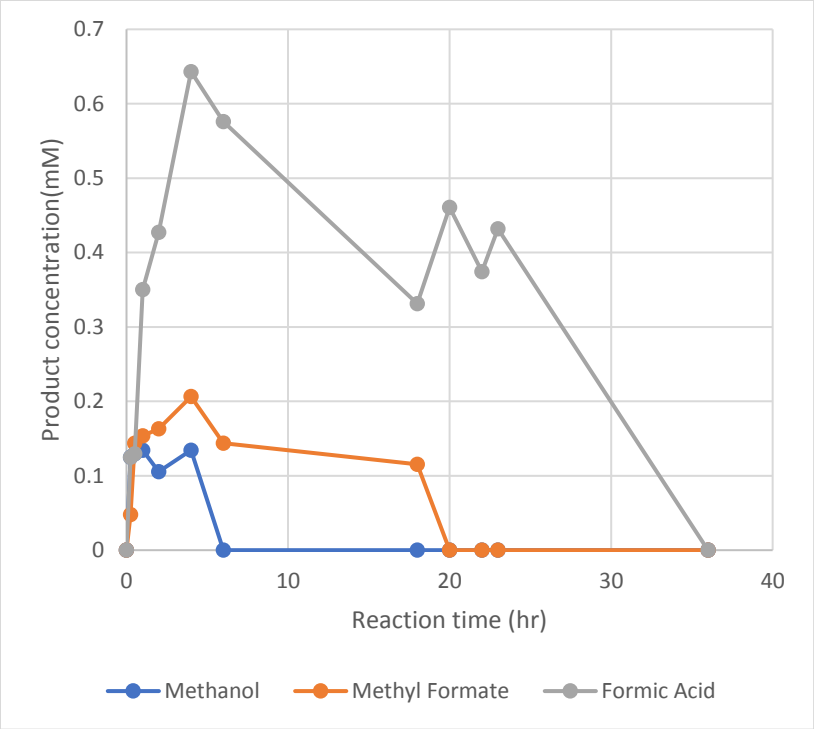

Figure 4-5. Concentration profiles of three oxycarbon products from methane activation along with reaction time in the presence of Pt

The Figure 4.5 graphically depicts the concentration profiles using the concentration date obtained from Table 4. For all three activation products, the concentration quickly increase, reaches a maximum value around 5 hours, and then decreases to zero eventually. The maximum concentrations 0.643 mM, 0.206 mM, and 0.135 mM for formic acid, methyl formate, and methanol.

The facilitating effect of the Pt surface is very obvious, and such facilitation is understandable: the adsorption of CH_4/CH_3• on metal surface must have drastically lowered the activation energy of methane reacting with HO•. And, this facilitation of metal surface also helps explain why the products with lower C−H bond strengths can survive in the same aggressive HO•-containing environment: The adsorption energies of the products on the same metal should be different from that of CH_4/CH_3•, and the adsorption of CH_4/CH_3• is more favored on the metal surface than that of the products under the test conditions.

The decomposition of the products will be investigated for better understanding in the next Chapter.

4.3.3 Palladium

From the same periodic group of platinum, palladium was also tested as well, with all other test conditions unchanged. ^{1}H NMR spectroscopy results along with reaction time are presented in Figure 4.6. Similar to the case of Pt, that same three product peaks are emerging in the presence of palladium.

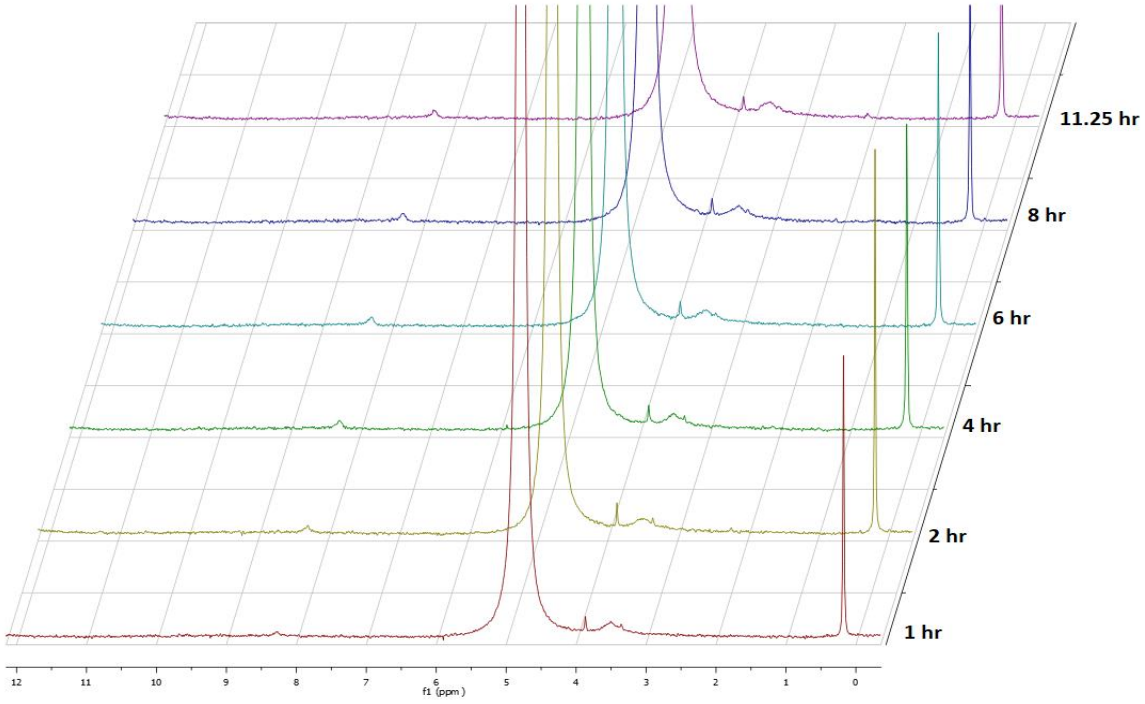

Figure 4-6. ^{1}H NMR spectra of reaction solution for methane activation with the presence of a Pd metal foil

Using the same quantitative method presented in section 4.3.2, we calculated the concentrations of the tree products of methane upgrading in the presence of palladium. Table 5, presents the concentration results of methanol, methyl formate, and formic acid in reaction solution. Figure.4.7 shows the concentration profiles of the three products along with reaction time.

TABLE 5

CALCULATED CONCENTRATIONS OF ACTIVATION PRODUCTSIN THE CASE OF PALLADIUM (Pd)

Time (hr.)	[CH_3OH] (mM)	[$HCOOCH_3$] (mM)	[HCOOH] (mM)
0	0	0	0
1	0.240	0.226	0.077
2	0.206	0.235	0.096
4	0.187	0.230	0.202
6	0.139	0.259	0.202
8	0.250	0.293	0.269
11.25	0	0.288	0.230
CH_4 concentration in solution is considered a constant of 1.44 mM for calculating other concentrations			

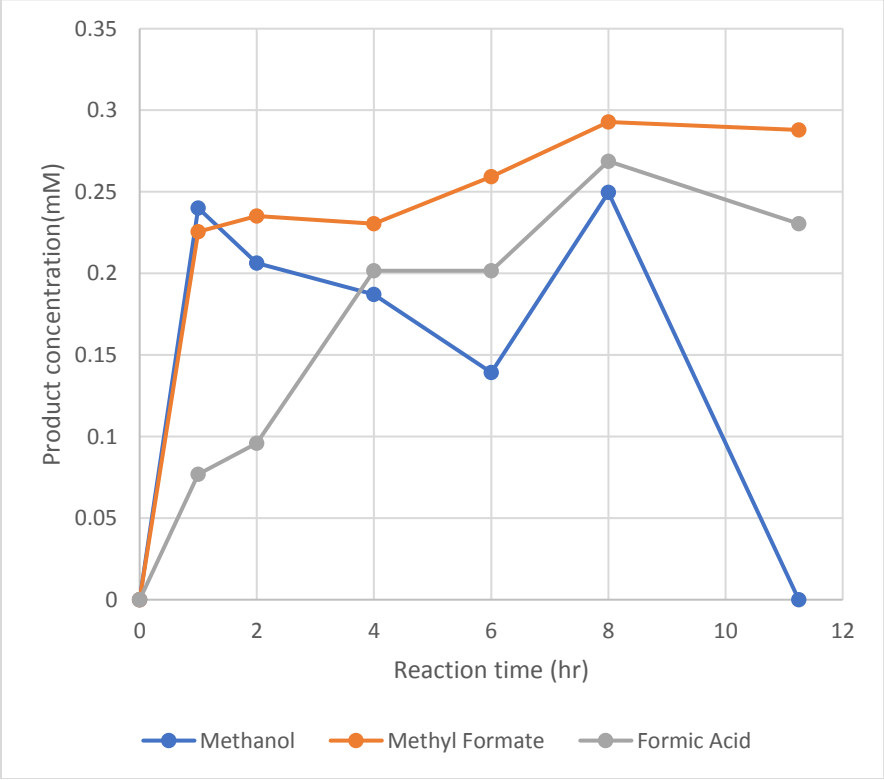

Figure 4-7. Concentration profiles of the three oxycarbon products from methane activation along with reaction time in the presence of Pd

As shown in the Figure 4.7, the concentrations of both methyl formate and formic acid initially increased, reached their peak concentrations at the reaction of 8 hours, and then decreased. The concentration of methanol is a bit complicated, and still it reached the peak value at the same reaction time of 8 hours.

The maximum concentrations observed are 0.250, mM, 0.293 mM, and 0.269 mM for methanol, methyl formate, and formic acid, respectively. Compared with the case of Pt, the production rates of using Pd surface are relatively slower, as evidenced by the less peak concentration and/or longer reaction time to reach the peak. This activation results again confirm the facilitating effect from a metal surface. Again, the decomposition of activation products is studied in the next Chapter.

4.3.4 Copper

As a stable metal from the neighboring periodic group of Pt and Pd, copper was used as the third metal for facilitating the methane activation in our system. ^{1}H NMR spectroscopy results along with reaction time are presented in Figure 4.8. Different from Pt and Pd, only one activation product, methyl formate (3.87 ppm), was observed in the case of Cu.. Using the same quantitative method presented in section 4.3.2 we calculated the concentrations of produced methyl formate for each reaction time in the case of Cu. Table 6, presents the calculated concentrations of methyl formate in reaction solution. Figure 4.9 shows the concentration profile of methyl formate along with reaction time in the presence of copper foil.

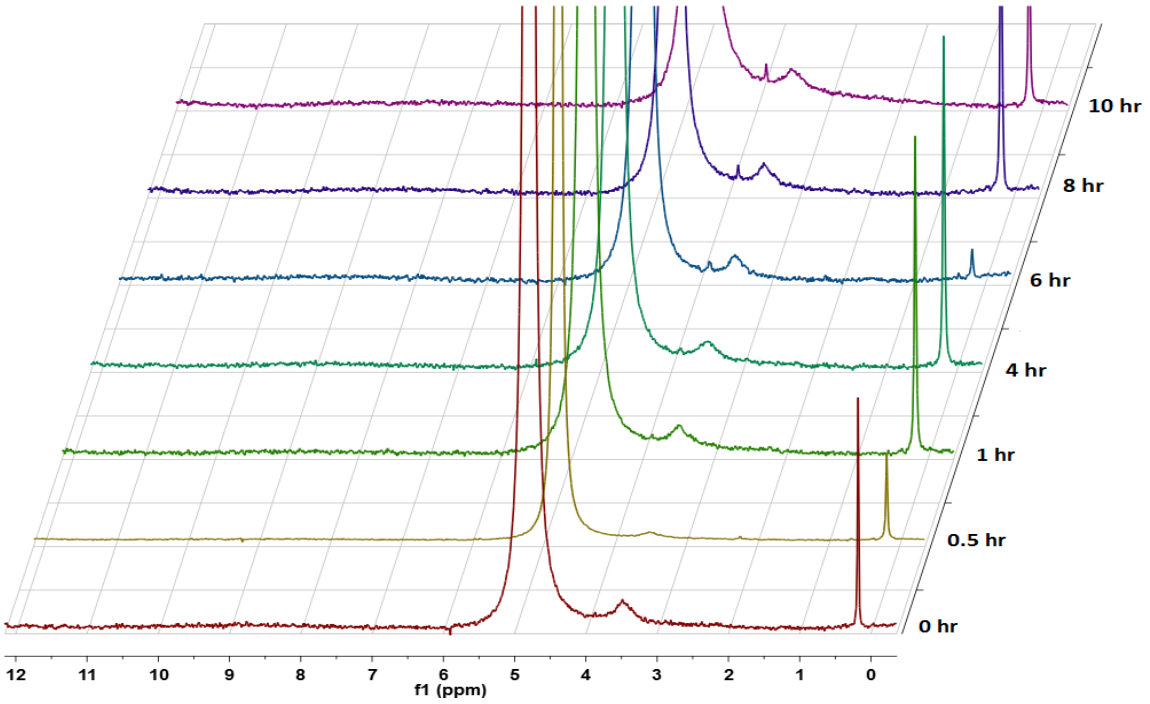

Figure 4-8. ^{1}H NMR spectra of reaction solution for methane activation with the presence of a Cu metal foil

TABLE 6

CALCULATED CONCENTRATIONS OF ACTIVATION PRODUCTSIN THE CASE OF COPPER (Cu)

Time (hr.)	$[CH_3OH]$ (mM)	$[HCOOCH_3]$ (mM)	[HCOOH] (mM)
0	0	0	0
0.5	0	0	0
1	0	0	0
4	0	0.134	0
6	0	1.253	0
8	0	0.154	0
10	0	0.437	0
11.75	0	0.149	0
CH_4 concentration in solution is considered a constant of 1.44 mM for calculating other concentrations			

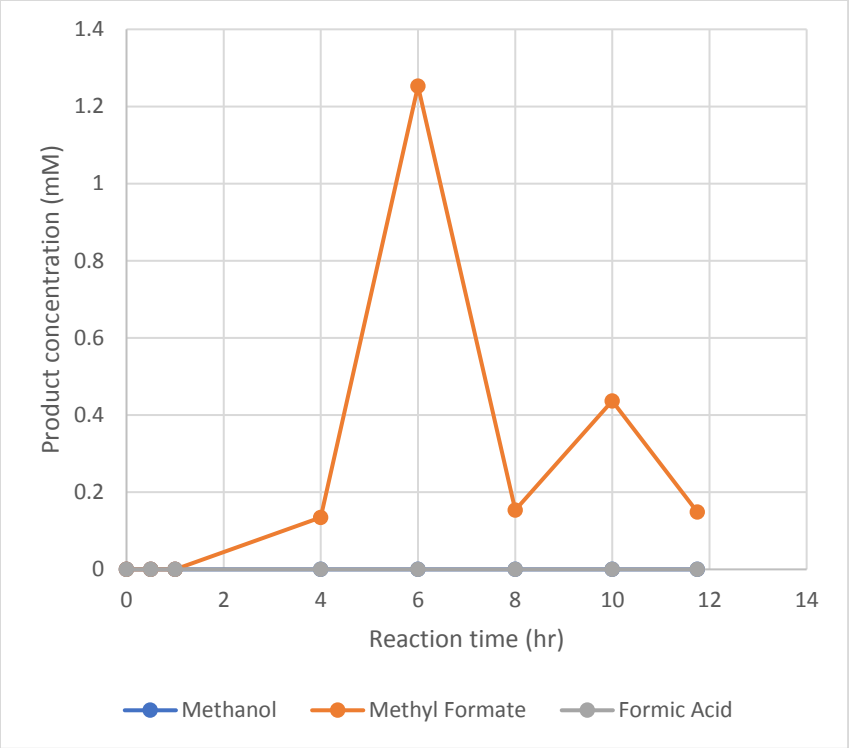

Figure 4-9. Concentration profiles of oxycarbon products from methane activation along with reaction time in the presence of Cu

From Figure 4.9, the concentration of methyl formate initially increased, reached the peak value, and then decreased eventually. The maximum value of 1.25 mM is obtained and then the same decomposition phenomenon appears for copper as well. Although only one activation product was observed, the results obtained here also confirm the facilitating effect of metal surface.

4.3.5 Gold

From the same periodic group of Cu, Au was studied for facilitating the methane activation as well. ^{1}H NMR spectroscopy results along with reaction time for 24 hours of reaction time are presented in Figure 4.10. The Au behaves much like Pt and Pd in terms of forming three activation products.

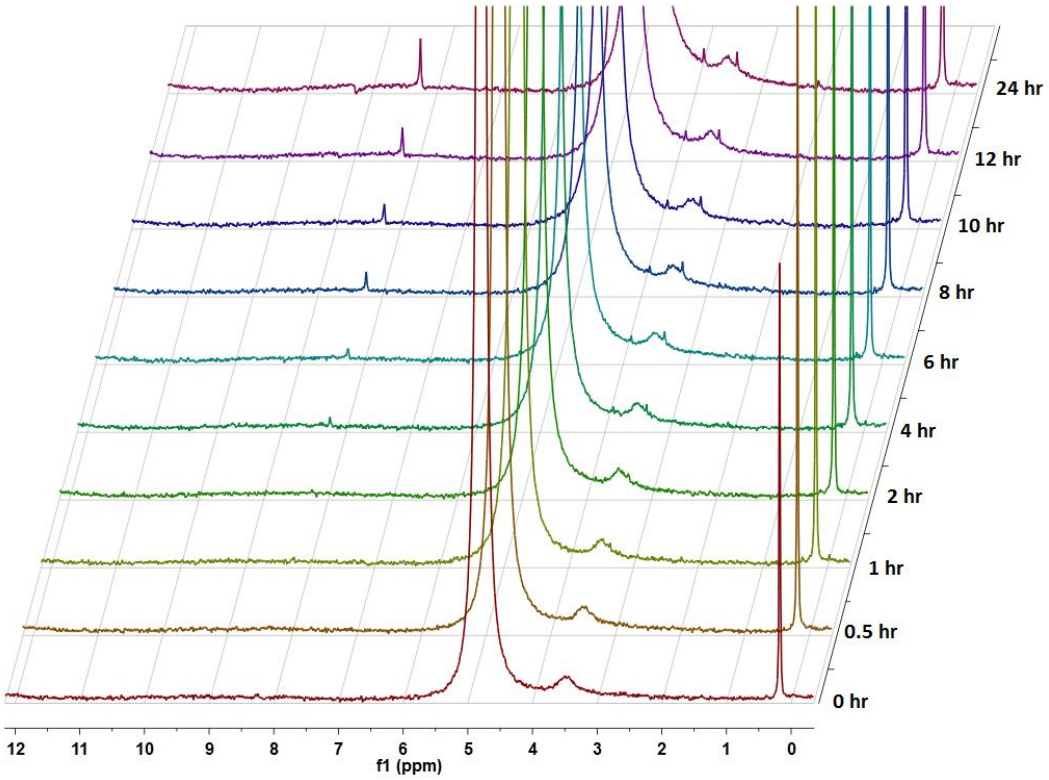

Figure 4-10. ^{1}H NMR spectra of reaction solution for methane activation with the presence of an Au metal foil

By using the same quantitative method presented in section 4.3.2 we calculated the concentrations of methanol, methyl formate, and formic acid in reaction solution in presence of gold. Table 7, presents the calculated concentrations of methanol, methyl formate and formic acid and Figure 4.11 shows concentration profiles of three activation products.

TABLE 7

CALCULATED CONCENTRATIONS OF ACTIVATION PRODUCTS IN THE CASE OF GOLD (Au)

Time (hr.)	$[CH_3OH]$ (mM)	$[HCOOCH_3]$ (mM)	[HCOOH] (mM)
0	0	0	0
4	0.120	0.115	0
6	0.154	0.130	0.014
8	0.173	0.168	0.106
10	0.139	0.130	0.101
12	0.144	0.149	0.211
24	0.187	0.226	0.379
CH_4 concentration in solution is considered a constant of 1.44 mM for calculating other concentrations			

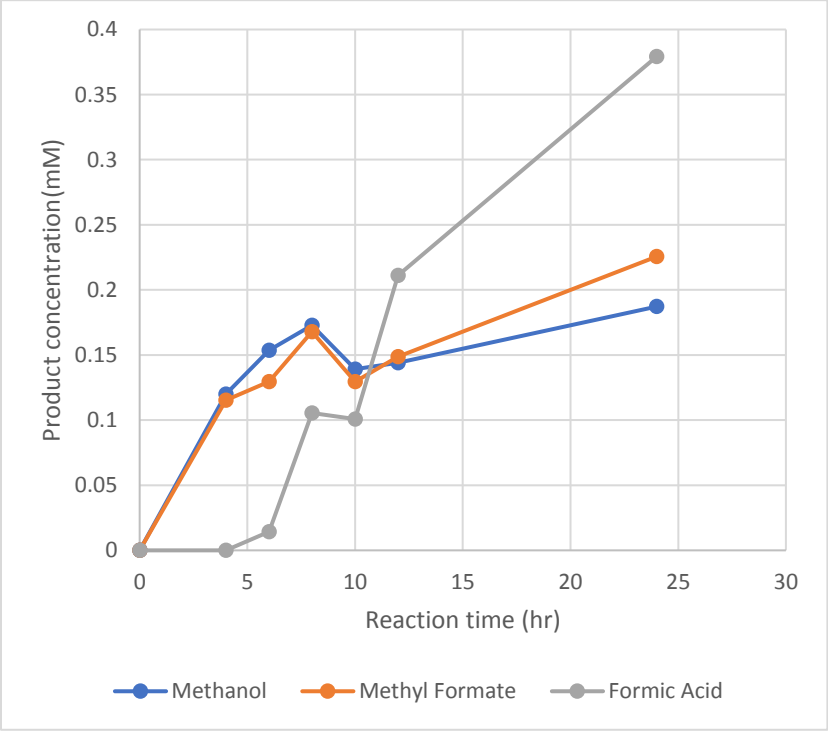

Figure 4-11. Concentration profiles of three oxycarbon products from methane activation along with reaction time in the presence of Au

Compared with Pt and Pd, the methane activation in the case of gold is relatively slow. In addition, the product concentrations are also low. For instance, the maximum concentration of formic acid reached only 0.37 mM after 24 hours.

The small Au foil (1 inch square) was used, and the activation rates are so low that in 24 hours the concentrations of none of three activation products showed the peak value. A big Au gauze (50 cm × 50 cm) was used, and concentrations of all three activation products reached peak values, and these results are presented in Appendix B.

4.3.6 Rhenium

Rhenium was also tested in our study, due to its stability in acidic environment. ^{1}H NMR spectroscopy results along with reaction time are presented in Figure 4.12. Same peaks at 3.36, 3.87 and 8.25 ppm are emerging in the presence of rhenium as well.

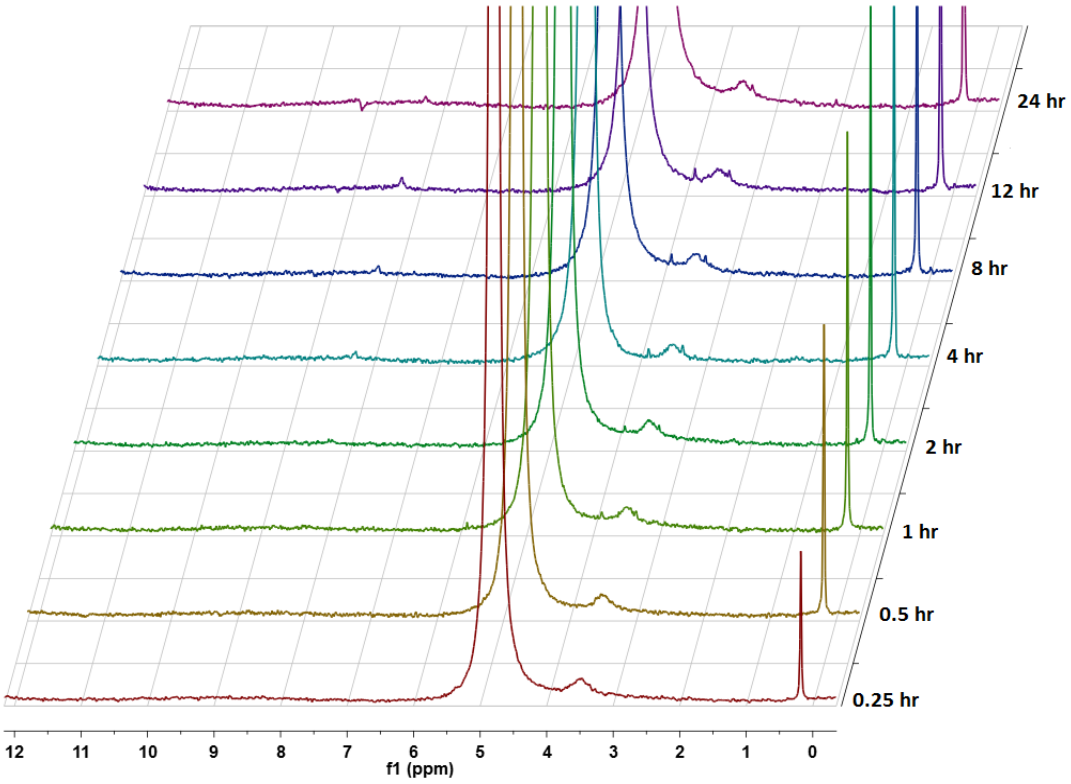

Figure 4-12. ^{1}H NMR spectra of reaction solution for methane activation with the presence of a Re metal foil

Using the same quantitative method presented in section 4.3.2 we calculated the concentrations of different products regarding to reaction time for methane upgrading. Table 8, presents the calculated concentrations of methanol, methyl formate and formic acid in reaction solution, and the Figure 4.13 shows the concentration profiles of activation products along with reaction time.

TABLE 8

CALCULATED CONCENTRATIONS OF ACTIVATION PRODUCTS IN THE CASE OF RHENIUM (Re)

Time (hr.)	$[CH_3OH]$ (mM)	$[HCOOCH_3]$ (mM)	[HCOOH] (mM)
0	0	0	0
1.25	0	0.139	0
2	0.221	0.187	0
4	0.115	0.062	0.154
8	0.269	0.331	0
10.5	0.182	0.163	0.197
24	0.139	0	0.216
CH_4 concentration in solution is considered a constant of 1.44 mM for calculating other concentrations			

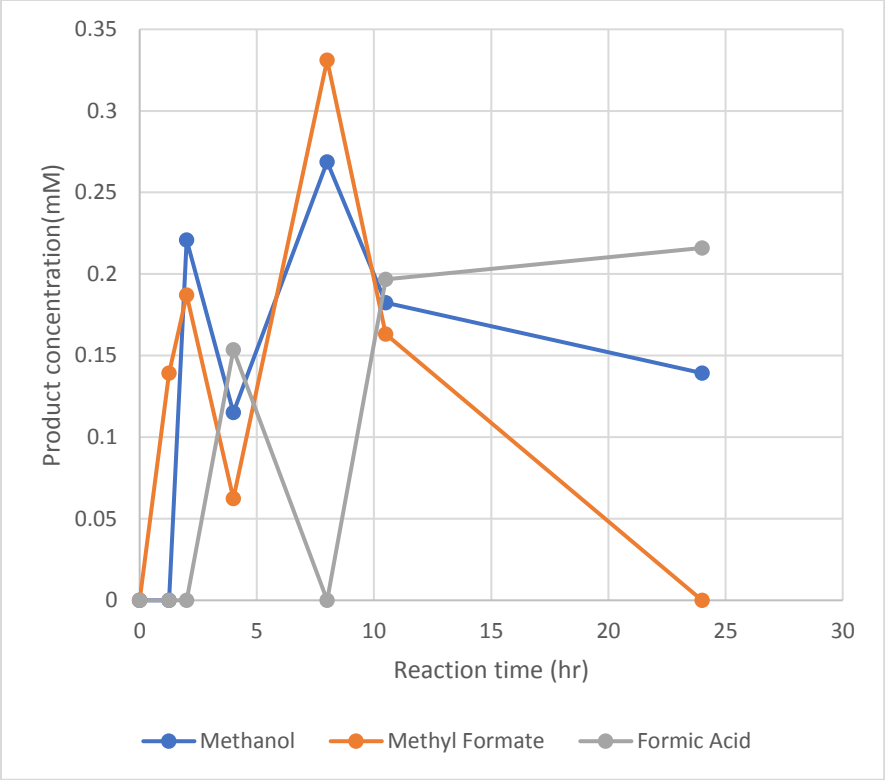

Figure 4-13. Concentration profiles of the three oxycarbon products from methane activation along with reaction time in the presence of Re

The concentration profiles show the peak concentrations: 0.216 mM, 0.269 m M, and 0.332 mM for formic acid, methyl formate, and methanol, respectively.

4.3.7 Silver

The last metal used here is silver that is from the same periodic group of Au and Cu. ^{1}H NMR spectroscopy results along with reaction time are presented in Figure 4.14. The methane activation over silver is very fast in the first hour and then all the generated products are decomposed. Same as the case of copper, the only observed activation product was methyl formate. Using the same quantitative method presented in section 4.3.2 we calculated the concentrations of methyl formate regarding to reaction time for methane upgrading.

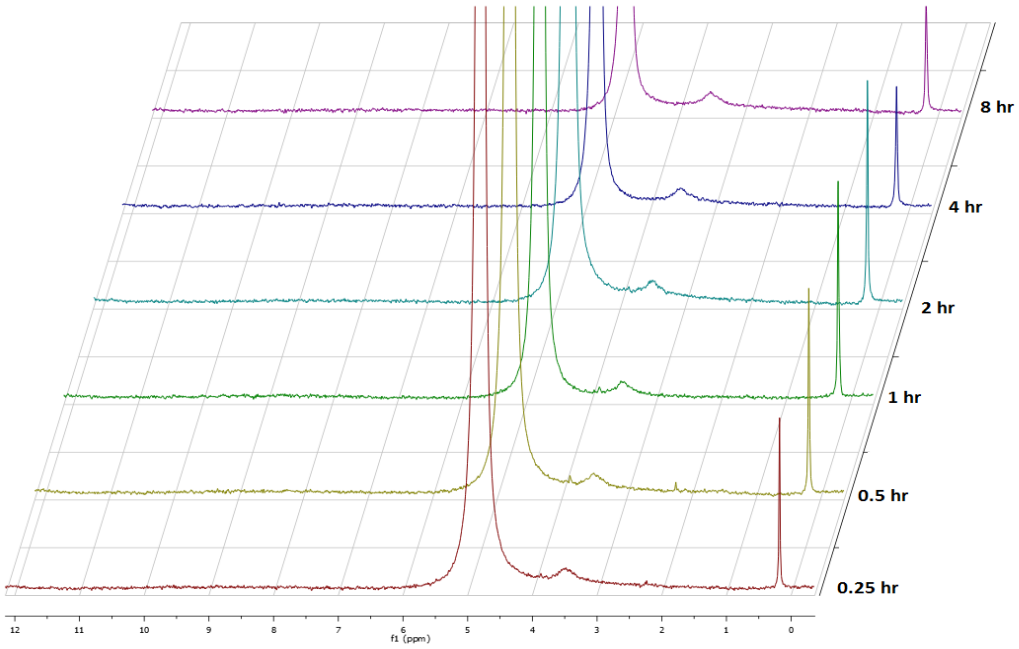

Figure 4-14. ^{1}H NMR spectra of reaction solution for methane activation with the presence of an Ag metal foil

Table 9, presents the calculated concentrations of methyl formate in reaction solution, and Figure.4.15 shows the concentration profile of methyl formate along with reaction time.

TABLE 9

CALCULATED CONCENTRATIONS ACTIVATION PRODUCTS IN THE CASE OF SILVER (Ag)

Time (hr.)	$[CH_3OH]$ (mM)	$[HCOOCH_3]$ (mM)	[HCOOH] (mM)
0	0	0	0
0.25	0	0.336	0
0.5	0	0.264	0
1	0	0.134	0
2	0	0	0
4	0	0	0
8	0	0	0
CH_4 concentration in solution is considered a constant of 1.44 mM for calculating other concentrations			

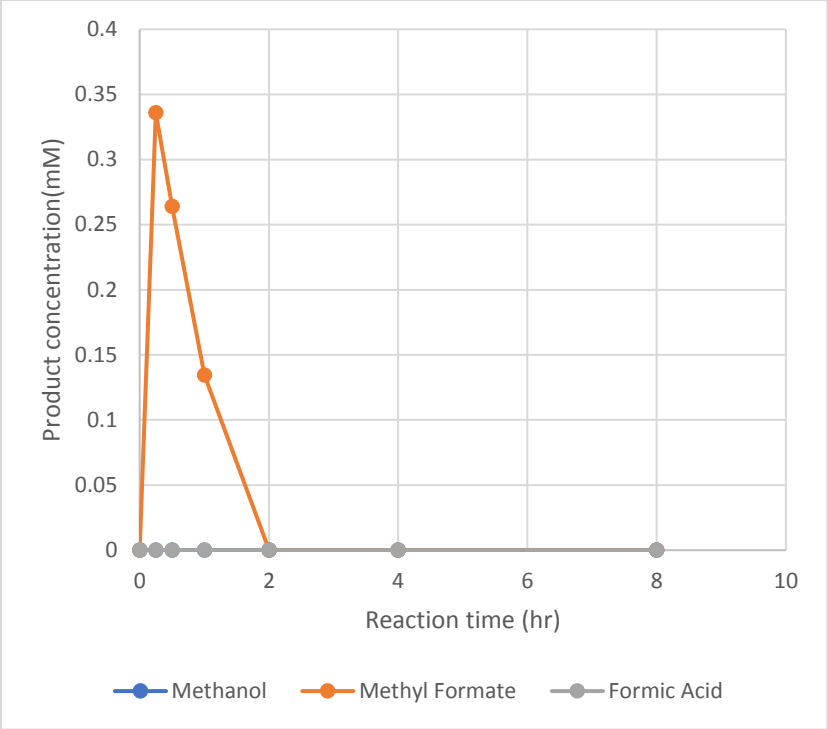

Figure 4-15. Concentration profiles of oxycarbon products from methane activation along with reaction time in the presence of Ag

The concentration of methyl formate rapidly rises in very beginning of the reaction and reaches its peak value of 0.336 mM in about 15 minutes.

4.3.8 Correlation between Methane Activation and Metal Binding Energy

In previous study, we have confirmed the powerful facilitating effect of metal surfaces on methane activation. And, we also observed that different metal surfaces result in varying activation rate and different activation products sometimes. It is of particular interest for us to investigate the underlying parameter that governs the activation kinetics. The best estimate for the generation rate of activation products for each metal surface is to use the very first data collected during each experiment setup. This is due to the fact that after a couple of hours the rather complicated evolution and decomposition of activation products occur when reaction proceeds longer (even over half of an hour).

There are three activation products: methanol, methyl formate, and formic acid; and they are different "average oxidation depth" (AOD) on carbon atom: 1, 2, and 3 of AOD for methanol, methyl formate, and formic acid. Note that, here we define the AOD with the average number of C−O bonds per carbon atom. Based on the AOD values and the experimental observations, methanol should be the earliest activation products, than methyl formate and formic acid.

As such, here we propose the production of CH_3OH via the following mechanism:

$$CH_4 + HO\bullet + M \longrightarrow CH_3\bullet_{ad} - M + H_2O$$
$$CH_3\bullet_{ad} - M + HO\bullet \longrightarrow CH_3OH_{ad} - M + H_2O$$
$$CH_3OH_{ad} - M \longrightarrow CH_3OH + M$$

This could be then followed by another series of reaction to generate deeper oxidized products such as formic acid in a mechanism as follows:

$$CH_3OH_{ad} - M + HO\bullet \longrightarrow HOCH_2\bullet_{ad} - M + H_2O$$
$$HOCH_2\bullet_{ad} - M + HO\bullet \longrightarrow HCHO_{ad} - M + 2H_2O$$
$$HCHO_{ad} - M + HO\bullet \longrightarrow OHC\bullet_{ad} - M + H_2O$$
$$OHC\bullet_{ad} - M + HO\bullet \longrightarrow HCOOH_{ad} - M + H_2O$$
$$HCOOH_{ad} - M \longrightarrow HCOOH_{ad} + M$$

The reactions between products themselves and also between products and hydroxyl radicals present in the reaction solution will make the system more and more complicated.

Based on the previous mechanisms, the most reasonable mechanism to generate methyl formate is as follow:

$$CH_3OH_{ad} - M + HCOOH_{ad} - M \longrightarrow HCOOCH_{3ad} - M + H_2O$$
$$HCOOCH_{3ad} - M \longrightarrow HCOOCH_3 + M$$

Generation rates of assorted products along with different metal surfaces could be expressed by unit of (μmol m^{-2} h^{-1}). Using the data obtained from ^1H NMR spectra, generation rates of CH_3OH and $HCOOCH_3$ oxycarbon products can be estimated with acceptable accuracy. Results from activation rates using different metal surfaces are presented in Table 10.

TABLE 10

CALCULATED PRODUCTION RATES OF TWO ACTIVATION PRODUCTS WITH DIFFERENT METAL SURFACES

Metal	Methanol (μmol m^{-2} h^{-1})	Methyl formate (μmol m^{-2} h^{-1})
Platinum	1290	1475
Palladium	299.5	351.4
Copper	0	121.6
Gold	115.0	119.0
Rhenium	1060	1069
Silver	0	0
Metal surface area is 0.00125 m^2 for all the metals used in experiment.		

For CH_3OH product, its generation rate on metal surfaces follows the descending order:

Pt > Re > Pd > Au

For $HCOOCH_3$ product, its generation rate on metal surfaces follows a similar trend:

Pt > Re > Pd > Cu > Au

By investigating adsorption energies of some species on metal surfaces, here we found that the CH_3•−M binding strength (with the most stable adsorption sites) follows the same descending order (Re data from the Ref [83, 84]):

Pt > Re > Pd > Cu > Au

In addition to the CH_3•−M binding energy, we also tried to use other binding energies including H•−M,[85] O•−M, [86] and HO•−M [86] for the correlation with production rate of oxycarbon products from methane activation, but none of them provides a better correlation. It becomes quite clear that CH_3•−M binding energy holds the bottleneck of the methane activation, which is consistent with the fact that the C−H breaking of methane is the rate-limiting step, similar to thermal activation [87, 88].

Figure 4.16, shows the correlation between the CH_3OH production rate and the CH_3•−M binding energy for four metal surfaces (Pt, Re, Pd, and Au). Copper is taken out form this chart since there was no methanol generated by copper surface facilitation.

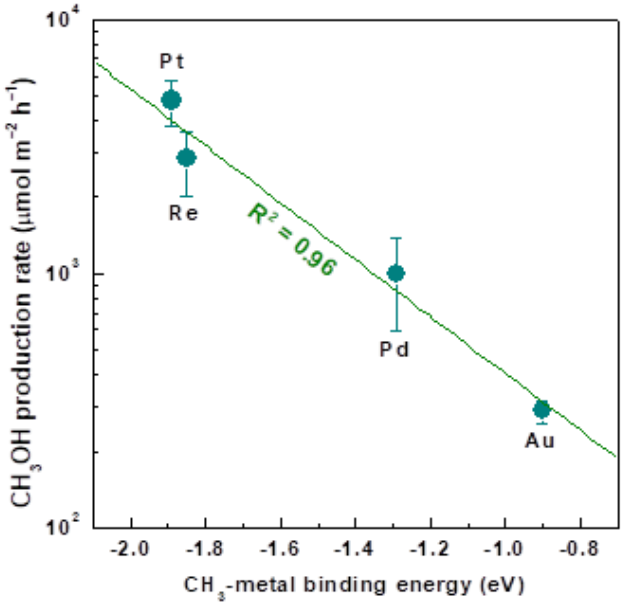

Figure 4-16. Correlation between CH_3OH production rate and CH_3•−M binding energy

Figure 4.17 shows the correlation between $HCOOCH_3$ production rate and the CH_3•−M binding energy for all five metal surfaces (Pt, Re, Pd, Cu, and Au). In fact, the generation rates of both CH_3OH and $HCOOCH_3$ oxycarbon products are similarly following the CH_3•−M binding strength, which quantitatively confirms the facilitation effect of the metal surface for methane activation.

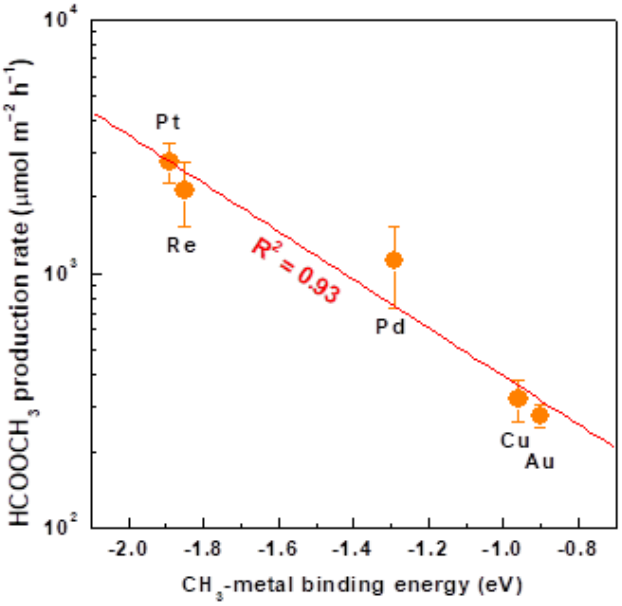

Figure 4-17. Correlation between $HCOOCH_3$ production rate and CH_3•−M binding energy

The correlation between HCOOH and CH_3•−M binding strength does not show a meaningful relationship. This could be explained by complexity of formic acid generation as other products are constantly getting more oxidized to deeper levels and for formic acid.

4.4 Chapter Summary

Facilitating impact from different metal surfaces on methane activation in reaction solution was studied, with For reaction conditions: as pH = 3, $[D_2O_2]$ = 12.5 mM, $[Fe^{2+}]$ = 0.25 mM (the ratio $[D_2O_2]/[Fe^{2+}]$ = 50). Platinum, palladium, copper, gold, rhenium, and silver were tested in our system regarding the facilitating effect on methane activation. From the ^1H NMR spectra of samples for each experiment setup regarding with time, three major products were identified as methanol, methyl formate, and formic acid. The facilitating effect can be reasoned by that the adsorption CH_3• on metal surfaces have been lowered the reaction barrier of C−H bond breaking of methane activation reacting with HO•. Based on the analysis of oxidation depth, the generation mechanisms of the activation products facilitated by metal surfaces have been proposed.

We have revealed a significant correlation between the production rate of methanol and methyl formate and CH_3•−M binding energies. The stronger CH_3•−M binding energy leads to the higher generation rats for methanol and methyl formate. Moreover, this correlation further supports with the metal facilitating effect where the adsorption of CH_3• on metal surface indeed lowers the reaction barrier of the C−H bond breaking of methane activation

Also, peak concentrations were observed for all three products. This is due to the complexity of reaction chain and over-oxidation phenomenon of generated products.

CHAPTER 5

THE EVOLUTION/DECOMPOSITION OF ACTIVATION PRODUCTS

5.1 Observation of Product Evolution and Destruction

As discussed in Chapter 4, we have discovered that metal surfaces can facilitate the methane activation by offering surface adsorption to methyl radicals. When increasing reaction time, the concentrations of oxycarbon products increase for all metal cases. However, the concentrations of oxycarbon products, for all metal surfaces, will decrease after reaching the peaks when reaction time is sufficiently extended. Obviously, the products decompose and eventually turn into CO_2. This product decomposition creates a serious challenge to utilize the decoupled methane activation for possible industry applications, because the products peak concentrations are fairly low (< 1 mM) that makes the product separation uneconomic.

The decomposition of those oxycarbon products may be explained by the metal-surface poisoning triggered by the high-concentration oxycarbon products in solution. Once the metal surface is poisoned, it is no longer favoring the methane adsorption and activation; but rather it is more favoring the adsorption oxycarbon products which leads to unfavorable deeply oxidized products such as CO_2.

It is very important to understand the decomposition kinetics of oxycarbon products, compared with the formation kinetics of oxycarbon products.

5.2 Methodology

As we discussed earlier in chapter 4, product evolution could be the reason for observation of only some particular compounds as reaction products. For instance, HCHO is expected to be generated in methane direct oxidation, but it was not observed. The absence of HCHO oxycarbon product implies that the formation of HCOOH likely goes through the following mechanism:

$$CH_3OH_{ad} - M + HO\bullet \longrightarrow HOCH_2\bullet_{ad} - M + H_2O$$
$$HOCH_2\bullet_{ad} - M + HO\bullet \longrightarrow HCHO_{ad} - M + 2H_2O$$
$$HCHO_{ad} - M + HO\bullet \longrightarrow OHC\bullet_{ad} - M + H_2O$$
$$OHC\bullet_{ad} - M + HO\bullet \longrightarrow HCOOH_{ad} - M + H_2O$$
$$HCOOH_{ad} - M \longrightarrow HCOOH_{ad} + M$$

Due to the product popularity and analysis simplicity, formic acid was used as the representing activation product to conduct the decomposition kinetics. In fact, choosing formic acid will help us simplify the reactions since there would be no chance to generate any other products, other than CO_2. Different metal surfaces were used for comparison, and same concentration of formic acid is introduced to the solution. ^{1}H NMR spectra are taken at different time intervals.

5.2.1 Materials and Reaction Conditions

For these experiments, high-purity D_2O (99.9%) solvent and $FeSO_4$ (99.0%) were obtained from Sigma-Aldrich. The solution of D_2O_2 in D_2O with 35 wt.% was obtained from Icon Isotopes Co, and sulfuric acid (98%, 17M) was supplied from Fisher-Scientific company. Formic acid (98+%) was also supplied by Sigma-Aldrich Co. 3-(Trimethylsilyl)propionic acid-D4 sodium salt for NMR spectroscopy reference with deuteration degree of $\geq$ 98% and purity of 99.96% is supplied by Sigma-Aldrich.

5.2.2 Testing Method of Products Evolution

For each test, both D_2O_2 and $FeSO_4$ are introduced in 12 mL of D_2O solvent. pH is then accurately set as 3 by adding H_2SO_4. The initial concentration of Fe^{2+} is 0.02 mM, and the initial molar ratio of D_2O_2 to Fe^{2+} is 50:1 (D_2O_2 concentration = 1.00 mM). At last, formic acid is added to the solution system at the initial concentration of 1 mM. The chance of external contaminations

from atmosphere is minimized by using closing the cap. Seen in Figure 5.1, the whole solution was held in a 25 mL glass vail with constant magnetic stirring.

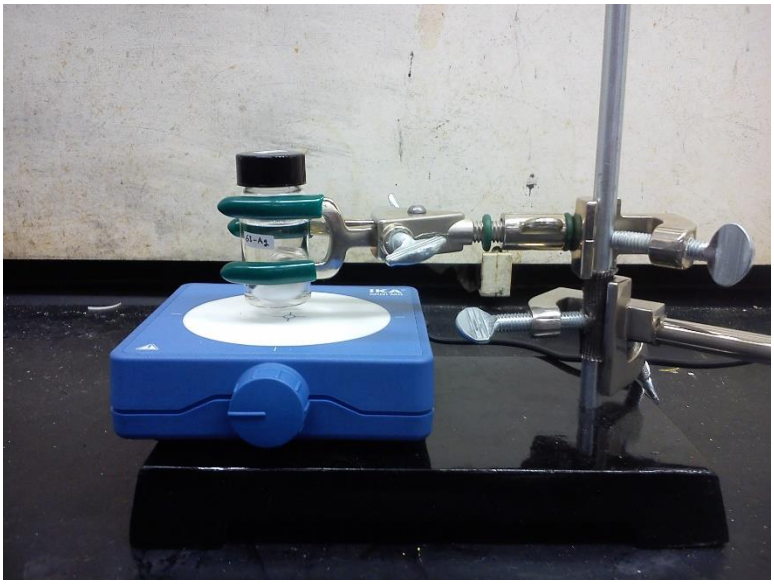

Figure 5-1. Experiment setup of decomposition study

A coaxial NMR insert filled with 1 mM solution of 3-(Trimethylsilyl)propionic acid-D4 sodium salt (DSS) was used as external NMR standard. For each ^{1}H NMR sample, 0.5 mL of the reaction solution was extracted and inserted into NMR tubes. Clean coaxial insert tube was then inserted into the NMR tube. The ^{1}H NMR spectroscopy was obtained with a number of 256 scans for each sample.

5.2.3 External NMR Standard

Different NMR reference standards are commercially available for different solvent. One of the most common ones is trimethylsilyl cyanide (TMS). However, this reference standard is not well soluble in water, and thus we used 3-(trimethylsilyl)propionic acid-D4 sodium salt (DSS) as the water-soluble reference standard. Note that the DSS cannot be used directly as the internal standard in our reaction solution, because it is not sufficiently stable against aggressive hydroxyl

radicals. We use a coaxial insert tube filled with DSS to serve as the external reference standard. For more detailed discussion on decomposition of reference standard, please refer to Appendix C.

The Figure 5.2 shows the typical coaxial insert tube that consists of an insert tube filled with the external reference solution and an outer tube filled with NMR sample solution. . The reference solution inside the insert tube and the sample solution in the outer tube are physically separated by the glass wall of the insert tube..

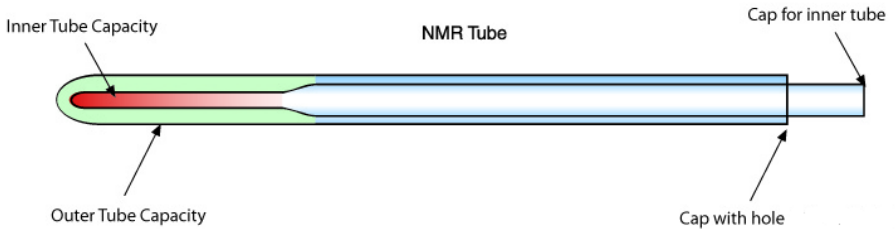

Figure 5-2. Schematic of coaxial insert NMR tube [89]

5.2.4 Selection of Initial Concentration for Decomposition Study

In the decomposition study of formic acid in the methane-activation system, we chose the initial value of 1 mM for all cases, since it is close to the maximum concentration of the products as possible.

5.2.5 Concentrations of Hydrogen Peroxide and Ferrous Sulfate

The concentration of hydrogen peroxide was 1 mM in the decomposition study, which is lower than that in methane activation (12.5 mM). This lowered concentration of hydrogen peroxide provides a mild decomposition condition for formic acid so that the impact of different metal surfaces can be distinguished. In fact, we tried the high concentration of D_2O_2 (12.5 mM) and we found for decomposition is too fast to see the difference among different metal surfaces. As shown in Figure 5.3, the H_2O_2 concentration of 1 mM ($[D_2O_2]/[Fe^{2+}]$ = 50:1) is mild enough for

decomposition of formic acid (. For this condition even after 12 hours, the concentration of formic acid (8.25 ppm) remains high enough to be distinguished from the effect of the metal surface.

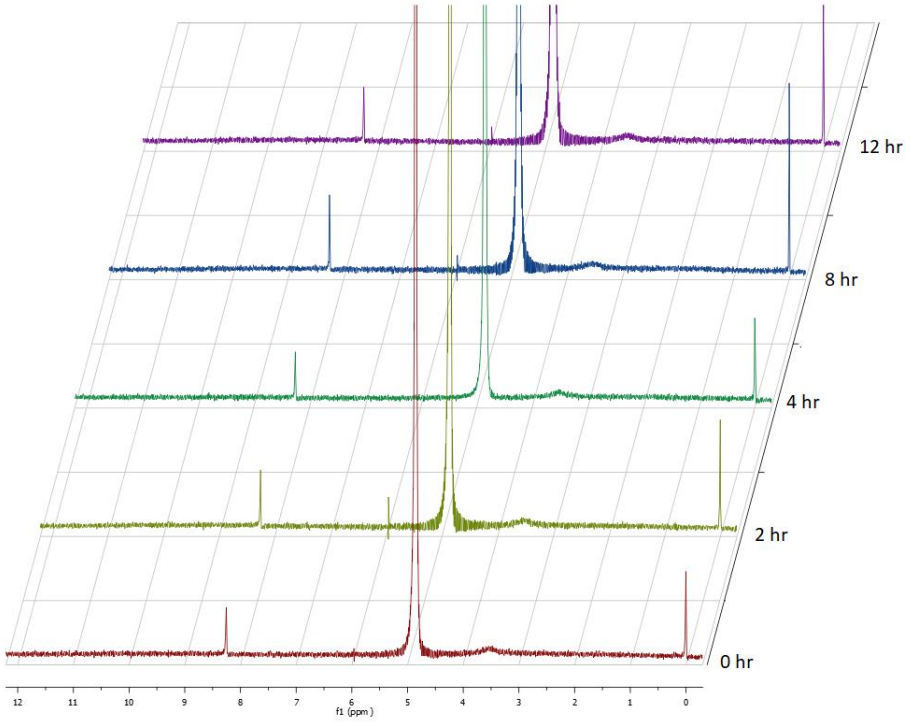

Figure 5-3. ^{1}H NMR spectra of reaction solution for decomposition of formic acid without any metal surfaces, [D_2O_2] as 1.0 mM

For more detailed discussions on this topic, please refer to Appendix D.

5.2.6 Pseudo-First Order Reactions

In kinetics of chemical reactions, the reaction order is defined as the relationship between the concentrations of species and the rate of a reaction. The order of a reaction indicates to what extend the rate of a reaction is influenced by the concentration of a species. This order could be defined in respect to a specific substance. [90]

In general, the experimenting is needed to determine the order of a reaction, and the final rate of a reaction is expressed as:

$$r = k[A]^x[B]^y ...$$

In this equation [A] and [B] are the concentrations of A and B spices, respectively. The order of a reaction is then simply determined as summation of the exponents

Overall reaction order = x + y + … [91]

If the reaction rate is not dependent of any concentrations of reactants, it is said to of the zeroth order. For zeroth order reactions, we have:

$$r = k = -\frac{d[A]}{dt}$$

By integrating the above equation, we have:

$$[A]_t = -kt + [A]_0$$

When the reaction is of the first order, it depends on the concentration of only one of the reactants and with the exponent of one. For the first order reactions, we can write the reaction rate as:

$$r = k[A] = -k\frac{d[A]}{dt}$$

By integrating the above equation, we have

$$\ln[A] = -kt + \ln[A]_0$$

The reaction rate for a second order reaction could be either $r = k[A]^2$ or more commonly $r = k[A][B]$. To avoid the complexities caused by two reactants A and B, here we use the pseudo-first order approximation [90, 92].

For that we need to assume that the concentration of one of the reactants is constant. Note: The reactant might be constantly supplied to the reaction or might have excess concentration such as to be assumed constant and with no change during the reaction. As a result, the fixed concentration could be included into the constant factor for the reaction rate and we have:

$$r = k[A][B],\ [B] = Const \Rightarrow r = k'[A]$$

$$-\frac{d[A]}{dt} = r = -k'\frac{d[A]}{dt} \quad \Rightarrow \ln[A] = -k't + \ln[A]_0$$

$$\Rightarrow -\ln\left(\frac{[A]}{[A]_0}\right) = k't$$

This pseudo-first order approximation was used and confirmed valid for determining the kinetics of the decomposition rate of formic acidic in our study.

5.3 Impact of Metal Surfaces on Evolution/Degradation Rate

Choices of metal have been made such as to match the cases of methane activation experiments, as this will provide the opportunity to compare the methane activation with product decomposition on the same metal. Hence, Platinum, palladium, copper, gold, rhenium and silver were tested. In addition, molybdenum and tungsten were also tested to give us a more comprehensive vision over the metal's impacts.

5.3.1 The Absence of Metal Surfaces

To make sure about the effect of metal surface over the decomposition of formic acid, the experiment was conducted once in the absence of any metal surfaces as the control experiment. The control experiment was extended to 36 hours and ^{1}H NMR samples were taken as shown in Figure 5.4. The formic acid remained at almost unchanged. This result sets the background decomposition of formic acid due to the solution itself (hydroxyl radical), and formic acid will not decompose too quickly.

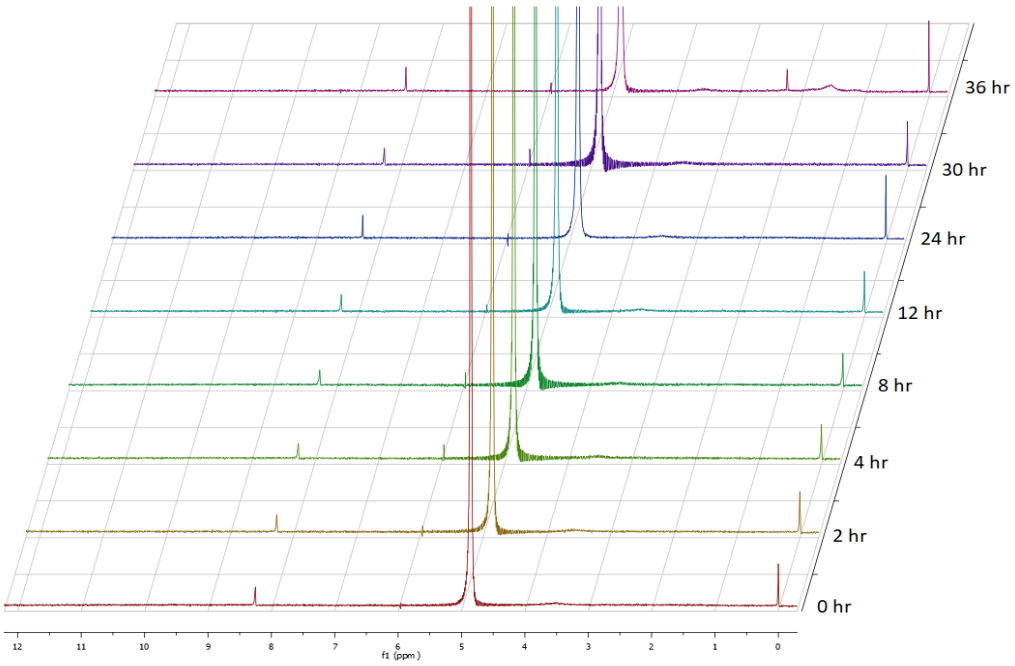

Figure 5-4. ^{1}H NMR spectra of reaction solution for decomposition of formic acid without any metal surfaces, ratio of $[D_2O_2]$ to $[Fe^{2+}]$ as 50 and $[D_2O_2]$ as 1.0 mM

In the beginning, both concentrations of formic acid and DDS external standard are equal to 1 mM. After some time from reaction, the concentration for formic acid changes while the concentration of DSS in coaxial insert tube is fixed at the value of 1 mM. Comparing the area-integral ratio of formic acid to DSS, enables us to calculate the remained amount of formic acid in reaction solution.

For instance, the integrated value of peaks at 0.00 ppm and 8.25 ppm at time zero in the absence of any metal surfaces are 1 and 0.77, respectively. (The value of peak at 0.00 ppm is set as 1 so as to be used as reference). As a result, we can conclude that the ratio of 0.77 for integrated area of the peaks represents 1 mM concentration for formic acid. Such ratio was used to calculate the concentration of formic acid in other NMR samples with extended reaction times.

The results have been calculated for all the ^{1}H NMR samples and are presented in Table 11.

TABLE 11

DECOMPOSION RATE OF FORMIC ACID IN THE ABSENCE OF ANY METAL SURFACE

Time (hr.)	Integrated value for formic acid (8.26 ppm)	Formic acid retention (%)
0	0.77	100
2	0.74	96.1
4	0.73	94.8
8	0.72	93.5
12	0.71	92.2
24	0.68	88.3
30	0.62	80.5
36	0.60	77.9
DSS peak at 0.00 ppm is considered as the standard peak. The area integrals of peaks at 0.00 ppm and 8.25 ppm at time zero are 1 and 0.77, respectively.		

The decomposition reaction for formic acid in the reaction solution could be written as:

$$HCOOH + HO\bullet \rightarrow H_2O + CO_2 + H\bullet \qquad [93]$$

Note that H• is used here to mainly simplify the reaction and in reality, other more complex radical or species is likely to be the product here. Consumption of H_2O_2 is determined by $[Fe^{2+}]$. If we assume that the concentration of HO• is constant during the reaction time, the pseudo-first order approximation applies.

As explained in section 5.2.6, the pseudo-first order approximation of reaction rate is expressed as:

$$-\ln\left(\frac{[A]}{[A]_0}\right) = k't, \qquad k' = k[B]$$

In this study, [A] is the concentration of formic acid (as a function of reaction time), $[A]_0$ is the initial concentration of formic acid (1 mM here), and [B] is the concentration of hydrogen peroxide as a constant (1 mM in this case). Furthermore, we include the area of metal surface in

this equation as a constant factor, and k' is then used to be distinct from k (k' = k × SA, where SA is the area of metal surface). Finally, the pseudo approximation equation is reorganized as follows:

$$-\ln\left(\frac{[A]}{[A]_0}\right) = k \cdot [B] \cdot (\mathrm{SA}) \cdot t$$

$$\Rightarrow -\ln\left(\frac{[\mathrm{HCOOH}]}{[\mathrm{HCOOH}]_0}\right) \times \left(\frac{1}{[\mathrm{H_2O_2}]_0 \cdot (\mathrm{SA})}\right) = k \cdot t$$

In the above equation, [HCOOH] is the concentration of HCOOH (a function of reaction time); $[HCOOH]_0$ is the initial concentration of HCOOH (1 mM); $[H_2O_2]_0$ is the initial concentration of H_2O_2; SA is the area of metal surface, k is reaction constant; and t is reaction time. By linear fitting the left part in the equation with the reaction time, we can obtain the reaction rate as the slope for regressed fitting. For fair comparison to metal surfaces, a virtual metal surface was assumed into the solution to make the units of decomposition rates uniform. Figure 5.5 shows such a fitting that reveals the reaction rate for the decomposition of formic acid: the slope as the rate constant is 0.5405 $(mM)^{-1}$ cm^{-2} h^{-1}. The coefficient of determination, R^2, is very high (0.94) for the fitting, which validates the pseudo-first order approximation in our study here.

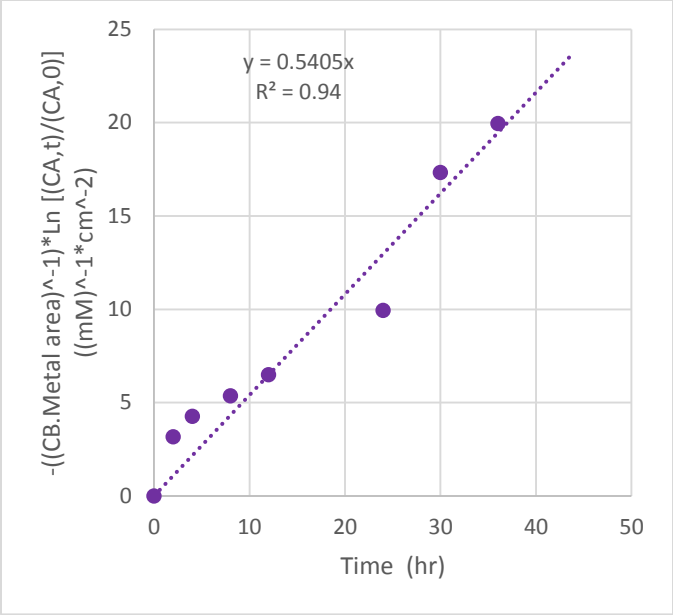

Figure 5-5. Fitting the rate constant (*k*) of formic-acid decomposition with pseudo-first order kinetics without using any metal

5.3.2 Platinum

Platinum was used to monitor the decomposition of formic acid. Using the same quantitative method presented in section 5.3.1 we calculated the retention percentage of formic acid in reaction solution. Table 12 presents the calculated remained formic acid in reaction solution in the presence of palladium at each time interval.

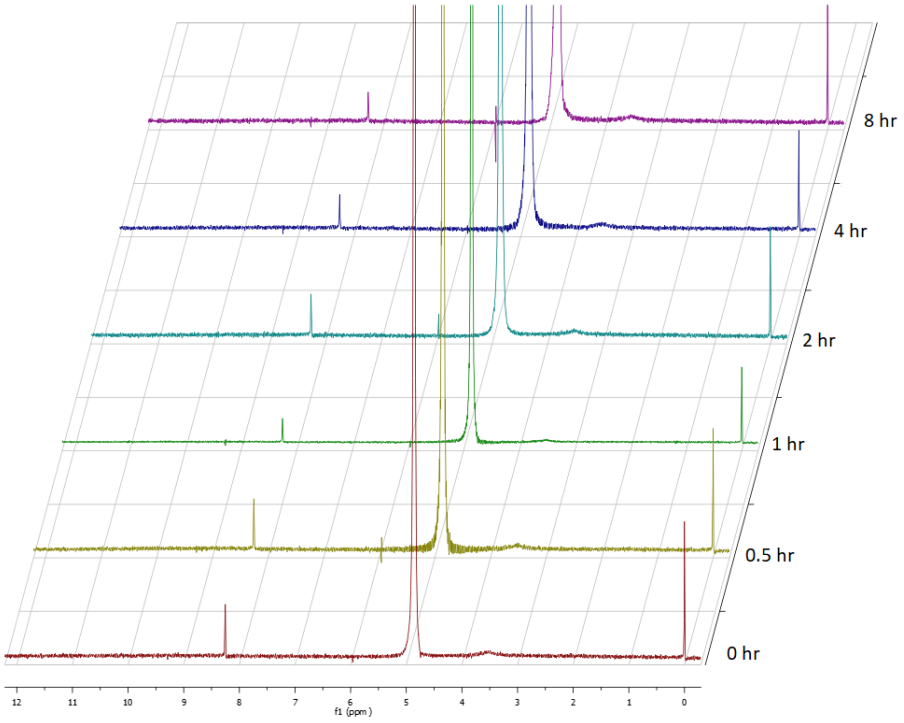

Figure 5-6. ^{1}H NMR spectra of reaction solution for decomposition of formic acid with the presence of a Pt metal foil, ratio of $[D_2O_2]$ to $[Fe^{2+}]$ as 50 and $[D_2O_2]$ as 1.0 mM

TABLE 12

DECOMPOSION RATE OF FORMIC ACID IN THE PRESENCE OF PLATINUM (Pt)

Time (hr.)	Integrated value for formic acid (8.26 ppm)	Formic acid retention (%)
0	0.78	100
0.5	0.70	90
1	0.65	83
2	0.59	76
4	0.51	65
8	0.32	41

DSS peak at 0.00 ppm is considered the standard peak
The area integrals of peaks at 0.00 ppm and 8.25 ppm at time zero are 1 and 0.77, respectively.

Figure 5.7 shows the fitted trendline for calculating the decomposition rate of formic acid in presence of platinum foil. Compared with the case free of metal surface [0.5405 $(mM)^{-1}$ cm^{-2} h^{-1}], Pt leads to a huge increase in rate constant of decomposition: k = 9.029 $(mM)^{-1}$ cm^{-2} h^{-1}, or 16.7 times The coefficient of determination (R^2) is very high: 0.9778..

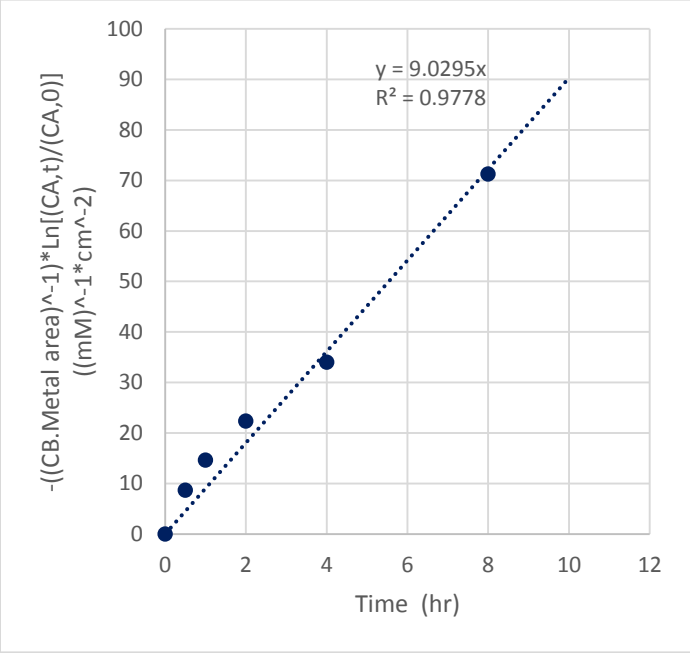

Figure 5-7. Fitting the rate constant (k) of formic-acid decomposition with pseudo-first order kinetics for Pt

5.3.3 Palladium

Pd was also used for the decomposition study. Using the same quantitative method presented in section 5.3.1, we calculated the retention percentage of formic acid in reaction solution. Table 13 presents the calculated remained formic acid in reaction solution in presence of palladium at each time interval.

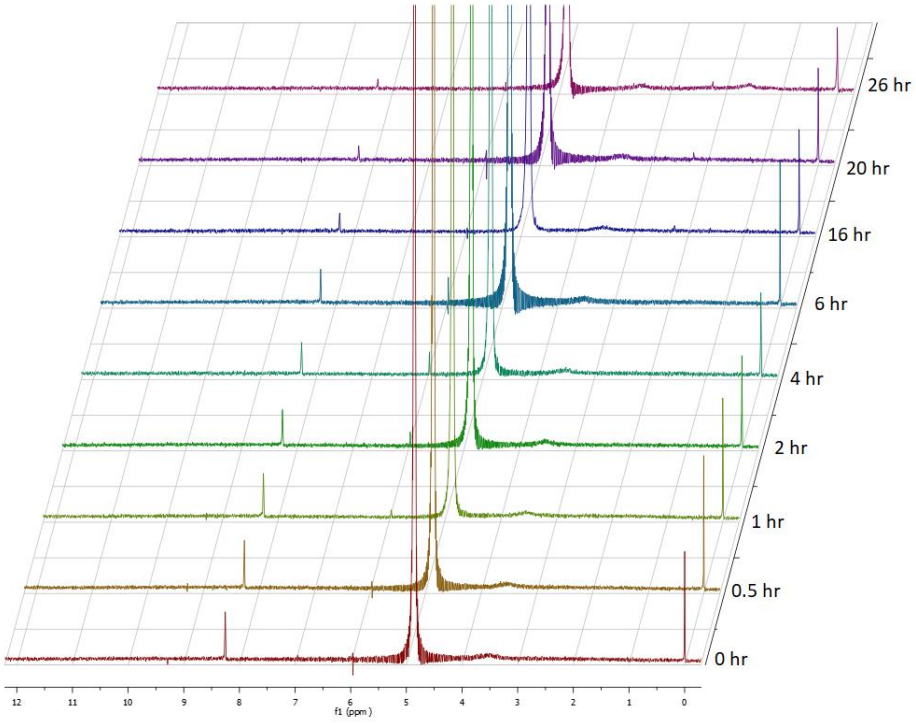

Figure 5-8. ^{1}H NMR spectra of reaction solution for decomposition of formic acid with the presence of a Pd metal foil, ratio of $[D_2O_2]$ to $[Fe^{2+}]$ as 50 and $[D_2O_2]$ as 1.0 mM

TABLE 13

DECOMPOSION RATE OF FORMIC ACID IN THE PRESENCE OF PALLADIUM (Pd)

Time (hr.)	Integrated value for Formic acid (8.26 ppm)	Formic acid Retention (%)
0	0.82	100
0.5	0.75	91.5
1	0.74	90.2
2	0.72	87.8
4	0.65	83.3
6	0.49	59.8
16	0.34	43.6
20	0.25	32.1
26	0.16	20.5
DSS peak at 0.00 ppm is considered the standard peak The area integrals of peaks at 0.00 ppm and 8.25 ppm at time zero are 1 and 0.82, respectively.		

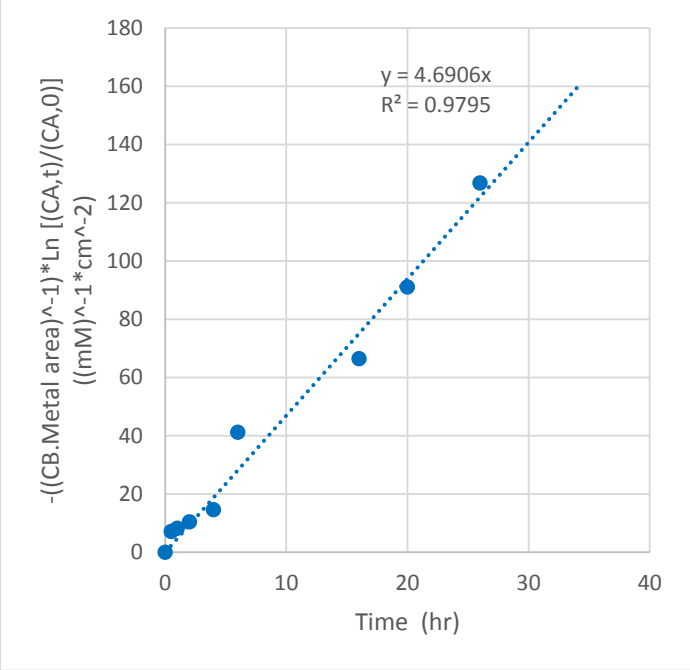

Figure 5-9. Fitting the rate constant (*k*) of formic-acid decomposition with pseudo-first order kinetics for Pd

Figure.5.9 shows the fitted trendline for calculating the reaction rate of formic acid decomposition in presence of palladium foil. The rate constant, k is 4.691 $(mM)^{-1}$ cm^{-2} h^{-1} for the case of Pd. The coefficient of determination (R^2) is very high: 0.9795.

5.3.4 Copper

When Cu is used, the size of Cu foil is reduced to 1/8 inch square. This is due to the very high reaction rate in presence of copper surface. ^{1}H NMR spectroscopy results along with reaction time are presented in Figure 5.8.

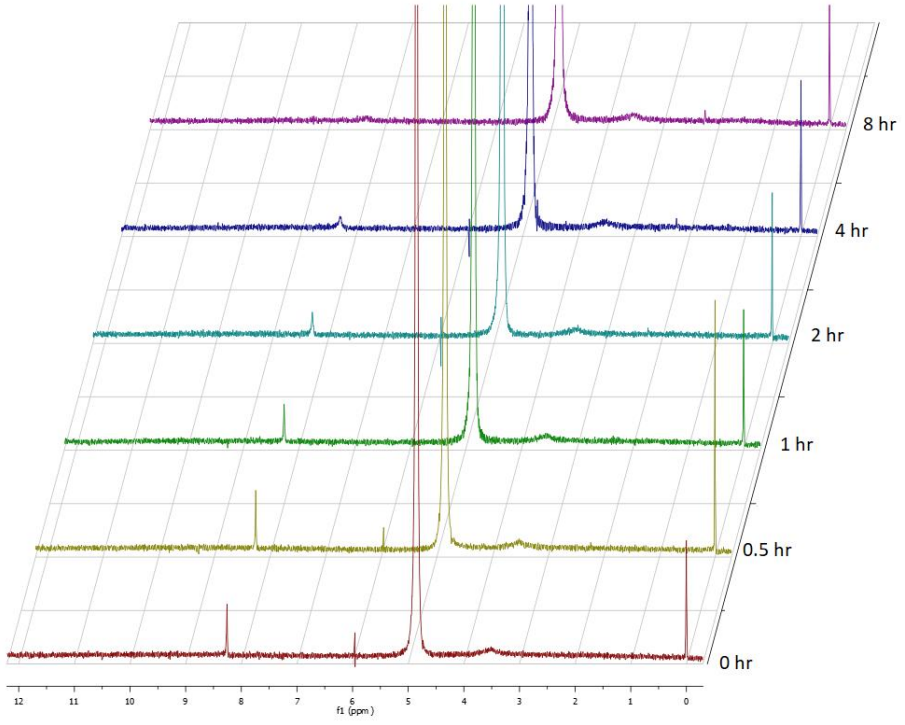

Figure 5-10. ^{1}H NMR spectra of reaction solution for decomposition of formic acid with the presence of a Cu metal foil, ratio of [D_2O_2] to [Fe^{2+}] as 50 and [D_2O_2] as 1.0 mM

Using the same quantitative method presented in section 5.3.1 we calculated the retention percentage of formic acid in reaction solution at every time interval. Table 14, presents the calculated remained formic acid in reaction solution in presence of copper at each time interval

TABLE 14

DECOMPOSION RATE OF FORMIC ACID IN THE PRESENCE OF COPPER (Cu)

Time (hr.)	Integrated value for Formic acid (8.26 ppm)	Formic acid Retention (%)
0	0.73	100
0.5	0.67	92
1	0.64	88
2	0.58	80
4	0.41	56
8	0	0.0

DSS peak at 0.00 ppm is considered the standard peak
The area integrals of peaks at 0.00 ppm and 8.25 ppm at time zero are 1 and 0.73, respectively.

Figure.5.11 shows the fitted trendline for calculating the reaction rate of formic acid decomposition in presence of copper foil. Note that the surface area has been taken into account, and the obtained rate constant, *k*, is 88.6 $(mM)^{-1}$ cm^{-2} h^{-1}. Such a rate constant is extremely high, and it is almost 10-fold that of Pt [9.0295 $(mM)^{-1}$ cm^{-2} h^{-1}]. The coefficient of determination (R^2) is very high: 0.9848.

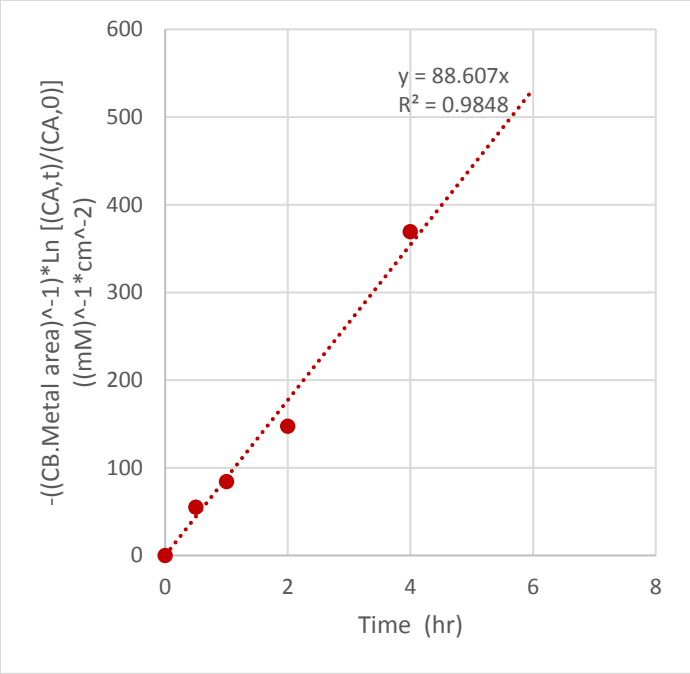

Figure 5-11. Fitting the rate constant (*k*) of formic-acid decomposition with pseudo-first order kinetics for Cu

5.3.5 Gold

Au was tested here as well. Using the same quantitative method presented in section 5.3.1 we calculated the retention percentage of formic acid in reaction solution. The data for calculated remained formic acid in reaction solution in presence of palladium at each time interval is presented in Table 15.

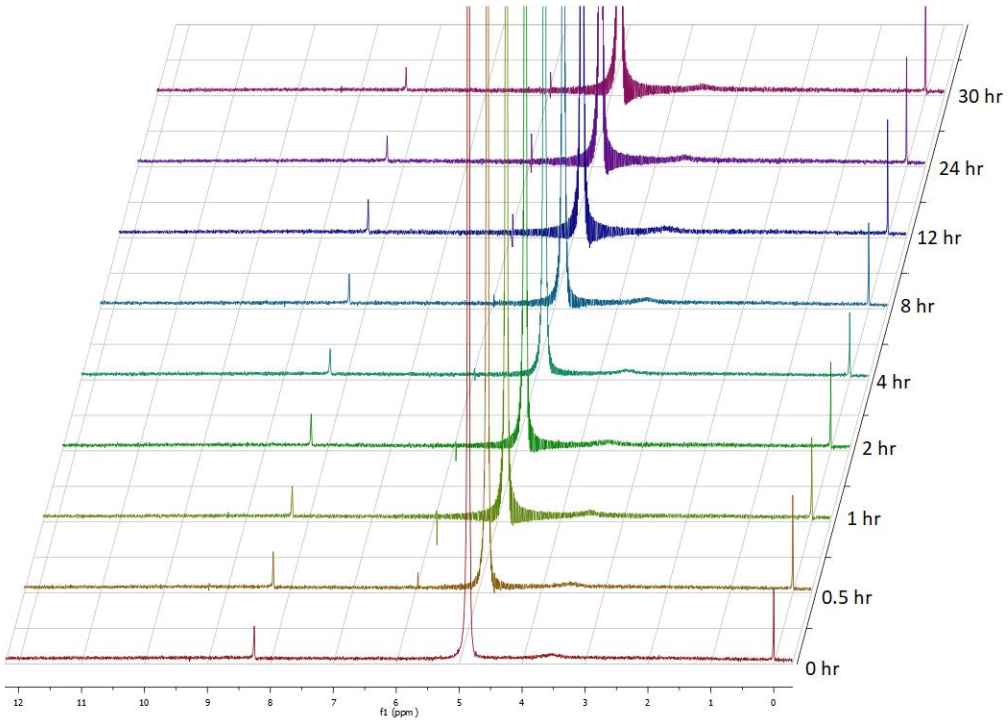

Figure 5-12. ^{1}H NMR spectra of reaction solution for decomposition of formic acid with the presence of a Au metal foil, ratio of $[D_2O_2]$ to $[Fe^{2+}]$ as 50 and $[D_2O_2]$ as1.0 mM

TABLE 15

DECOMPOSION RATE OF FORMIC ACID IN THE PRESENCE OF GOLD (Au)

Time (hr.)	Integrated value for Formic acid (8.26 ppm)	Formic acid Retention (%)
0	0.80	100
0.5	0.77	96
1	0.75	94
2	0.74	93
4	0.71	89
8	0.70	88
12	0.66	83
24	0.53	66
30	0.39	49

DSS peak at 0.00 ppm is considered the standard peak
The area integrals of peaks at 0.00 ppm and 8.25 ppm at time zero are 1 and 0.80, respectively.

Figure.5.13 shows the fitted trendline for calculating the reaction rate of formic acid decomposition in the presence of gold foil. The rate constant of decomposition, is 1.667 $(mM)^{-1}$ cm^{-2} h^{-1}. Compared with Pt, the rate constant is relatively small (about 1/5 of that of Pt). The coefficient of determination (R^2) is very high: 0.9381.

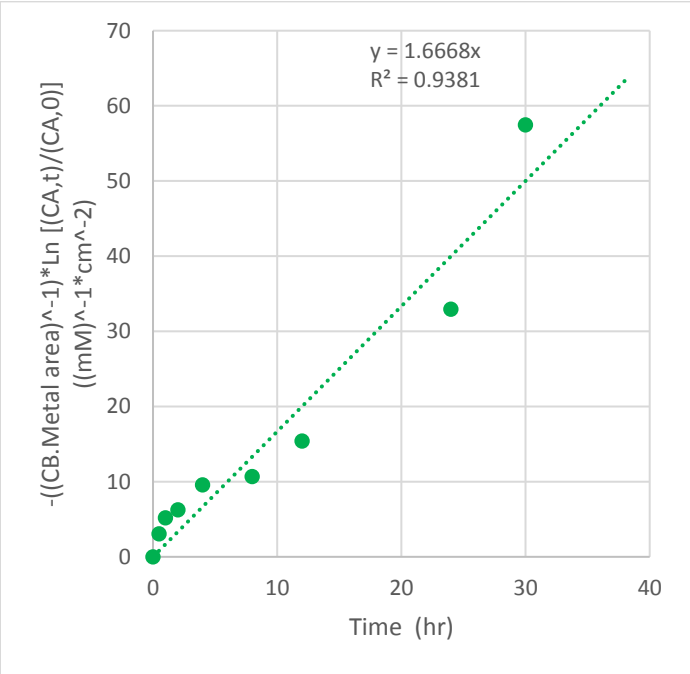

Figure 5-13. Fitting the rate constant (k) of formic-acid decomposition with pseudo-first order kinetics for Au

5.3.6 Rhenium

Similarly, Re was tested here. Using the same quantitative method presented in section 5.3.1 we calculated the retention percentage of formic acid in reaction solution. The data for calculated remained formic acid in reaction solution in presence of rhenium at each time interval is presented in Table 16.

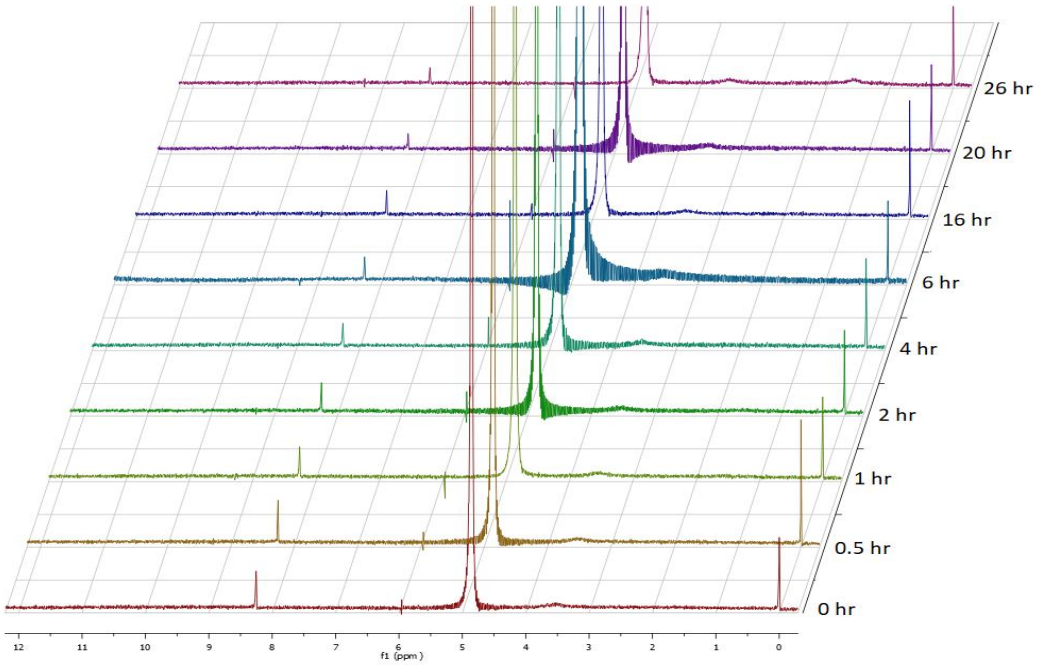

Figure 5-14. ^{1}H NMR spectra of reaction solution for decomposition of formic acid with the presence of a Re metal foil, ratio of $[D_2O_2]$ to $[Fe^{2+}]$ as 50 and $[D_2O_2]$ as 1.0 mM

TABLE 16

DECOMPOSION RATE OF FORMIC ACID IN THE PRESENCE OF RHENIUM (Re)

Time (hr.)	Integrated value for Formic acid (8.26 ppm)	Formic acid Retention (%)
0	0.81	100.0
0.5	0.69	93
1	0.67	91
2	0.62	84
4	0.48	65
6	0.44	60
16	0.40	49
20	0.30	37
26	0.26	32

DSS peak at 0.00 ppm is considered the standard peak
The area integrals of peaks at 0.00 ppm and 8.25 ppm at time zero are 1 and 0.81, respectively.

Figure 5.15 shows the fitted trendline for calculating the decomposition rate of formic acid in the presence of rhenium foil. The rate constant for the case of Re, *k*, is 3.803 $(mM)^{-1}$ cm^{-2} h^{-1}. The coefficient of determination (R^2) is 0.8984.

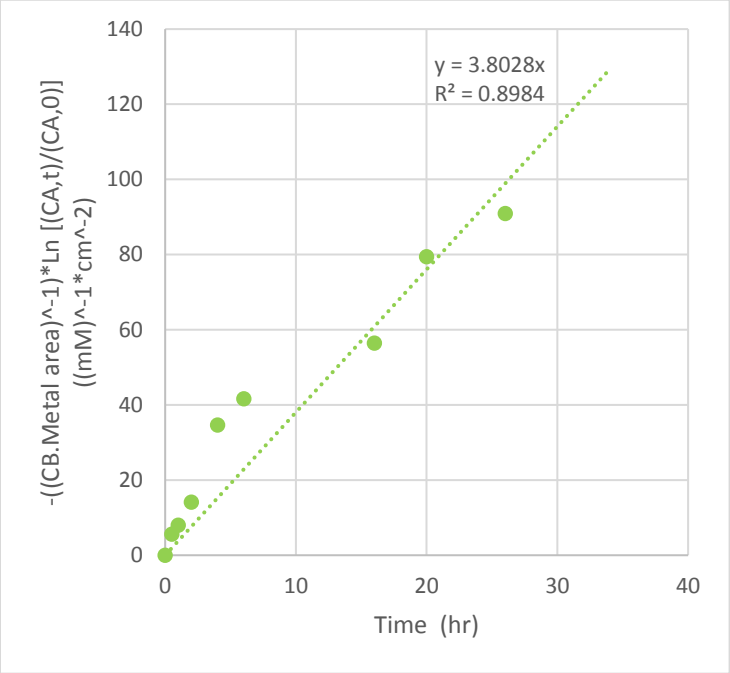

Figure 5-15. Fitting the rate constant (*k*) of formic-acid decomposition with pseudo-first order kinetics for Re

5.3.7 Silver

Using the same quantitative method presented in section 5.3.1 we calculated the retention percentage of formic acid in reaction solution. The data for calculated remained formic acid in reaction solution in the presence of silver at each time interval is presented in Table 17.

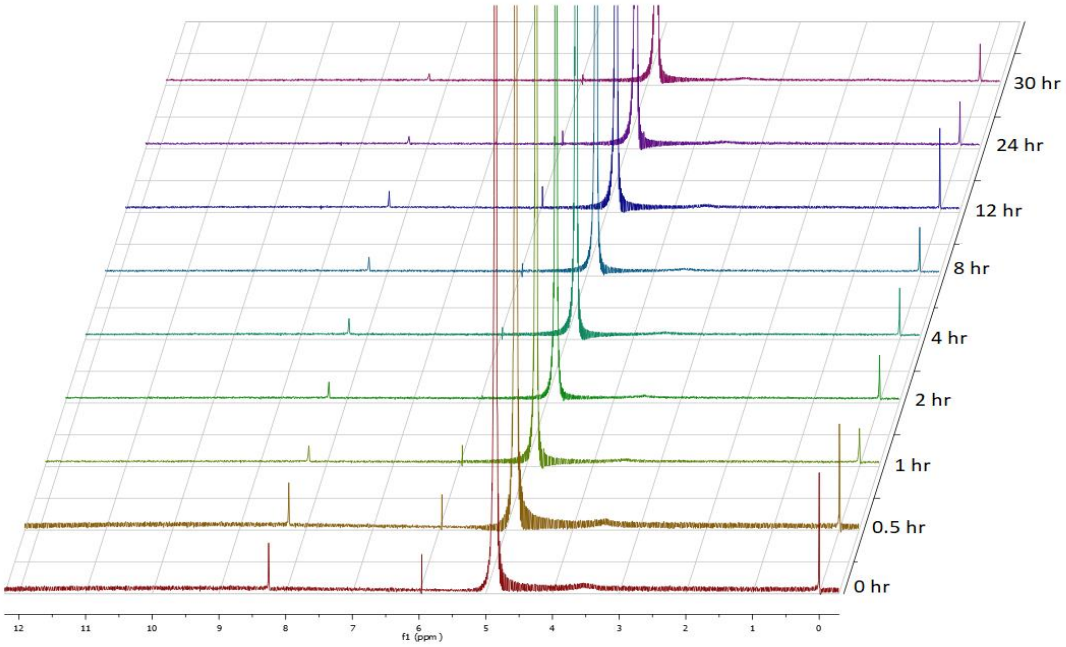

Figure 5-16. ^{1}H NMR spectra of reaction solution for decomposition of formic acid with the presence of a Ag metal foil, ratio of $[D_2O_2]$ to $[Fe^{2+}]$ as 50 and $[D_2O_2]$ as 1.0 mM

TABLE 17

DECOMPOSION RATE OF FORMIC ACID IN THE PRESENCE OF SILVER (Ag)

Time (hr.)	Integrated value for Formic acid (8.26 ppm)	Formic acid Retention (%)
0	0.79	100
0.5	0.77	98
1	0.73	92
2	0.71	90
4	0.62	79
8	0.57	72
12	0.52	66
24	0.32	41
30	0.26	33

DSS peak at 0.00 ppm is considered the standard peak
The area integrals of peaks at 0.00 ppm and 8.25 ppm at time zero are 1 and 0.79, respectively.

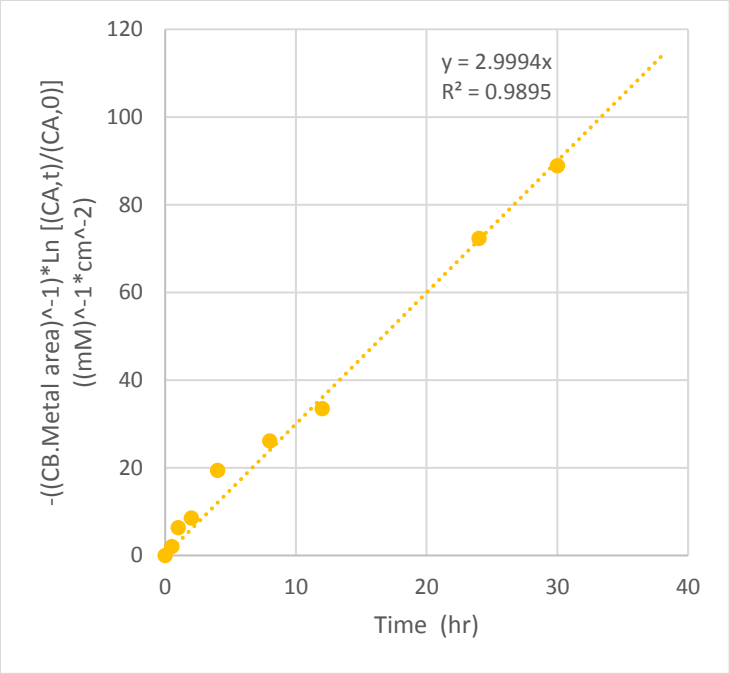

Figure 5-17. Fitting the rate constant (*k*) of formic-acid decomposition with pseudo-first order kinetics for Ag

Figure.5.17 shows the fitted trendline for calculating the decomposition rate of formic acid in the presence of silver foil. The rate constant for the case of Ag, *k* is 2.999 $(mM)^{-1}$ cm^{-2} h^{-1}. The coefficient of determination (R^2) is very high: 0.9895.

5.3.8 Tungsten

In addition to the above metals that were used in methane activation, two new metals were also introduced here: tungsten and molybdenum (discussed in the next subsection). ^{1}H NMR spectroscopy results along with reaction time are presented in Figure 5.18. Using the same quantitative method presented in section 5.3.1 we calculated the retention percentage of formic acid in reaction solution.

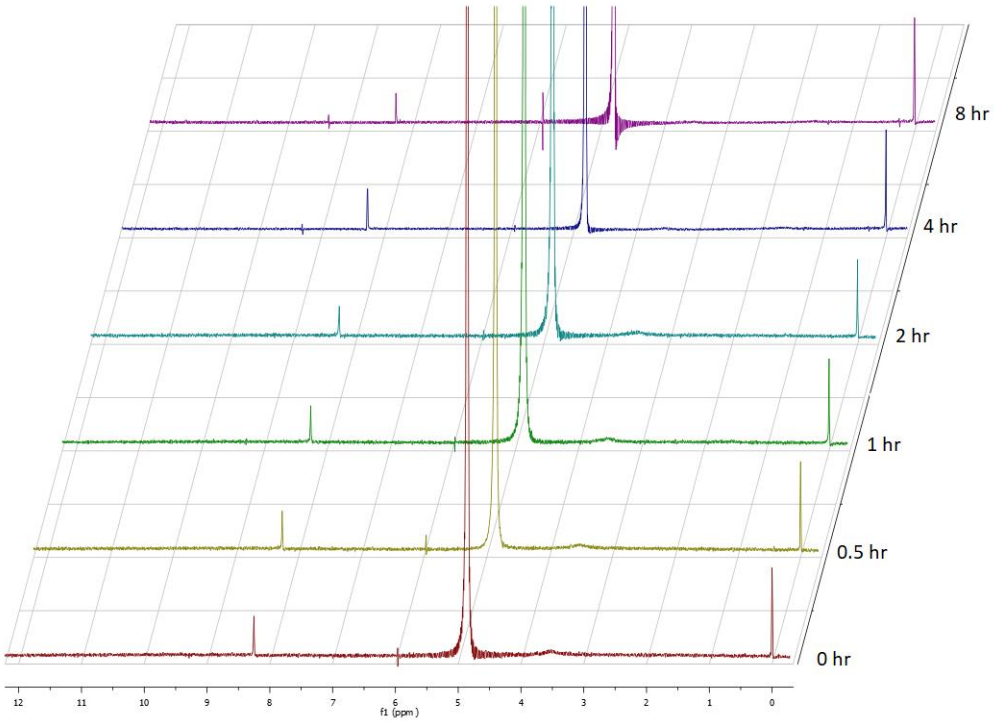

Figure 5-18. ^{1}H NMR spectra of reaction solution for decomposition of formic acid with the presence of a W metal foil, ratio of $[D_2O_2]$ to $[Fe^{2+}]$ as 50 and $[D_2O_2]$ as 1.0 mM

The data for calculated remained formic acid in reaction solution in the presence of tungsten at each time interval is presented in Table 18

TABLE 18

DECOMPOSION RATE OF FORMIC ACID IN THE PRESENCE OF TUNGSTEN (W)

Time (hr.)	Integrated value for Formic acid (8.26 ppm)	Formic acid Retention (%)
0	0.78	100.0
0.5	0.78	100.0
1	0.76	97.4
2	0.72	92.3
4	0.54	69.2
8	0.32	41.0
DSS peak at 0.00 ppm is considered the standard peak The area integrals of peaks at 0.00 ppm and 8.25 ppm at time zero are 1 and 0.78, respectively.		

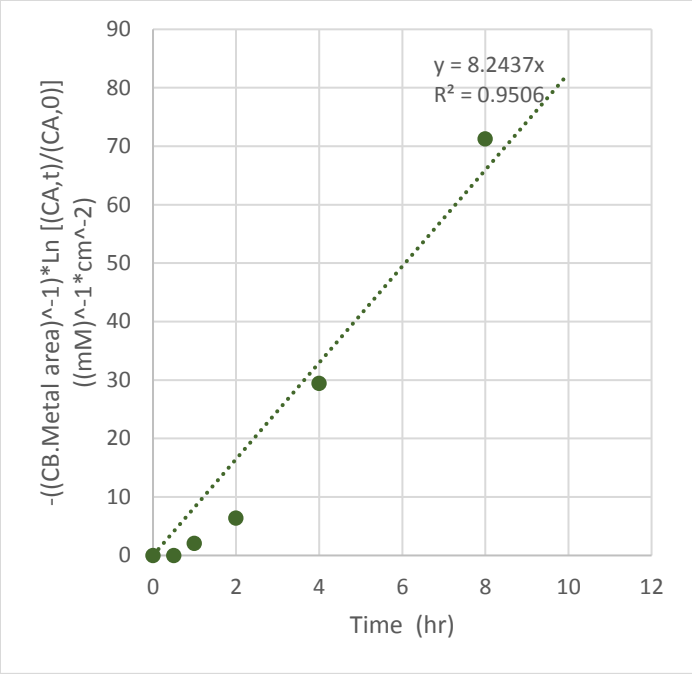

Figure 5-19. Fitting the rate constant (*k*) of formic-acid decomposition with pseudo-first order kinetics for W

Figure 5.19 shows the fitted trendline for calculating the decomposition rate of formic acid in the presence of silver foil. The rate constant for the case of W, *k*, is 8.2437 $(mM)^{-1}$ cm^{-2} h^{-1}. The coefficient of determination (R^2) is very high: 0.9506.

5.3.9 Molybdenum

The molybdenum is the last metal we used for the decomposition study. ^1H NMR spectroscopy results along with reaction time are presented in Figure 5.20. Using the same quantitative method presented in section 5.3.1 we calculated the retention percentage of formic acid in reaction solution.

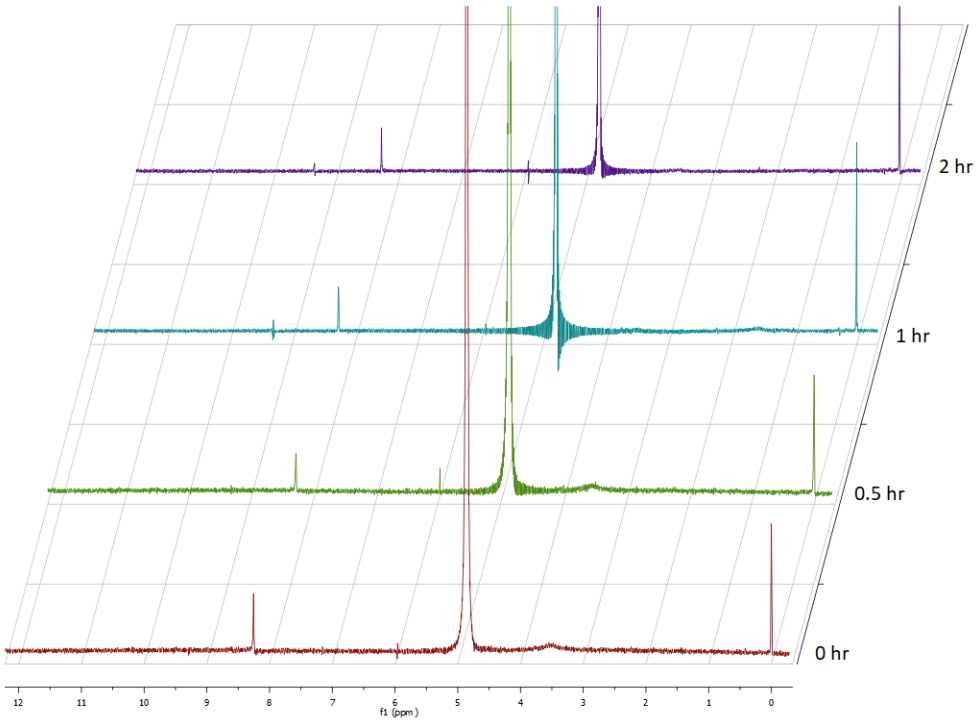

Figure 5-20. ^{1}H NMR spectra of reaction solution for decomposition of formic acid with the presence of a Mo metal foil, ratio of $[D_2O_2]$ to $[Fe^{2+}]$ as 50 and $[D_2O_2]$ as 1.0 mM

The data for calculated remained formic acid in reaction solution in the presence of tungsten at each time interval is presented in Table 19. We only carry out the reaction for two hours, because of the surface change on Mo foil over two hours due to oxidization by aggressive solution.

TABLE 19

DECOMPOSION RATE OF FORMIC ACID IN THE PRESENCE OF MOLYBDENUM (Mo)

Time (hr.)	Integrated value for Formic acid (8.26 ppm)	Formic acid Retention (%)
0	0.73	100
0.5	0.64	88
1	0.45	62
2	0.36	492
DSS peak at 0.00 ppm is considered the standard peak The area integrals of peaks at 0.00 ppm and 8.25 ppm at time zero are 1 and 0.37, respectively.		

Figure.5.21 shows the fitted trendline for calculating the decomposition rate of formic acid in the presence of molybdenum foil. The rate constant for the case of Mo, k is 29.919 $(mM)^{-1}$ cm^{-2} h^{-1}. The coefficient of determination (R^2) is very high: 0.9465.

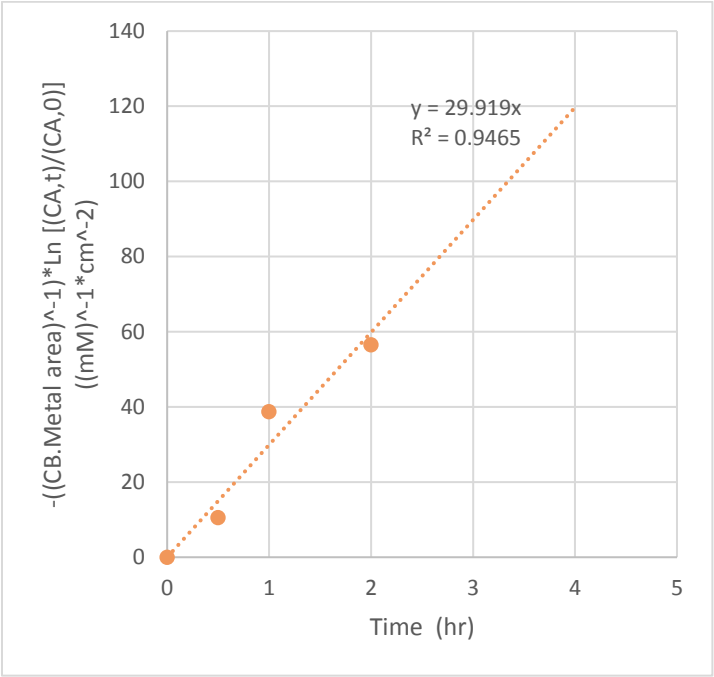

Figure 5-21. Fitting the rate constant (k) of formic-acid decomposition with pseudo-first order kinetics for Mo

5.4 Correlation between Metal Binding Energy and Decomposition Rate

The decomposition trend of formic acid in presence of different metals has been shown in Figure 5.21. The decomposition trend of the control experiment that is free of any metal surface is also included for comparison. Clearly, the presence of a metal surface facilitates the decomposition of formic acid, just like the facilitating effect on the methane activation. And, different metals have varying impact on the decomposition rate.

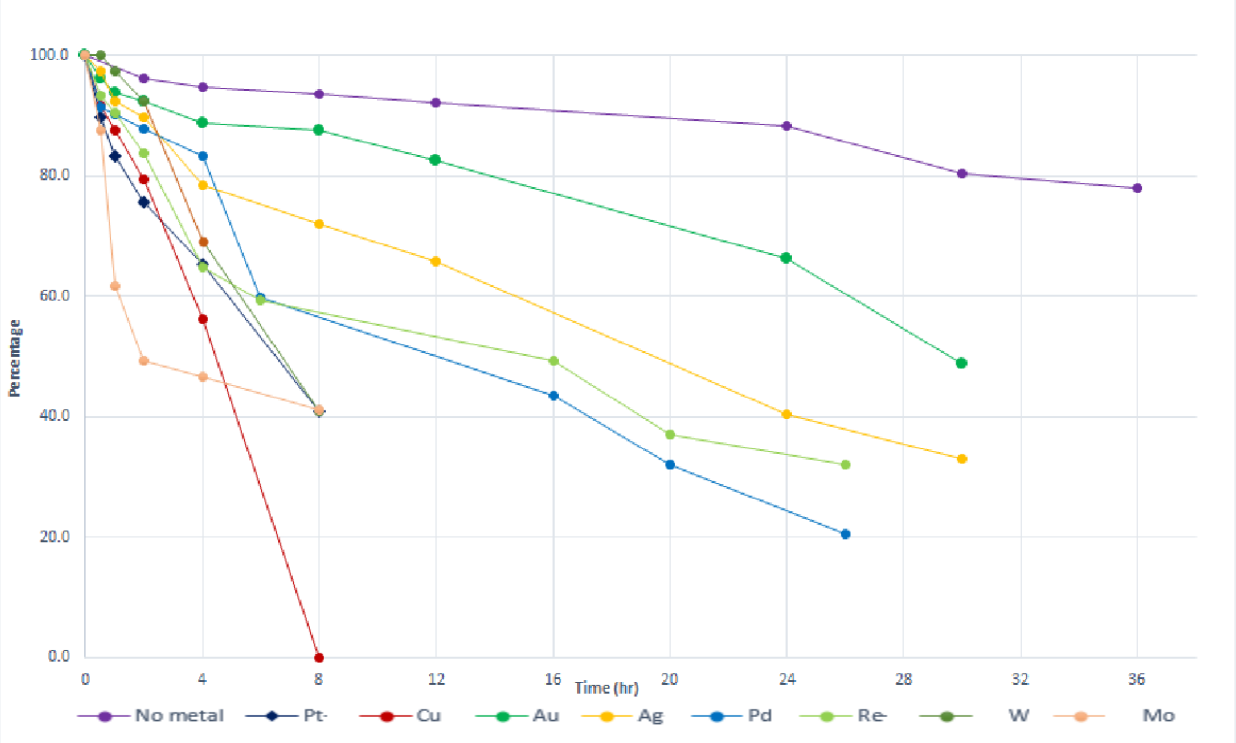

Figure 5-22. Decreasing trend of [HCOOH] over time in the absence of any metal surface and the presence of different metal surfaces

For formic acid, its decomposition rate on metal surfaces follows the descending order:

Cu > Mo > Pt > W > Pd > Re > Ag > Au > no metal

The binding energy between different spices such as O•, HO•, H•, and CH_3• with aforesaid metals is investigated and it seems that the decomposition of formic acid is much related to the M−O binding energy [83, 84, 86, 94]. As shown in Figure 5.22, the decomposition rate of formic

acid reveals a volcano plot regarding the M−O binding energies. This shows that the lower absolute value of Metal−O binding energy, the higher decomposition rate of formic acid.

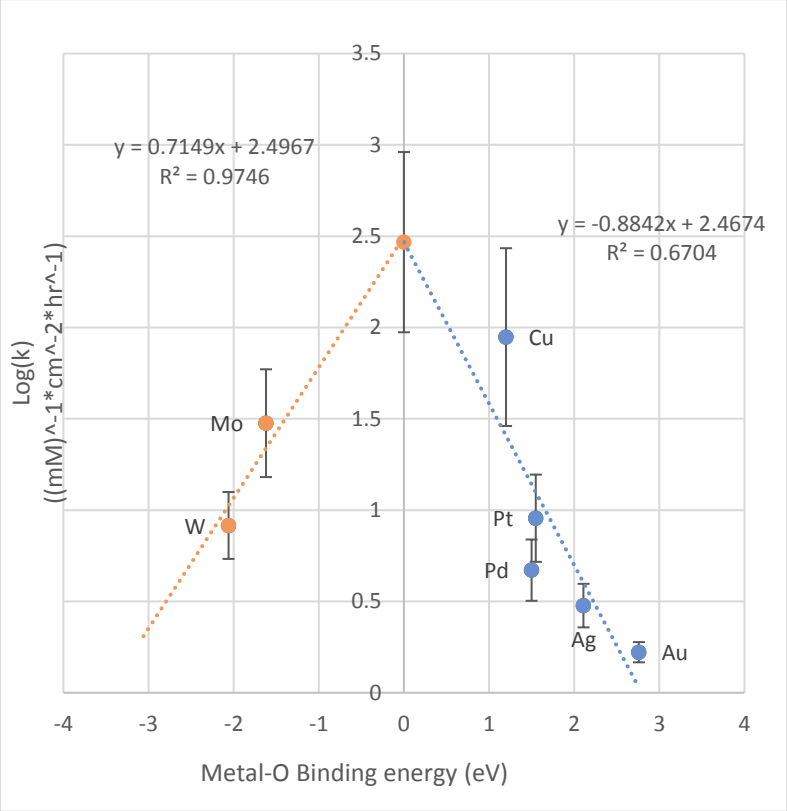

Figure 5-23. Corelation between decomposition rate, *k*, and M−O binding energy

When fitting the leg of the volcano plot, we used a virtual metal that has zero M−O binding energy. The virtual metal was obtained by extrapolating the fitted trendline of the right leg. If the volcano plot is true, then a metal on top of the volcano that has a zero M−O binding energy would result the least decomposition rate. The virtual point $x = 0$ and $y = 2.4674$. In fact, ruthenium (Ru) has a M−O binding energy of −0.05 eV, which is the closest among the known metals [86]. Due to very high cost of this metal, Ru was not tested in this study. Re will be tested in the future research when available.

The Figure 5.22 shows that the fitted trendline for right leg has the acceptable coefficient of determination (R^2) value of 67.04%. Using the virtual point obtained from the right leg, the

fitted trendline is fitted with a very high coefficient of determination (R^2) of 97.46%. This result will help us better understand the decomposition procedure of oxycarbons generated form methane upgrading.

For attempts using on other binding energies, please refer to Appendix E.

5.5 Chapter Summery

Formic acid was used as a representing activation product of methane activation for composition study. The initial concentration of 1 mM was chosen for formic acid, based on the observed concentration in methane activation. The initial concentration of hydrogen peroxide was carefully chosen as well to ensure the effectiveness of control experiment. The reaction rate was calculated by implementing the pseudo-first order approximation.

In comparison to the case of metal-free decomposition, a metal surface leads to a much faster decomposition. The decomposition rate of formic acid on metal surfaces follows the descending order:

Cu > Mo > Pt > W > Pd > Re > Ag > Au > no metal

We have made the correlation between decomposition rate and the M−O binding energy, and a volcano plot is revealed. This volcano plot indicates that smaller the absolute value of M−O binding energy, higher the decomposition reaction rate would be. This correlation casts the light in the underlying parameter who governs the decomposition of activation products, and it can also guide us to choose the suitable metal surfaces with lower decomposition rate to best preserve the activation products.

CAHPTER 6

CONCLUSIONS

The massively increasing methane production worldwide, especially in the USA, calls for new methods of upgrading this inexpensive natural resource into value-added oxycarbon products. Natural gas can be liquefied by cooling process, but it is rather costly, compared with common liquid products. More importantly, oxycarbon products from natural gas, such as methanol and formic acid, can serve as a platform of precursor chemicals for use in many industrial applications.. Conventional methods of methane upgrading, such as Fischer-Tropsch, are energy-intense and infrastructure-complicated. By contrast, an energy-efficient and mild-conditioned electrochemical approach is highly desired for alternative methane upgrading. .

In this study, we extend the cathodic electrochemical upgrading of methane by decoupling the radical generation and methane activation. The focus has been laid on the methane activation which is the bottleneck of the whole process of methane upgrading. The hydroxyl radical was chosen as the powering agent to break the C−H bonds of methane, and hydrogen peroxide was used to generate the hydroxyl radial with the help of $FeSO_4$ Fenton's catalyst in acidic solution of the pH of 3. .

For methane activation, we have discovered that the powerful facilitating effect of metal surfaces on the methane activation, and this facilitation can be reason by by offering the adsorption of CH_3• on metal surface that in turn lowers the reaction barrier of breaking C−H bond reacting with HO•. With facilitation of metal surfaces, three activation products have been observed in the methane activation: methanol, methyl formate, and formic acid. Based on the experimental observations and theoretical analysis, we also proposed the generation mechanisms of all three activation products.

A group of metal surfaces has been tested for the facilitating effect: Pt, Pd, Cu, Au, Ag, and Re. The metals regarding the generation rate of methanol and methyl formate followed the descending order as:

$$Pt > Re > Pd > Cu > Au$$

This order of the metals is the same as the descending order for CH_3−M binding energy. We have correlated the generation rates and the CH_3−M binding energy, leading to a very high coefficient of determination (R^2) for fitted trendline: 0.96 and 0.93 for methanol and methyl formate, respectively.

In addition to the astonishing discovery of the powerful facilitating effect of metal surfaces, we also observed that all of the activation products decompose given enough reaction time. It is important for us to study the decomposition behavior of the activation products. Formic acid was chosen as the representing product of methane activation for the product decomposition study in our reaction system. Similarly, the metal surfaces also apparently facilitate the decomposition reaction of the formic acid, compared with the case of metal-free decomposition. In order to quantitatively study the decomposition kinetics, pseudo-first order approximation method was assumed and implemented in reaction rate calculation. As a result, the rate constants of decomposition were obtained with very high coefficient of determination (mostly > 0.95).

We correlated the rate constant of decomposition with a few metal binding energies, and the M−O binding energy fits the best. A volcano plot is revealed: the smaller the absolute value of M−O binding energy, the higher the decomposition reaction rate would be. This correlation casts the light in the underlying parameter who governs the decomposition of activation products, and it can also guide us to choose the suitable metal surfaces with lower decomposition rate to best preserve the activation products.

From both studies on methane activation and product decomposition, the metal facilitation could provide a fantastic opportunity for us to design and engineer the unique methane upgrading. With deeper understanding of reaction mechanisms and better optimizing reaction conditions, it is possible to drastically increase the concentration of activation products which may lead to final industrial practices.

CHAPTER 7

FUTURE RESEARCH

7.1 Increasing Product Concentrations

By better understanding the mechanisms of both methane activation and product decomposition, we will design a system that will give much higher product concentrations that are critically required for possible commercialization. Some metal alloys can be used, instead of pristine metals, by taking advantage of the insight over the binding energies.

7.2 Onsite Electrosynthesis of H_2O_2 from water

One of the main consumables in this process is H_2O_2 that is the source for hydroxyl radicals. H_2O_2 could be generated onsite by electrolysis of water. Recent research breakthroughs on this field have demonstrated that a Pt-Hg catalyst may be active enough for such duty: it has over one order magnitude of improvement in mass activity for direct electrochemical H_2O_2 generation in 0.1 M $HClO_4$ over all reported materials in literature [95, 96]. Note that, we are aware of another choice of electrochemically generating H_2O_2: the combination of oxygen reduction at cathode and oxygen evolution at anode. But, the overall efficiency of this choice should be a bit lower than the one we plan to introduce.

7.3 Introducing the photo-reduction of Fe^{3+} to Fe^{2+}

Hydroxyl radicals are generated through oxidation process of H_2O_2 catalyzed by Fe^{2+} ions. To constantly provide the HO• supply to reaction system, we may utilize photo-reduction of Fe^{3+} to Fe^{2+} to regenerate Fenton reagent. The photon-reduction of Fe^{3+} to Fe^{2+} has been well established [69, 97]. Different aspects of this process such as light wavelength [75, 98] radiation intensity, exposure time, and temperature [99], and pH [100] have been studied. By some

necessary modifications, we may use the same method to regenerate Fenton reagent in methane activation process.

Combining the methods presented above, here we schematically show the system for methane upgrading using the decoupled mechanism for methane activation as shown in Figure 7.1. H_2O_2 is generated onsite through electrolysis of water and by a photo-reduction, HO• is generated. By utilizing UV radiation, we are able to regenerate the Fe^{2+} ions so as to keep the HO• generation reaction continuous. Once generated, HO• is used for methane activation in the presence of a proper metal surface to generate oxycarbons and other value-added products.

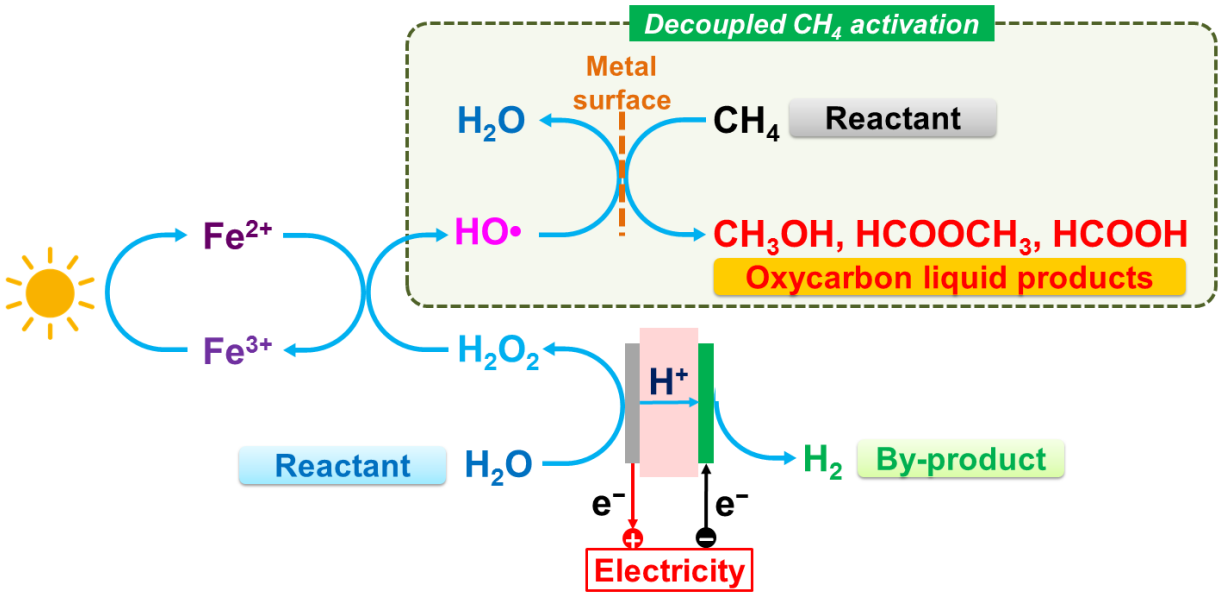

Figure 7-1. Proposed concept for upgrading methane to oxycarbon products (liquid fuels) and hydrogen

Notes:

1- Methanol is used as the example of the liquid product.
2- The species are not balanced for simplification.
3- Oxygen-evolution reaction in the photo-reduction is omitted for clarity.

REFERENCES

REFERENCES

1. Gupta, A., et al., *Measurements of methane hydrate heat of dissociation using high pressure differential scanning calorimetry*. Chemical Engineering Science, 2008. **63**(24): p. 5848-5853.

2. Brown, W.H., et al., *Organic chemistry*, *Cengage Learning.* Inc., Belmont, CA, 2008.

3. Kietäväinen, R. and L. Purkamo, *The origin, source, and cycling of methane in deep crystalline rock biosphere.* Frontiers in microbiology, 2015. **6**.

4. Cramer, B. and D. Franke, *Indications for an active petroleum system in the Laptev Sea, NE Siberia.* Journal of Petroleum Geology, 2005. **28**(4): p. 369-384.

5. Khalil, M., *Non-CO2 greenhouse gases in the atmosphere.* Annual Review of Energy and the Environment, 1999. **24**(1): p. 645-661.

6. March, J., *Advanced organic chemistry: reactions, mechanisms, and structure*. 1992: John Wiley & Sons.

7. Thunnissen, D., et al. *Advanced space storable propellants for outer planet exploration*. in *40th AIAA/ASME/SAE/ASEE Joint Propulsion Conference and Exhibit*. 2004.

8. Eberhardt, J.J., E. Efficiency, and R. Energy. *Fuels of the Future for Cars and Trucks*. in *2002 Diesel Engine Emissions Reduction (DEER) Workshop*. 2002.

9. Lunsford, J.H., *Catalytic conversion of methane to more useful chemicals and fuels: a challenge for the 21st century*. Catalysis Today, 2000. **63**(2): p. 165-174.

10. Myhre, G., et al., *Anthropogenic and natural radiative forcing.* Climate change, 2013. **423**: p. 658-740.

11. Stocker, T., *Climate change 2013: the physical science basis: Working Group I contribution to the Fifth assessment report of the Intergovernmental Panel on Climate Change*. 2014: Cambridge University Press.

12. Lashof, D.A. and D.R. Ahuja, *Relative contributions of greenhouse gas emissions to global warming.* Nature, 1990. **344**(6266): p. 529-531.

13. Agency, U.S.E.P. *Understanding Global Warming Potentials*. 2017 [cited 2017 12 June]; Available from: https://www.epa.gov.

14. Schwarz, H., *Chemistry with methane: concepts rather than recipes.* Angewandte Chemie International Edition, 2011. **50**(43): p. 10096-10115.

15. Fokin, A.A. and P.R. Schreiner, *Selective alkane transformations via radicals and radical cations: Insights into the activation step from experiment and theory.* Chemical reviews, 2002. **102**(5): p. 1551-1594.

16. De María, R., et al., *Industrial methanol from syngas: kinetic study and process simulation.* International Journal of Chemical Reactor Engineering, 2013. **11**(1): p. 469-477.

17. Ryndin, Y.A., et al., *Effects of metal-support interactions on the synthesis of methanol over palladium.* Journal of Catalysis, 1981. **70**(2): p. 287-297.

18. Kikuzono, Y., et al., *Selective hydrogenation of carbon monoxide on palladium catalysts.* Faraday Discussions of the Chemical Society, 1981. **72**: p. 135-143.

19. Kelly, K.P., et al., *Methanol synthesis over palladium supported on silica.* Journal of Catalysis, 1986. **101**(2): p. 396-404.

20. Fleisch, T., et al., *Dimethyl ether: a fuel for the 21st century.* studies in surface science and catalysis, 1997. **107**: p. 117-125.

21. Periana, R.A., et al., *Catalytic, oxidative condensation of CH4 to CH3COOH in one step via CH activation.* Science, 2003. **301**(5634): p. 814-818.

22. Periana, R.A., et al., *Platinum catalysts for the high-yield oxidation of methane to a methanol derivative.* Science, 1998. **280**(5363): p. 560-564.

23. Periana, R.A., et al., *A Mercury-Catalyzed, High-Yield System for the.* Science, 1993. **259**: p. 15.

24. Ding, X.-L., et al., *C–H bond activation by oxygen-centered radicals over atomic clusters.* Accounts of chemical research, 2011. **45**(3): p. 382-390.

25. Yoshizawa, K., Y. Shiota, and T. Yamabe, *Methane− Methanol Conversion by MnO+, FeO+, and CoO+: A Theoretical Study of Catalytic Selectivity.* Journal of the American Chemical Society, 1998. **120**(3): p. 564-572.

26. Schulz, H., *Short history and present trends of Fischer–Tropsch synthesis.* Applied Catalysis A: General, 1999. **186**(1): p. 3-12.

27. Vannice, M., *The catalytic synthesis of hydrocarbons from H2CO mixtures over the group VIII metals: I. The specific activities and product distributions of supported metals.* Journal of Catalysis, 1975. **37**(3): p. 449-461.

28. Otsuka, K. and Y. Wang, *Direct conversion of methane into oxygenates.* Applied Catalysis A: General, 2001. **222**(1): p. 145-161.

29. Hargreaves, J.S., G.J. Hutchings, and R.W. Joyner, *Control of product selectivity in the partial oxidation of methane.* Nature, 1990. **348**(6300): p. 428-429.

30. Jiang, Y., I. Yentekakis, and C. Vayenas, *Methane to ethylene with 85 percent yield in a gas recycle electrocatalytic reactor-separator.* SCIENCE-NEW YORK THEN WASHINGTON-, 1994: p. 1563-1563.

31. Mimoun, H., et al., *Oxypyrolysis of natural gas.* Applied catalysis, 1990. **58**(1): p. 269-280.

32. Fang, X., et al., *Oxidative coupling of methane on W–Mn catalysts.* J. Mol. Catal, 1992. **6**(6): p. 427-433.

33. Pak, S., P. Qiu, and J.H. Lunsford, *Elementary Reactions in the Oxidative Coupling of Methane over Mn/Na2WO4/SiO2and Mn/Na2WO4/MgO Catalysts.* Journal of Catalysis, 1998. **179**(1): p. 222-230.

34. Schweer, D., L. Meeczko, and M. Baerns, *OCM in a fixed-bed reactor: limits and perspectives.* Catalysis today, 1994. **21**(2-3): p. 357-369.

35. Pak, S. and J.H. Lunsford, *Thermal effects during the oxidative coupling of methane over Mn/Na 2 WO 4/SiO 2 and Mn/Na 2 WO 4/MgO catalysts.* Applied Catalysis A: General, 1998. **168**(1): p. 131-137.

36. Wang, L., et al., *Dehydrogenation and aromatization of methane under non-oxidizing conditions.* Catalysis Letters, 1993. **21**(1): p. 35-41.

37. Betteridge, S., et al., *A study of the iron/sodalite catalyst for the partial oxidation of methane to methanol*, in *Methane and Alkane Conversion Chemistry*. 1995, Springer. p. 187-193.

38. Wang, Y. and K. Otsuka, *Selective Oxidation of Methane to Methanol over FePO4 Using N2O and H2 at Low Temperatures.* Chemistry letters, 1994. **23**(10): p. 1893-1896.

39. Solymosi, F., A. Erdöhelyi, and A. Szöke, *Dehydrogenation of methane on supported molybdenum oxides. Formation of benzene from methane.* Catalysis Letters, 1995. **32**(1): p. 43-53.

40. Weckhuysen, B.M., et al., *Conversion of methane to benzene over transition metal ion ZSM-5 zeolites: II. Catalyst characterization by X-ray photoelectron spectroscopy.* Journal of catalysis, 1998. **175**(2): p. 347-351.

41. Zeng, J.L., et al., *Nonoxidative dehydrogenation and aromatization of methane over W/HZSM-5-based catalysts.* Catalysis letters, 1998. **53**(1): p. 119-124.

42. Lu, Y., et al., *Methane aromatization in the absence of an added oxidant and the bench scale reaction test.* Catalysis letters, 1999. **62**(2): p. 215-220.

43. Hammond, C., S. Conrad, and I. Hermans, *Oxidative methane upgrading.* ChemSusChem, 2012. **5**(9): p. 1668-1686.

44. Yilmaz, A., et al., *Bromine mediated partial oxidation of ethane over nanostructured zirconia supported metal oxide/bromide.* Microporous and mesoporous materials, 2005. **79**(1): p. 205-214.

45. Lorkovic, I.M., et al., *C 1 oxidative coupling via bromine activation and tandem catalytic condensation and neutralization over CaO/zeolite composites: II. Product distribution variation and full bromine confinement.* Catalysis today, 2004. **98**(4): p. 589-594.

46. Lorkovic, I.M., et al., *A novel integrated process for the functionalization of methane and ethane: bromine as mediator.* Catalysis today, 2004. **98**(1): p. 317-322.

47. Li, F. and G. Yuan, *Hydrated Dibromodioxomolybdenum (VI) Supported on Zn-MCM-48 for Facile Oxidation of Methane.* Angewandte Chemie International Edition, 2006. **45**(39): p. 6541-6544.

48. Lin, M. and A. Sen, *Direct catalytic conversion of methane to acetic acid in an aqueous medium.* Nature, 1994. **368**(6472): p. 613-615.

49. Kirillova, M.V., et al., *Direct and efficient transformation of gaseous alkanes into carboxylic acids catalyzed by vanadium containing heteropolyacids.* Applied Catalysis A: General, 2007. **332**(1): p. 159-165.

50. Shteinman, A., *The role of metal-oxygen intermediates in biological and chemical monooxygenation of alkanes.* Russian chemical bulletin, 2001. **50**(10): p. 1795-1810.

51. Otsuka, K., I. Yamanaka, and Y. Wang, *Reductive activation of oxygen for partial oxidation of light alkanes.* Studies in surface science and catalysis, 1998: p. 15-24.

52. Fan, Q., *Method for producing methanol from methane*. 2014, Google Patents.

53. Zhang, Y., et al., *Electro-oxidation of methane on roughened palladium electrode in acidic electrolytes at ambient temperatures.* Analytical Letters, 2010. **43**(6): p. 1055-1065.

54. Jacquinot, P., et al., *Determination of methane and other small hydrocarbons with a platinum–Nafion electrode by stripping voltammetry.* Analytica chimica acta, 2001. **432**(1): p. 1-10.

55. Hahn, F. and C. Melendres, *Anodic oxidation of methane at noble metal electrodes: an 'in situ'surface enhanced infrared spectroelectrochemical study.* Electrochimica acta, 2001. **46**(23): p. 3525-3534.

56. Otagawa, T., S. Zaromb, and J.R. Stetter, *Electrochemical Oxidation of Methane in Nonaqueous Electrolytes at Room Temperature Application to Gas Sensors.* Journal of the Electrochemical Society, 1985. **132**(12): p. 2951-2957.

57. Sustersic, M., W. Triaca, and A. Arvía, *The electrosorption of methane and its potentiodynamic electrooxidation on platinized platinum.* Journal of the Electrochemical Society, 1980. **127**(6): p. 1242-1248.

58. Hsieh, S. and K. Chen, *Anodic oxidation of methane.* Journal of the Electrochemical Society, 1977. **124**(8): p. 1171-1174.

59. TAYLOR, A. and S. BRUMMER. *ANODIC OXIDATION OF METHANE ON PT*. in *JOURNAL OF THE ELECTROCHEMICAL SOCIETY*. 1968. ELECTROCHEMICAL SOC INC 10 SOUTH MAIN STREET, PENNINGTON, NJ 08534.

60. BINDER, H., A. KOHLING, and G. SANDSTEDE. *ANODIC OXIDATION OF METHANE, ETHANE, PROPANE, BUTANE, AND CARBON MONOXIDE IN PHOSPHORIC ACID AT 110-DEGREES-C.* in *JOURNAL OF THE ELECTROCHEMICAL SOCIETY*. 1964. ELECTROCHEMICAL SOC INC 65 SOUTH MAIN STREET, PENNINGTON, NJ 08534.

61. Tomita, A., J. Nakajima, and T. Hibino, *Direct oxidation of methane to methanol at low temperature and pressure in an electrochemical fuel cell.* Angewandte Chemie, 2008. **120**(8): p. 1484-1486.

62. Cook, R.L. and A.F. Sammells, *Ambient Temperature Methane Activation to Condensed Species Under Cathodic Conditions.* Journal of The Electrochemical Society, 1990. **137**(6): p. 2007-2008.

63. Frese Jr, K.W., *Partial electrochemical oxidation of methane under mild conditions.* Langmuir, 1991. **7**(1): p. 13-15.

64. Blanksby, S.J. and G.B. Ellison, *Bond dissociation energies of organic molecules.* Accounts of chemical research, 2003. **36**(4): p. 255-263.

65. Cruickshank, F.R. and S.W. Benson, *The Carbon-Hydrogen Bond Strength in Dimethyl Ether and Some Properties of Iodomethyl Methyl Ether.* International Journal of Chemical Kinetics, 1969. **1**: p. 381-390.

66. Solly, R.K. and S.W. Benson, *Carbon-Hydrogen Bond Strengths in Methyl Formate and the Kinetics of the Reaction with Iodine.* International Journal of Chemical Kinetics, 1969. **1**: p. 427-437.

67. Jeong, J. and J. Yoon, *pH effect on OH radical production in photo/ferrioxalate system.* Water Research, 2005. **39**(13): p. 2893-2900.

68. Kang, Y.W. and K.-Y. Hwang, *Effects of reaction conditions on the oxidation efficiency in the Fenton process.* Water research, 2000. **34**(10): p. 2786-2790.

69. Zepp, R.G., B.C. Faust, and J. Hoigne, *Hydroxyl radical formation in aqueous reactions (pH 3-8) of iron (II) with hydrogen peroxide: the photo-Fenton reaction.* Environmental Science & Technology, 1992. **26**(2): p. 313-319.

70. Buxton, G.V., et al., *Critical review of rate constants for reactions of hydrated electrons, hydrogen atoms and hydroxyl radicals (·OH/·O− in aqueous solution.* Journal of physical and chemical reference data, 1988. **17**(2): p. 513-886.

71. Kang, N., D.S. Lee, and J. Yoon, *Kinetic modeling of Fenton oxidation of phenol and monochlorophenols.* Chemosphere, 2002. **47**(9): p. 915-924.

72. Barbeni, M., et al., *Chemical degradation of chlorophenols with Fenton's reagent (Fe2++ H2O2).* Chemosphere, 1987. **16**(10-12): p. 2225-2237.

73. Safarzadeh-Amiri, A., J.R. Bolton, and S.R. Cater, *Ferrioxalate-mediated solar degradation of organic contaminants in water.* Solar Energy, 1996. **56**(5): p. 439-443.

74. Safarzadeh-Amiri, A., J.R. Bolton, and S.R. Cater, *Ferrioxalate-mediated photodegradation of organic pollutants in contaminated water.* Water Research, 1997. **31**(4): p. 787-798.

75. Weller, C., S. Horn, and H. Herrmann, *Photolysis of Fe (III) carboxylato complexes: Fe (II) quantum yields and reaction mechanisms.* Journal of Photochemistry and Photobiology A: Chemistry, 2013. **268**: p. 24-36.

76. Matheson, L.J. and P.G. Tratnyek, *Reductive dehalogenation of chlorinated methanes by iron metal.* Environmental Science & Technology, 1994. **28**(12): p. 2045-2053.

77. Goddard, P.J. and R. Lambert, *Adsorption-desorption properties and surface structural chemistry of chlorine on Cu (111) and Ag (111).* Surface Science, 1977. **67**(1): p. 180-194.

78. Sonntag, C., *The reaction of methyl radicals with hydrogen peroxide.* Journal of the Chemical Society, Perkin Transactions 2, 1999(4): p. 673-676.

79. Zins, E.L., et al., *Reactivity between non-energetic hydroxyl (OH) radicals and methane (CH4).* J Phys Chem A, 2012. **116**(50): p. 12357-63.

80. Graf, E., et al., *Iron-catalyzed hydroxyl radical formation. Stringent requirement for free iron coordination site.* Journal of Biological Chemistry, 1984. **259**(6): p. 3620-3624.

81. Chen, S.x. and P. Schopfer, *Hydroxyl-radical production in physiological reactions.* European Journal of Biochemistry, 1999. **260**(3): p. 726-735.

82. Duesterberg, C.K., S.E. Mylon, and T.D. Waite, *pH effects on iron-catalyzed oxidation using Fenton's reagent.* Environmental science & technology, 2008. **42**(22): p. 8522-8527.

83. Abild-Pedersen, F., et al., *Scaling properties of adsorption energies for hydrogen-containing molecules on transition-metal surfaces.* Phys Rev Lett, 2007. **99**(1): p. 016105.

84. Hahn, K. and M. Mavrikakis, *Atomic and Molecular Adsorption on Re(0001).* Topics in Catalysis, 2013. **57**(1-4): p. 54-68.

85. Sheng, W., et al., *Correlating the hydrogen evolution reaction activity in alkaline electrolytes with the hydrogen binding energy on monometallic surfaces.* Energy & Environmental Science, 2013. **6**(5): p. 1509-1512.

86. Nørskov, J.K., et al., *Origin of the overpotential for oxygen reduction at a fuel-cell cathode.* The Journal of Physical Chemistry B, 2004. **108**(46): p. 17886-17892.

87. Psofogiannakis, G., A. St-Amant, and M. Ternan, *Methane oxidation mechanism on Pt (111): a cluster model DFT study.* The Journal of Physical Chemistry B, 2006. **110**(48): p. 24593-24605.

88. Lanza, R., P. Canu, and S.G. Järås, *Methane partial oxidation over Pt–Ru catalyst: An investigation on the mechanism.* Applied Catalysis A: General, 2010. **375**(1): p. 92-100.

89. Wilmad-labglass. *Coaxial insert NMR tube*. 2017 [cited 2017; Available from: http://www.wilmad-labglass.com.

90. Chang, R., *Physical chemistry for the biosciences*. 2005: University Science Books.

91. Braslavsky, S.E., *Glossary of terms used in photochemistry, (IUPAC Recommendations 2006).* Pure and Applied Chemistry, 2007. **79**(3): p. 293-465.

92. Connors, K.A., *Chemical kinetics: the study of reaction rates in solution*. 1990: John Wiley & Sons.

93. Jolly, G.S., et al., *Rates of hydroxyl radical reactions. Part 14. Rate constant and mechanism for the reaction of hydroxyl radical with formic acid.* The Journal of Physical Chemistry, 1986. **90**(24): p. 6557-6562.

94. Varma, C.M. and A.J. Wilson, *Systematics of the binding energy of oxygen and hydrogen on transition-metal surfaces. I.* Physical Review B, 1980. **22**(8): p. 3795-3804.

95. Siahrostami, S., et al., *Enabling direct H2O2 production through rational electrocatalyst design.* Nature materials, 2013. **12**(12): p. 1137-1143.

96. Verdaguer-Casadevall, A., et al., *Trends in the electrochemical synthesis of H2O2: Enhancing activity and selectivity by electrocatalytic site engineering.* Nano letters, 2014. **14**(3): p. 1603-1608.

97. Ruppert, G., R. Bauer, and G. Heisler, *The photo-Fenton reaction—an effective photochemical wastewater treatment process.* Journal of Photochemistry and Photobiology A: Chemistry, 1993. **73**(1): p. 75-78.

98. Laglera, L.M. and C.M. Van den Berg, *Wavelength dependence of the photochemical reduction of iron in Arctic seawater.* Environmental science & technology, 2007. **41**(7): p. 2296-2302.

99. Liu, W., et al., *UV–Vis spectrophotometric and XAFS studies of ferric chloride complexes in hyper-saline LiCl solutions at 25–90 C.* Chemical Geology, 2006. **231**(4): p. 326-349.

100. Vermilyea, A.W. and B.M. Voelker, *Photo-Fenton reaction at near neutral pH.* Environmental science & technology, 2009. **43**(18): p. 6927-6933.

101. Edwards, J.C., *Principles of NMR.* Process NMR Associates LLC, 87A Sand Pit Rd, Danbury CT, 2009. **6810**.

102. Fulmer, G.R., et al., *NMR chemical shifts of trace impurities: common laboratory solvents, organics, and gases in deuterated solvents relevant to the organometallic chemist.* Organometallics, 2010. **29**(9): p. 2176-2179.

103. Gottlieb, H.E., V. Kotlyar, and A. Nudelman, *NMR chemical shifts of common laboratory solvents as trace impurities.* The Journal of organic chemistry, 1997. **62**(21): p. 7512-7515.

APPENDICES

APPENDIX A

NUCLEAR MAGNETIC RESONANCE SPECTROSCOPY

A.1. Basic Principles

The developments of Nuclear Magnetic Resonance (NMR) spectroscopy goes back to 1946 simultaneously at M.I.T and Stanford universities, in the USA. NMR mainly owes its development to advanced improvements in radar technologies, especially hardware developments, which took place during World War (II). Physicists and chemists used all those advanced technologies to tackle the problems they were facing. As a result in 50 years, NMR is considered as one of the most powerful tools for analytical problems in physics and chemistry. One of the most well-known devices developed from the basis of NMR spectroscopy is Magnetic Resonance Imaging (MRI). MRI is widely used in medical radiology field to get picture cuts of delicate tissues in the human body. With new advancements in NMR technology one would be able to take high resolution NMR spectra in a process environment.

Generally NMR instruments are divided into two categories of a) Continuous wave (CW) and b) Fourier Transform (FT). Continuous wave spectrometers share more basics with optical spectrometers in which a strong magnetic field is applied over a fixed sample and the source frequency is then slowly scanned. Continuous wave NMR instruments were taken over by development of Fourier Transform type. Fourier Transform NMR devices, are much faster and can give better qualities and resolutions in the output spectroscopy due to the fact that they irradiate all the frequencies at the same time. This irradiation will excite the nuclei to different energy state. By observing the relaxation time required for nuclei to get back to its thermal equilibrium a time domain signal could be digitized and recorded, called Free Induction Decay (FID). As shown in

Figure 2.5, by applying a Fourier transformation over the FID data, a frequency domain spectrum could be obtained [101].

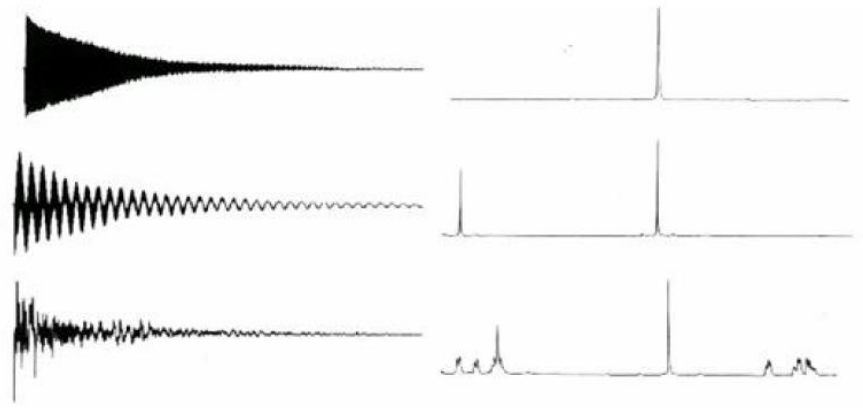

Figure A. 1. Fourier transformation of FID data to frequency domain spectrum [101]

A.2. Processing Free Induced Decay Signals

By conducting NMR spectroscopy, we can obtain a free induction decay (FID) signals corresponding to the spectrum. This signal consists of set of sine and cosine waves that are measured as a function of time. These waves are decaying towards zero, at an exponential rate. This row data is also known as analogue data. An Analogue-to Digital-Converter (ADC) is then used to convert these recorded intensities as integer values and store them. The digital information now could be processed using Fourier Transformation (FT) technique. This even could be improved by Fast Fourier Transformation (FFT) and processing time could be reduced if the number of points that are being processed is exactly 2^n.

The continuous form of Fourier Transformation is expressed as:

$$F(\omega) = \int_{-\infty}^{+\infty} f(t)\, \mathrm{e}^{-i\omega t}\, dt$$

Where $f(t) = FID$ which is a function of time, $F(\omega)$ is transformed form of the same date in frequencies domain and "i" is $\sqrt{-1}$ This could furthermore be expressed as:

$$F(\omega) = \int_{-\infty}^{+\infty} f(t)\left[\cos(\omega t) - i\sin(\omega t)\right]dt$$

By separating the real from the imaginary part, we have

$$F(\omega) = \int_{-\infty}^{+\infty} f(t)\cos(\omega t)dt - i\int_{-\infty}^{+\infty} f(t)\sin(\omega t)dt$$

Continuous Fourier Transformation (CFT) is replaced by Discrete Fourier Transform (DFT) in order to meet the needs of pulse NMR where the FID is sampled at short but discreet intervals. DFT is expressed as:

$$X(n) = \frac{1}{N}\sum_{n=0}^{N-1}\left[f(n)\frac{\cos(2\pi kn)}{N} - i\, f(n)\frac{\sin(2\pi kn)}{N} \right]$$

Where N is the number of samples, "n" is the n^{th} sample and $2\pi k$ is used to convert the n^{th} point to corresponding frequency form of ωt .

More advanced techniques are also implemented to reduce the required computation time and also to provide a better and smoother plot. The Cooley-Tukey fast-Fourier algorithm (FFT) is an example which reduces the number of required calculation in discrete FT from $N \times N$ to $N \log_2 N$ for instance if the number of points is 1024, by applying Cooley-Tukey FFT, the number of calculation would be reduced to 7098 from 1048576 which shows almost 93% reduction in required calculations. The only drawback for implementing this method is the restriction on the number of samples, which should be a power of 2.

A.3. Locking and Shimming

In order to get a good spectroscopy out of the sample, we need to set the lock and shimming level properly. The main purpose of lock system is to maintain a constant magnetic field at the sample while the static magnetic field of the superconductor changes with the time. As a result, the resonance of the deuterium in solvent will coincide with the frequency of the lock.

Another very important factor to obtain a good quality NMR spectroscopy is shimming. A good shimming will provide a homogeneous magnetic field over the whole sample volume, which is critical for a clear spectroscopy. Increase in non-homogeneousness of the field will increase the distortions and poor resolution in the results. Changing the applied current of the coils that are surrounding the probe, one can easily set the shimming level. The changes in the current will vary the magnetic field generated and will let us to accomplish the shimming process and obtain a perfectly homogeneous field.

A.4. Proton NMR Chemical Shifts for Common Functional Groups

Chemical shift is expressed as variations in magnetic resonances of same nuclei. This shift is calculated with respect to a standard reference frequency which is chosen intentionally to have minimum distorted electron distribution. Different nucleus will cause different shift. A row estimation of these shifts is shown in Figure 2.6 [101].

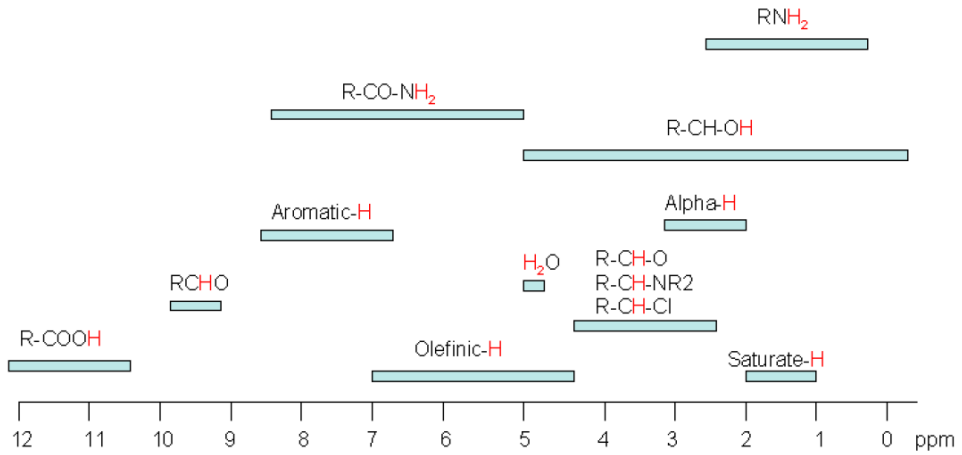

Figure A. 2. Chemical shift for different compounds [101]

For instance, electronegative groups tend to shift NMR signals from neighboring protons further to the "downfield" which means to higher ppm values. The same thing is true about alkenes, aromatic and carbonyls as well. Chemical shift for different compounds in common solvents has been well organized for better analysis of NMR spectra [102, 103].

APPENDIX B

GOLD GAUZE WITH EXTENDED SURFACE FOR METHANE ACTIVATION

To extend the gold available surface area a gold gauze is purchased from Alfa-Aesar Co. with purity of 99.9%. By using a gold gauze instead of gold foil, the available surface area of the metal for methane activation reaction could be increased by factor of 6.34. ^{1}H NMR spectroscopy results along with reaction time are presented in Figure Appendix A.1. Using the same quantitative method presented in section 4.3.2 we are would be able to calculate the concentrations of different products regarding to reaction time for methane upgrading. Table Appendix A.1, presents the final calculated concentrations of products in reaction solution in presence of gold gauze. Figure Appendix A.2, shows the graphically depicted trend of methane activation and generation of products

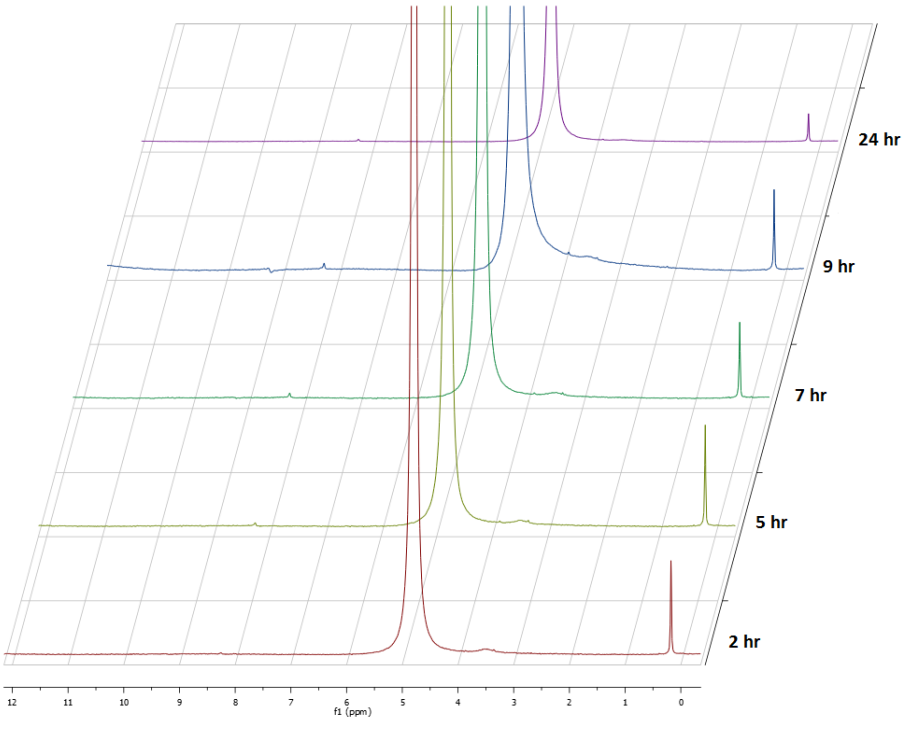

Figure B. 1. ^{1}H NMR spectra of reaction solution for methane activation with the presence of Au gauze

APPENDIX B TABLE. 1

CALCULATED CONCENTRATIONS OF ACTIVATION PRODUCTSIN THE CASE OF USING GOLD GAUZE (Au)

Time (hr.)	$[CH_3OH]$ (mM)	$[HCOOCH_3]$ (mM)	[HCOOH] (mM)
2	0.163	0.182	0.106
5	0.235	0.240	0.322
7	0.715	1.046	0.879
9	0.202	0.312	0.437
24	0	0	0.331
Concentration of methane in solution is considered as a constant of 1.44 mM for calculating other concentrations			

APPENDIX C

DECOMPOSITION OF INTERNAL STANDARD IN SOLUTION

The Figure C.1 shows that the peak for DSS standard reference at 0.00 ppm appears as a dual peak and starts altering regarding the time. This shows instability of this compound and its decomposition in the reaction solution regarding time. As a result, this chemical cannot be internally used for NMR reference in this reaction solution and use of coaxial insert tube for NMR spectroscopy is inevitable.

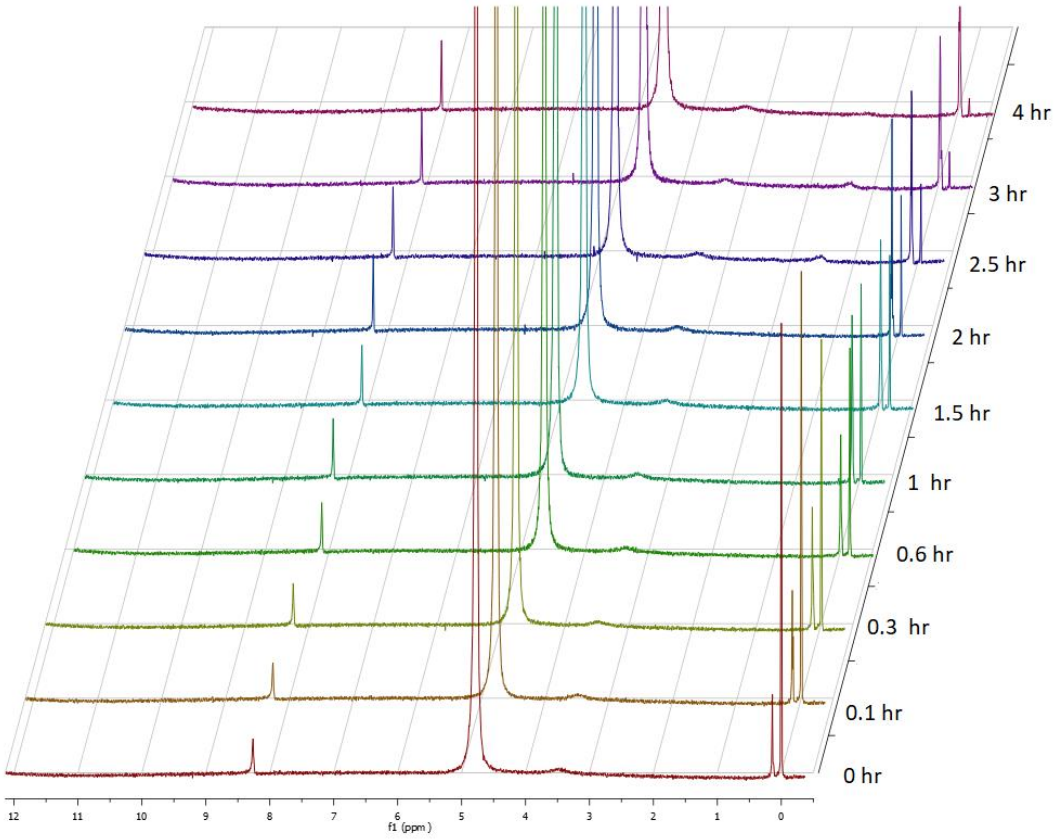

Figure C. 1. Decomposition of DSS in solution

APPENDIX D

CONTROL EXPERIMENT FOR THE DECOMPOSION STUDY OF FORMIC ACID OVER DEFFERENT CONCENTRATIONS OF H_2O_2

Same concentration of 1 mM formic acid was tested in different concentrations of D_2O_2 and Fe^{2+} ions, making the same ration of 50:1. The Figure D.1 shows that the same concentrations of $[D_2O_2]$ = 12.5 mM vs. $[Fe^{2+}]$ = 0.25 mM is too intense for formic acid and the decomposition will take place spontaneously

Keeping the same ratio of 50:1 between $[D_2O_2]$ and $[Fe^{2+}]$ and lowering the concentration of them reduced the intensity of the reaction solution condition to decompose formic acid in absence of any metal surfaces. This could be seen in Figures Appendix D. 2 to 4. Concentration of D_2O_2 has varied from 7.5 mM to 5.0 mM and 2.5 mM respectively. As mentioned in section 5.2.2, the most stable reaction condition was achieved once the concentration of D_2O_2 was set as

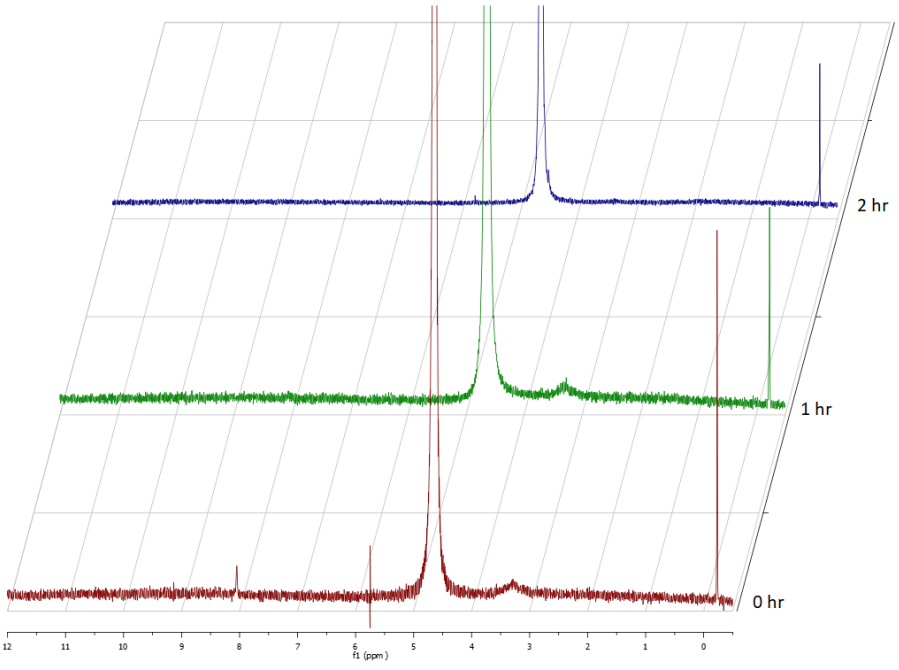

Figure D. 1. ^1H NMR spectra of reaction solution for decomposition of formic acid in absence of any metal surfaces with ratio of $[D_2O_2]$ to $[Fe^{2+}]$ as 50 and $[H_2O_2]$ = 12.5 mM

1 mM. This provided the opportunity to investigate the impact of metal surfaces on decomposition rate of formic acid in reaction solution.

Figure D.2 shows the decomposition of formic acid in absence of any metal once the initial concentration of D_2O_2 is set as 7.5 Mm with ratio of 50:1 to [Fe^{2+}]. It can be seen that after almost 10 hours all the formic acid will disappear.

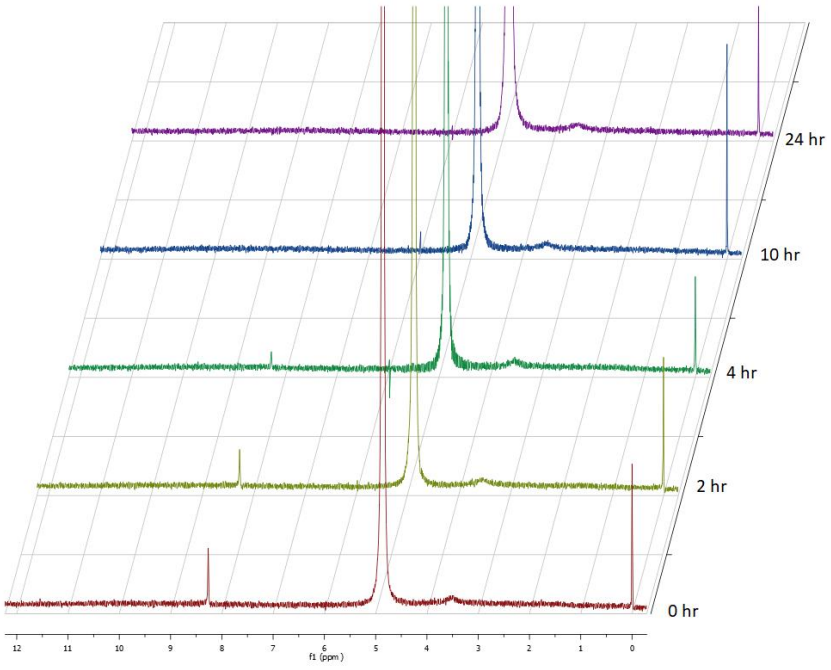

Figure D. 2. ^1H NMR spectra of reaction solution for decomposition of formic acid in absence of any metal surfaces with ratio of [D_2O_2] to [Fe^{2+}] as 50 and [D_2O_2] = 7.5 mM

Figure D.3 shows the decomposition of formic acid in absence of any metal once the initial concentration of D_2O_2 is set as 7.5 mM with ratio of 50:1 to [Fe^{2+}]. It can be seen that after almost 10 hours all the formic acid will disappear

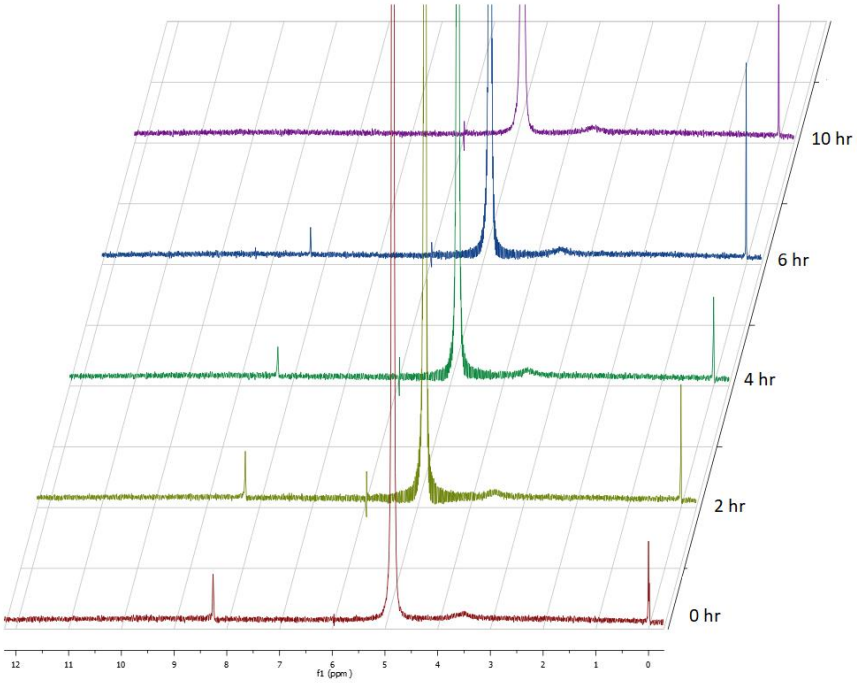

Figure D. 3. ^1H NMR spectra of reaction solution for decomposition of formic acid in the absence of any metal surfaces with ratio of [D_2O_2] to [Fe^{2+}] as 50 and [H_2O_2] = 5.0 mM

Figure D.4 shows the decomposition of formic acid in absence of any metal once the initial concentration of D_2O_2 is set as 7.5 mM with ratio of 50:1 to [Fe^{2+}]. It can be seen that after almost 12 hours more than 50% of the formic acid will disappear

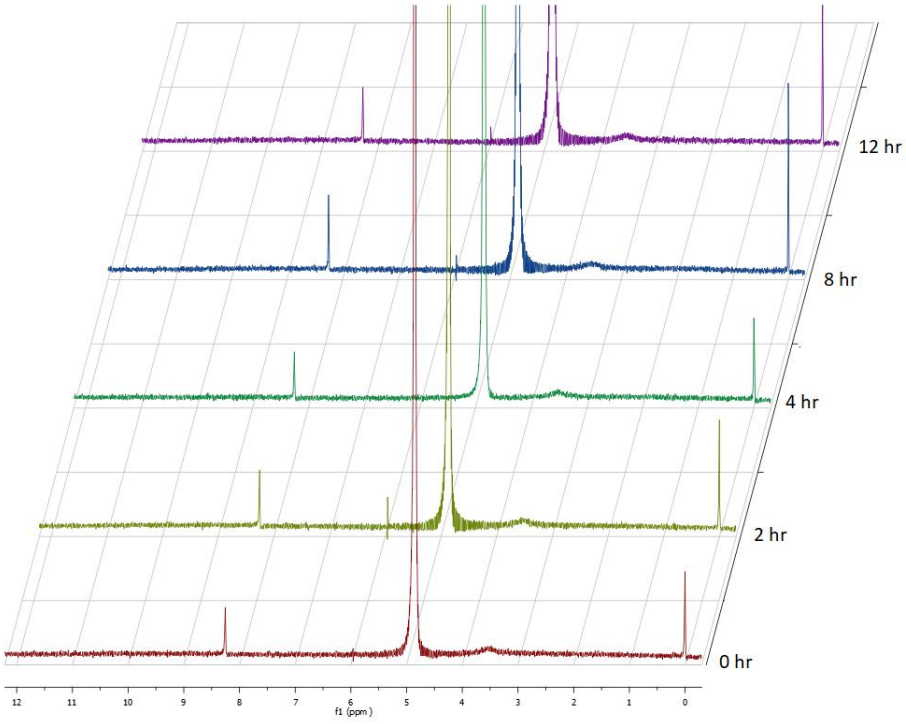

Figure D. 4. ^1H NMR spectra of reaction solution for decomposition of formic acid in the absence of any metal surfaces with ratio of [D_2O_2] to [Fe^{2+}] as 50 and [H_2O_2] = 2.5 mM

APPENDIX E

DECOMPOSION RATE VS. DIFFERENT METAL BINDING ENERGIES

Figure E.1 depicts graphical outline for reaction rates for decomposition of formic acid in presence of different metals, verses metal−OH binding energies. As is clear, there is no significant correlation between these data and not a useable interpretation could be made.

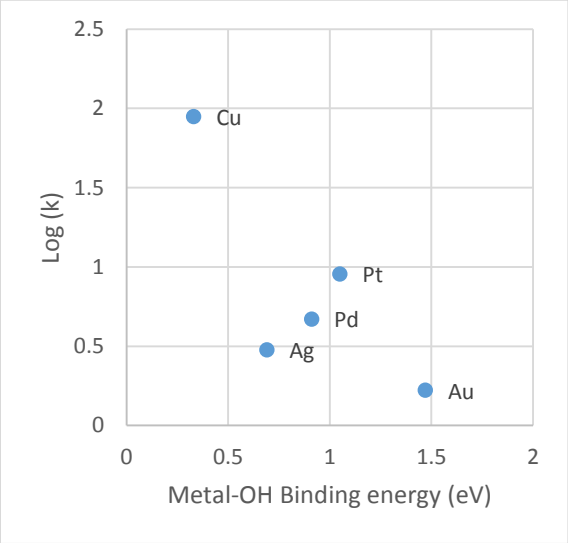

Figure E. 1. Correlation between *k* value and metal−HO binding energy

Figure E.2 depicts graphical outline for reaction rates for decomposition of formic acid in presence of different metals, verses metal−CH_3 binding energies. As is clear, there is no significant correlation between these data and not a useable interpretation could be made.

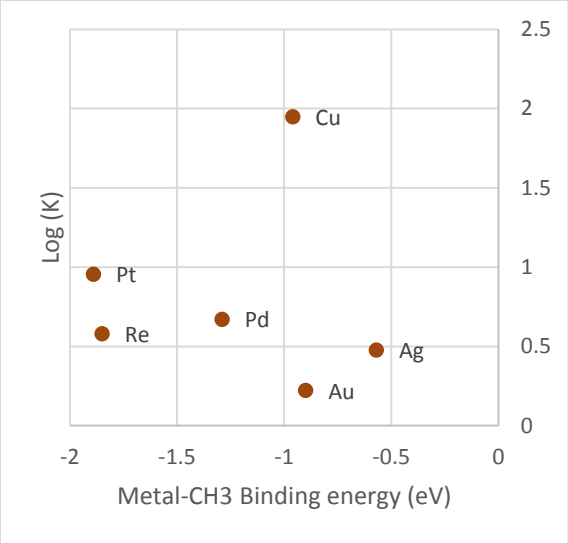

Figure E. 2. Correlation between *k* value and metal−CH_3 binding energy

Figure E.3 depicts graphical outline for reaction rates for decomposition of formic acid in presence of different metals, verses metal−H binding energies. As is clear, there is no significant correlation between these data and not a useable interpretation could be made.

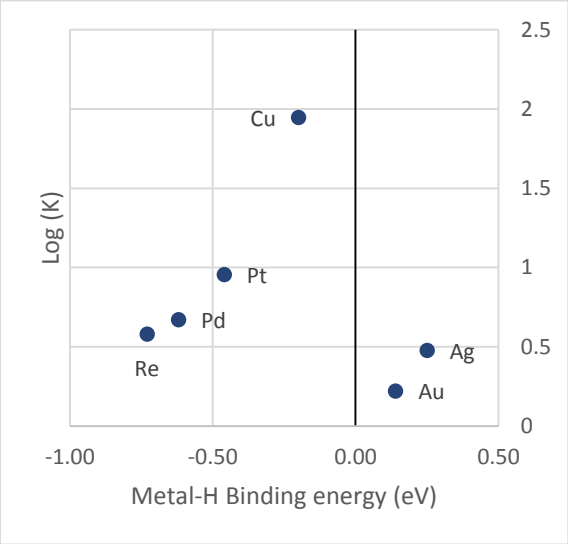

Figure E. 3. Correlation between *k* value and metal−H binding energy